Development of Tools and Guidance for Damage Assessment of Prestressed Concrete Girder Bridges

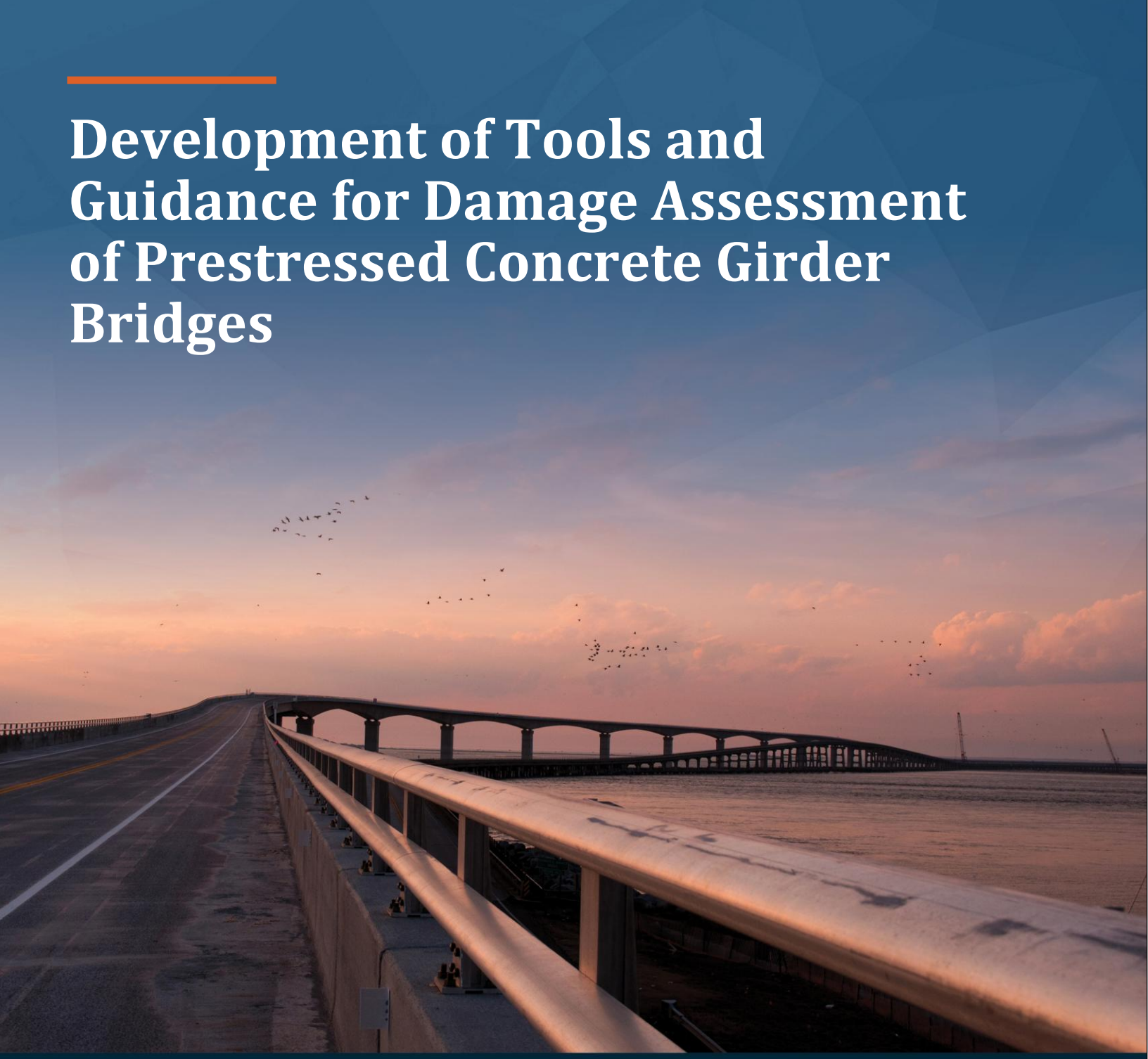

NCDOT Project 2023-06
FHWA/NC/2023-06
December 2025

Nicole Braxtan, Ph.D., et al.
Department of Civil and Environmental Engineering
University of North Carolina at Charlotte

RESEARCH & DEVELOPMENT

Technical Report Documentation Page

1. Report No. FHWA/NC/2023-06	2. Government Accession No.	3. Recipient's Catalog No.
4. Title and Subtitle Development of Tools and Guidance for Damage Assessment of Prestressed Concrete Girder Bridges		5. Report Date December 23rd, 2025
		6. Performing Organization Code
7. Author(s) Nicole L. Braxtan, Matthew Whelan, Shen-En Chen, Amirmohammad Samadzad, Seth Cathey		8. Performing Organization Report No.
9. Performing Organization Name and Address Department of Civil and Environmental Engineering, University of North Carolina at Charlotte 9201 University City Blvd, Charlotte, NC 28223		10. Work Unit No. (TRAIS)
		11. Contract or Grant No.
12. Sponsoring Agency Name and Address North Carolina Department of Transportation Research and Development Unit 104 Fayetteville Street Raleigh, North Carolina 27601		13. Type of Report and Period Covered Final Report August 01, 2022 - September 30, 2025
		14. Sponsoring Agency Code RP2023-06
Supplementary Notes:		

16. Abstract

The collision of overheight vehicles and objects with bridge girders is a not uncommon occurrence that requires timely inspection and engineering assessment to determine if repair or replacement is required. When girders of prestressed concrete bridges are impacted, this assessment is particularly challenging due to the potential for internal damage that is not readily detected by conventional visual inspection. Furthermore, when girders are damaged during the construction of the bridge, subjectivity in the assessment may lead to disputes with liable parties that can lead to litigation and delay construction. The primary objective of this research project was to produce a physics-based approach to support the assessment of prestressed concrete girders impacted by overheight vehicles. The research leverages high-fidelity finite element (FE) modeling with advanced constitutive and contact models, while building on verified techniques for collision simulations. A key innovation is the development of a Collision Analysis Engine (CAE), an automated script library that generates detailed 3D models of bridge superstructures from basic parameters, incorporating elements like girders, decks, diaphragms, reinforcement, and elastomeric bearings. Additionally, the research introduces the first high-fidelity finite element model of a dump truck with raised bed to permit simulation of the most common vehicle involved in overheight collisions. A case study involving impact damage to girders of a prestressed concrete bridge under construction is used to validate the plausibility of the model. Furthermore, insight into differences in failure mechanisms and vulnerabilities of girders during construction are produced through simulations and the effect of the presence and type of intermediate diaphragm on girder resistance to impact damage is explored, resulting in guidance for inspection of prestressed concrete girders when impacted prior to the construction of the deck The research advances the state of knowledge by providing the first comprehensive parametric studies of raised bed dump truck collisions with prestressed concrete girder bridges, revealing critical insight into the effects of bridge characteristics and truck velocity, angle of raised bed, impact location, and vertical underclearance violation on the resulting damage and producing empirical model to predict impact force characteristics. Lastly, a framework for risk-based, simplified prediction of damage severity based on iso-damage curves is formulated and demonstrated using a detailed model of a representative superstructure.

17. Key Words Prestressed concrete bridges, impact damage, finite element analysis, iso-damage curve	18. Distribution Statement		
19. Security Classif. (of this report) Unclassified	20. Security Classif. (of this page) Unclassified	21. No. of Pages 121	22. Price

Form DOT F 1700.7 (8-72) **Reproduction of completed page authorized**

DISCLAIMER

The contents of this report reflect the views of the author(s) and not necessarily the views of the University. The author(s) are responsible for the facts and the accuracy of the data presented herein. The contents do not necessarily reflect the official views or policies of either the North Carolina Department of Transportation or the Federal Highway Administration at the time of publication. This report does not constitute a standard, specification, or regulation.

ACKNOWLEDGMENTS

The research team acknowledges the North Carolina Department of Transportation for supporting and funding this project (RP 2023-06). We extend our gratitude to the Steering and Implementation Committee and the managers and engineers of the Structures Management Units: Trey Carroll, Mustansir Kadibhai, Brian Hanks, Gichuru Muchane, Tim Sherrill, Beth Quinn, Aaron Earwood, Cabell Garbee, Larry Carpenter, Brian Hedrick, Jason Civils, Phillip Brewer, Chuck White, Daniel Muller (FHWA), Todd Whittington, and Matt Hilderbran. The research team also acknowledges assistance provided by Justin Sprumont, who served as an undergraduate research assistant during the first year of the project and assisted with identifying relevant background literature. The High-Performance Computing resources maintained by University Research Computing at the University of North Carolina at Charlotte were leveraged by the research team to enable the large-scale parametric finite element analysis presented in this report. The research team would like to specifically acknowledge support provided by Jonathan Halter and Tien Bui of the Research Computing Team for their assistance with the use of these resources.

EXECUTIVE SUMMARY

This report presents the findings of NCDOT Research Project RP 2023-06, aimed at addressing the challenges associated with assessing damage to bridges with prestressed concrete girders caused by overheight vehicle collisions, particularly during construction. Overheight impacts are a frequent issue, with over 12,000 bridge-vehicle collisions reported annually in the U.S., often leading to costly delays, litigation, or safety risks due to inadequate visual inspections that may fail to detect or underestimate the severity of internal damage like strand debonding or prestress loss. The primary objective was to develop a fundamental understanding of how the impacting object characteristics (e.g., type, velocity, location), bridge features (e.g., girder type, diaphragms), and construction stage influence external and internal damage in prestressed concrete girder bridges. A practical goal was to create physics-based tools and guidelines for rapid, risk-informed damage assessments to guide do-nothing/repair/replace decisions.

The research leveraged high-fidelity finite element (FE) modeling with advanced constitutive and contact models using LS-DYNA, while building on verified techniques for collision simulations. A key innovation was the development of a Collision Analysis Engine (CAE), an automated script library that generates detailed 3D models of bridge superstructures from basic parameters, incorporating elements like girders, decks, diaphragms, reinforcement, and elastomeric bearings. This CAE allows for the rapid development of high-fidelity finite element models of bridge superstructures from bridge plans, ensures consistency in model development, and afforded the research team with a means to perform parametric analysis at a scale significantly larger than any prior research. Models were initialized to replicate construction sequences, ensuring accurate prestress and camber simulation. Constitutive models were evaluated and selected for concrete (e.g., CSCM for high-strain-rate behavior) and steel, by benchmarking model performance against data from impact experiments. Novel contributions included the development of a finite element model for a dump truck with raised beds to provide a means of simulating one of the most frequent culprits of overheight collisions. A case study involving accidental collision of a raised bed dump truck with girders of a bridge under construction was simulated to provide validation of the plausibility of this dump truck model. A series of parametric analyses were then performed to address three specific gaps in the existing knowledgebase. The first investigated differences in failure modes and susceptibility of prestressed concrete girders to damage from overheight vehicle impact at different stages of construction as well as the influence of the presence and type of intermediate diaphragm on the girder response. Significantly different failure modes and significantly reduced resistance to lateral impact forces were predicted for girders prior to the placement of the deck. The vulnerability of such girders to severe damage adjacent to the sole plate connection, a damage mechanism also observed in a real-world case study, was specifically highlighted. The second parametric analysis examined the effect of initial truck velocity, angle of raised bed, impact location, and vertical underclearance violation on the severity of damage using a model of a representative prestressed concrete girder bridge. This parametric analysis resulted in the development of a framework for creating simplified and intuitive iso-damage curves that could be used by bridge engineers to quickly estimate the likelihood of superficial, moderate, or severe damage without running additional computationally intensive finite element analysis. Lastly, a large parametric analysis consisting of 864 simulations conducted with models of three different bridges was performed to investigate the effect of bridge and dump truck features on the impact force characteristics needed to utilize the iso-damage curves in practice. Specifically, prediction models for peak lateral impact force and impulse associated with raised

bed dump truck impacts were successfully developed using nonlinear regression and the models were shown to exhibit high confidence.

The research advances the state of knowledge by providing the first comprehensive parametric study of raised bed dump truck collisions with prestressed concrete girder bridges, revealing critical insight into the effects of bridge characteristics and truck velocity, angle of raised bed, impact location, and vertical underclearance violation on the impact force characteristics and resulting damage. Products include:

- Extensive software libraries for rapid and automated generation of high-fidelity finite element models from bridge plans, enabling event-specific simulations to support forensic analysis of real-world incidents.
- Unique capability to explicitly simulate the collision of dump trucks with raised beds using a high-fidelity model of a representative construction vehicle.
- A framework for risk-based, simplified assessment of the likelihood and severity of damage to prestressed concrete girders from overheight collisions based on iso-damage curves.
- Statistical models to predict the impact force characteristics needed for practical utilization of the iso-damage curves.
- Guidance related to the inspection of prestressed concrete bridge girders when subjected to accidental lateral impacts prior to the construction of the bridge deck.

These tools could empower NCDOT engineers to mitigate risks, reduce litigation, and ensure long-term bridge safety over 75 to 100-year service lives. Additionally, this work could enhance bridge management practices, potentially saving costs and improving public safety. Since the developed framework for risk-based, simplified assessment of the likelihood and severity of damage is based on iso-damage curves that are described with only three parameters, the framework is suitable for being generalized to any prestressed concrete girder bridge. Future research should be directed towards the development of a surrogate model for predicting this limited set of iso-damage curve parameters from bridge characteristics so that a tool applicable to the entire inventory of the state's prestressed concrete girder bridges can be developed for use by practitioners. Additional recommendations for future research, such as expanding the research to excavators carried on flatbed trailers, are also provided.

TABLE OF CONTENTS

1. MOTIVATION AND BACKGROUND

In 2022 alone, 12,339 vehicle collisions with bridges were reported throughout the United States (National Center for Statistics and Analysis, 2025). Overheight collisions with bridge girders occur significantly more frequently than vehicular collisions with bridge piers or abutments and the majority of overheight collisions are attributed to trucks and trailers carrying construction equipment, materials, and other objects (Agrawal, et al. 2011). Although minimum underclearance standards generally mitigate the risk of overheight collisions to in-service bridges by vehicles of legal height, both overpass bridges under active construction as well as overpass bridges in service are at particularly elevated risk to accidental collisions from dump trucks with unintentionally raised beds and overheight excavators on flatbed trailers.

Bridges of all materials and design types may be affected by overheight vehicle collisions, but prestressed concrete girder bridges are of particular concern to NCDOT due to their prevalence and the challenges associated with their damage assessment. According to 2025 National Bridge Inventory data (LTBP InfoBridge, 2025), prestressed concrete girder or beam bridges account for over 40% of all bridges constructed in North Carolina within the past five years and over 20% of the entire statewide bridge inventory owned and maintained by NCDOT. Although prestressed concrete generally offers greater resistance to impact loading than reinforced concrete, the collision of overheight vehicles with prestressed concrete girders can produce significant damage that in many cases may not be visually apparent and is difficult to accurately assess. Specifically, the following unique challenges are associated with damage assessment of prestressed concrete girders: 1) debonding of the prestressing strands and loss of effective prestressing force can often not be visually observed since the strands are embedded in the concrete; 2) even if spalling exposes strands, it is difficult to assess the redevelopment of prestressing force to undamaged regions of the girder; 3) the most common damage pattern associated with impacts from overheight vehicles is torsion-induced shear cracking, but the nature of the prestressing can causes crack closure making complete observation of the damage pattern difficult; and, 4) exterior girders may have beneficial composite action with the barrier wall and other structural components that may be compromised by impact damage (Harries, 2012). The significance of damage in prestressed concrete girders introduced by overheight impacts is not limited to direct reductions in the strength of the section. Harries et al. (2012) summarized additional considerations that inform decisions to repair damaged girders. For example, cracks and minor spalls may reduce the durability of the girder by accelerating chloride ingress and weakening the resistance to corrosion-induced damage. Also, effective prestress losses may extend beyond visibly exposed or ruptured strands, as compromised concrete may inhibit the ability of nearby strands to fully transfer prestress.

Based on analysis of the incident rate of collisions involving prestressed concrete girder bridges over a five-year period in Texas, Feldman et al. (1996) estimated that at least two-thirds of all overheight collisions with prestressed concrete girder bridges result in only minor damage limited to cracks, shallow spalls, and scrapes. Moderate damage, characterized by either large cracks or spalling extensive enough to expose undamaged strands, occurred in 20% of the incidents, while severe damage was noted in only 14% of the reported incidents. This finding is generally consistent with an earlier NCHRP study that surveyed 36 state DOTs and found that 72 percent of incidents to prestressed concrete bridges resulted in only minor damage (Shanafelt and Horn, 1980). These statistics are based on accidental overheight collisions occurring to fully constructed, in-service bridges. Existing research on damage to highway bridges from overheight collisions

has focused almost exclusively on in-service bridges. However, prestressed concrete bridge girders under active construction may be particularly vulnerable to damage from overheight collisions, as the beneficial stiffness and inertial contributions provided by intermediate diaphragms, the deck, and parapets or railings may or may not be provided depending on the stage of construction during the impact. Post-impact assessment of such girders requires a determination of whether to accept repair or require replacement of the affected bridge components while considering the near and long-term risks of acceptance, effect on project timeline and cost, and potential for litigation by the responsible party.

1.1 Research Needs and Objectives

This research is in response to the NCDOTs need to perform timely and accurate assessment of prestressed concrete girder bridges impacted by overheight vehicles and equipment while overcoming the significant challenges related to visual inspection of this construction type. This need is most frequently associated with active construction sites, where overheight collisions result in a difficult decision presented to NCDOT engineers on whether to accept or reject the affected girder or girders. Unnecessarily requiring the replacement of an impact-damaged girder can lead to significant delay and cost to the responsible party, especially if the collision occurs when the bridge is near completion. The party carrying such liability for the replacement may pursue litigation, which further adds to scheduling delay and project costs. However, accepting a repaired girder based only on visual inspection presents a safety risk to the public since safety-critical damage mechanisms in prestressed concrete, such as debonding of strands and loss of prestress, can occur without exhibiting clear, externally visible symptoms. Furthermore, this risk is carried for the remainder of the 75~100-year service life of the bridge. A related challenge faced by NCDOT engineers is the accurate assessment of in-service prestressed concrete girder bridges following accidental overheight vehicle collisions to inform appropriate and cost-effective do-nothing/repair/replace decisions.

The research leverages existing verified and validated finite element modeling techniques to analyze the impact of overheight collisions on prestressed concrete girder bridges, expands the modeling methodology to include active construction site objects and vehicles, and integrates both into an analysis framework that is referred to as a Collision Analysis Engine (CAE). The CAE is an automated workflow that accepts a set of parameters defining the general bridge characteristics and the nature of the overheight impact, constructs an input file for finite element analysis of the scenario, and performs nonlinear analyses to generate high-fidelity predictions of both observable and internal damages to the affected structure. The CAE is used to conduct large-scale parametric analysis to develop an understanding of the correlations between impact object/location, velocity at impact, and bridge characteristics with the location/type/severity of damage developed from the collision. By introducing novel models for vehicle collision analysis at active construction sites (i.e. dump trucks with raised beds) as well as producing the first comprehensive parametric analysis of factors affecting the impact resistance of prestressed girders, the research addresses fundamental gaps in the current knowledge base. Strategically, the design of the research approach also results in valuable products that could enable NCDOT to perform rapid assessments of probable damage and associated girder capacity reduction without placing an increased burden on Structures Management Unit engineers, produce actionable guidance for damage inspection, and mitigate risk and potential litigation following overheight collisions at active bridge construction sites.

The principal research objective of this project is to develop a fundamental understanding of the effect of impact object, intensity, and location, as well as bridge characteristics (such as girder type, number of girders, and intermediate diaphragm design) on external and internal damages in prestressed concrete

bridges resulting from overheight vehicle impacts occurring during either active construction or during service. This research objective builds on recently published literature that has established verified and validated high-fidelity finite element models for simulating the collision of typical construction objects and vehicles with prestressed concrete bridge girders. However, the research conducted to-date has focused on utilizing such high-fidelity modeling to improve the design of prestressed concrete girders against overheight collisions, rather than to inform damage inspections and condition assessments of bridges following impacts. Furthermore, the modeling of impact forces on highway bridges in the literature has largely been limited to vehicles and objects likely to collide with a bridge during service, rather than on construction vehicles and objects likely to collide during construction. Consequently, there are significant gaps in the existing knowledge base on how to appropriately model the impact from construction equipment and how the properties of the object impacting the bridge, location of the impact, intensity of the impact force, and characteristics of the bridge affect the severity and nature of damage and the capacity of the structure.

The practical objective of satisfying these gaps in the existing knowledgebase is to produce risk-based guidelines and tools for damage assessment and inspection of impact-damaged prestressed concrete girder bridges that are informed by the underlying physics, as predicted by high-fidelity finite element analysis. Statistical classification of the results from the large-scale parametric analysis results in easily implemented iso-damage curves that will inform NCDOT engineers of the case-specific risk of accepting impact-damaged girders during construction or choosing do-nothing action following in-service collisions. Furthermore, the analysis tools developed to conduct the large-scale parametric analysis lead to an automated framework of scripts capable of generating site-specific finite element models and establishing the required analysis steps with only simple parametric input from the user on the general bridge design characteristics and nature of the impact force. This developed capability enables the research team to assist NCDOT with simulation of specific real-world incidents to investigate the likelihood and nature of internal damage resulting from overheight collision of raised bed dump trucks with girders of prestressed concrete bridges.

1.2 Literature Review

1.2.1 Field observations of damages to bridges with prestressed concrete girders

Several prior studies have documented real-world cases of accidental overheight collision damage in bridges with prestressed concrete girders. Zobel, et al. (1997) described damages to four prestressed concrete girder bridges following accidental overheight vehicle impact. One incident involving impact from the boom of a truck-mounted crane resulted in total collapse of a span. From direct observation of the collapsed span, the authors were able to conclude that shear failure at the interface between the web and upper flange of the girders led to the collapse. Another incident involving a vehicle with unknown overheight cargo resulted in severe damage in the form of exposed and severed strands in the exterior girder at the location of impact. Notably, the authors also described moderate damage in the adjacent girder that was also impacted, while highlighting evidence of a reinforced concrete intermediate diaphragm near the impact location acting as a reaction point based on the propagation of cracking observed in the bottom flange. Furthermore, instrumentation and in-situ load testing of the damaged span and a nominally identical undamaged adjacent span revealed little difference in the deflection of the spans despite the complete severing of at least four strands. The authors concluded that the damage was repairable based on the in-situ testing. Harries et al. (2012) provides photographs of additional damage observations from overheight vehicle collisions, although commentary on the individual incidents is limited.

Both Zobel et al. (1997), Harries et al. (2012), and Brice (2013) describe typical failure modes for prestressed concrete girders subjected to overheight vehicle impacts. A typical observation in a severely damaged girder is depicted graphically in Figure 1.1. The bottom flange on the impacted side of the girder often experiences localized spalling across the surface directly impacted by the vehicle. In some cases, the spalling is significant enough to expose strands, which can lead to rupture. The response of the girder to the impact force is characterized by shear-torsional behavior, which can lead to shear cracking throughout the web and bottom flange of the girder and horizontal cracking along the web-to-top flange transition. In cases of severe damage, a D-shaped shear failure of the girder is often observed on the rear surface of the girder. Zobel et al. (1997) also observed in two incidents the presence of cracking along the bottom surface of the girder extending to the location of an intermediate diaphragm. The presence of this cracking was attributed to the stiffness of the diaphragm introducing a reaction force to the girder under the lateral impact load. A typical observation in a moderately damaged girder is depicted in Figure 1.2. In such cases, the observable damage is often restricted to the bottom flange of the girder. In addition to any spalling on the impacted surface, a shear push-out failure is developed that is characterized by delamination symmetrically extending diagonally from the location of the impact. In some cases, the delaminated concrete will separate from the girder and prestressing strands will be exposed.

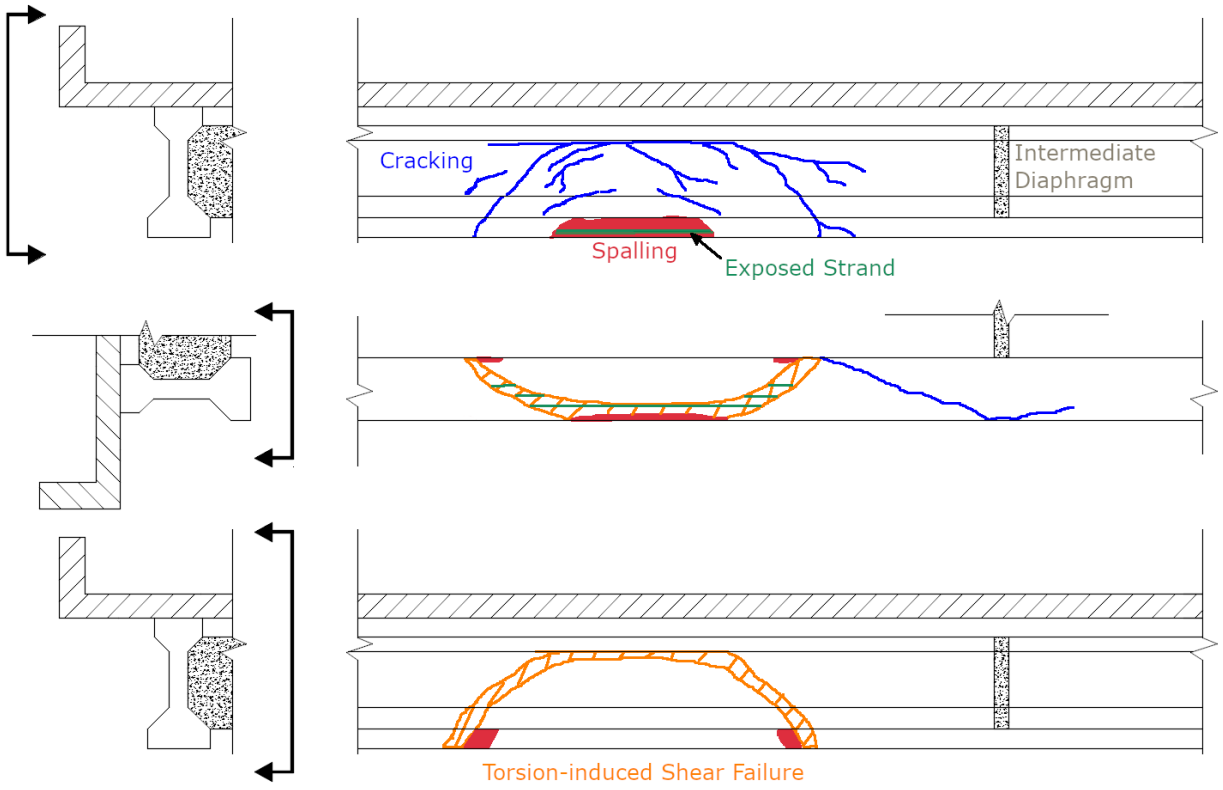

Figure 1.1. Depiction of typical case of severe damage to a prestressed concrete girder from overheight vehicle impact

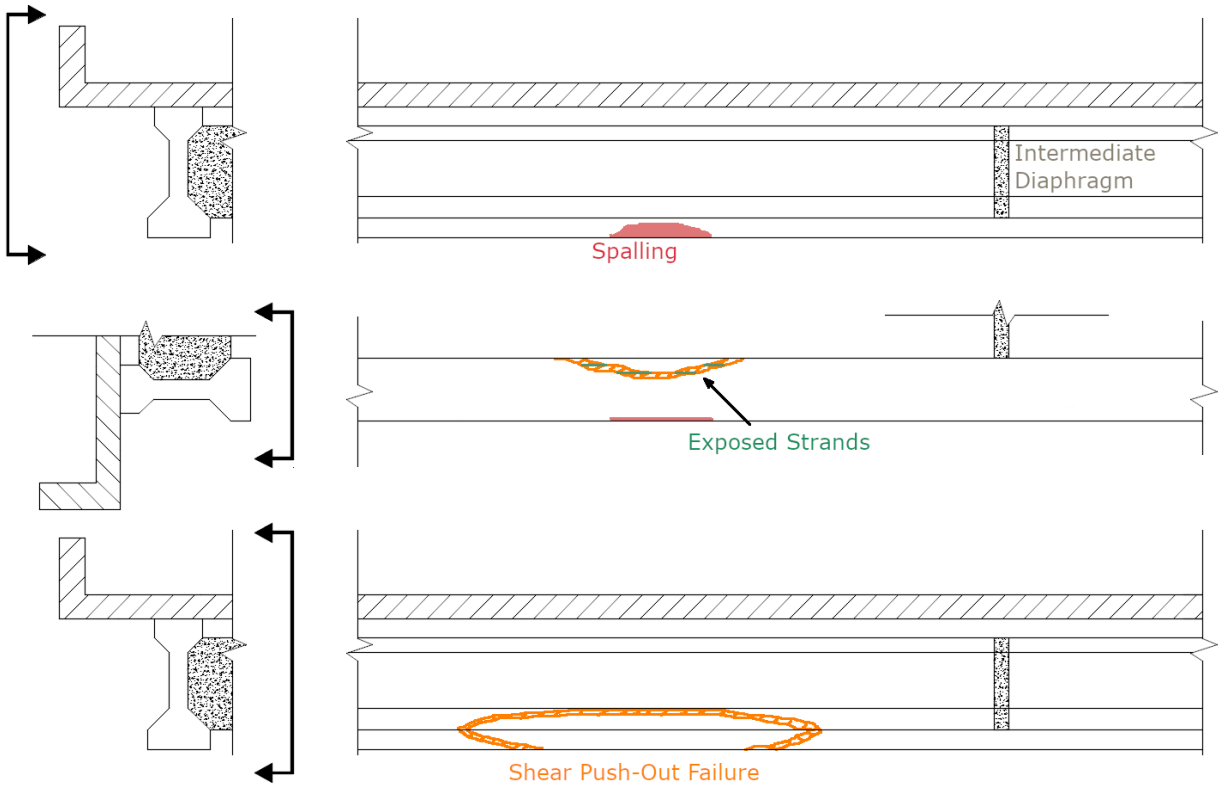

Figure 1.2. Depiction of typical case of moderate damage to a prestressed concrete girder from overheight vehicle impact

1.2.2 Damage assessment for prestressed concrete bridges

Each year, there are approximately a thousand reported cases of impact damage to highway bridges (Gangi et al. 2017), with impact damage identified as the third most significant cause of bridge failures (Nguyen and Brilakis 2016). This widespread issue has been examined by various state Departments of Transportation (DOTs), primarily focusing on the repair of impact damage to prestressed bridge girders (Shanafelt and Horn 1985; El Safty and Graef, 2012; Harris et al. 2012; Pino and Nanni 2015a; Ghaffary and Moustafa 2020, among others). Notable studies regarding the behavior of prestressed girders under impact damage have been conducted by Rizkalla et al. (2011), Xu et al. (2013), Nguyen and Brilakis. (2016), and Oppong et al. (2021), which include extensive finite element modeling and laboratory analyses. To evaluate and determine suitable repair options, several recommendations have been proposed, including assessing the prestressed tendon stress levels at various sections (Tabatabai et al. 2019) and utilizing an evaluation table (Table 1.1) that categorizes damage levels (Das et al. 2022). Nevertheless, there is a notable lack of specific literature addressing impact damage on prestressed girder bridges during construction – highlighting a critical gap in the current research.

Table 1.1. Damage Classification (Das et al., 2022)

Damage Classification	SEVERE I	SEVERE II	SEVERE III	SEVERE IV
Repair philosophy	Preventing further deterioration	ULS only	ULS and SLS	-
Action	Not required	Non post- or pre-tensioned repair	Post- or pre-tensioned repair	Replace
Live load capacity replacement	-	Up to 5%	Up to 30%	100%
Ultimate load capacity replacement	-	Up to 8%	Up to 15%	100%
Replace lost strands	< 5% strand loss	2-3 strands (>5%)	Up to 8 strands (>20%)	>8 strands (>35%)
Vertical deflection (camber)	Partial loss of camber	Complete loss of camber	Up to 0.5% of span	>0.5% of span

Literature regarding the inspection of prestressed concrete bridge girders was surveyed as part of the research effort. Several reports proposed qualitative rankings of damage severity. For instance, ABC-UTC (2020) introduced a five-level damage severity classification. Table 1.2 describes this damage classification to aid in determining repair strategies. Tabatabai et al. (2019) elaborated on these five levels, categorizing them as Minor, Moderate, Significant, Serious, and Severe, and provided additional qualitative metrics for assessing crack widths and the percentage of severed strands. For an automatable assessment process, a flowchart or algorithm is typically required, such as one suggested by Feldman et al. (1996). However, Feldman's algorithm lacks comprehensiveness as it does not take into account minor and moderate damage scenarios. Harries et al. (2012) conducted a thorough review of collision damage and repair strategies for concrete girders. Their report includes a decision flowchart for the repair versus replacement of prestressed I girders, addressing damage classifications from minor to severe, as well as a table estimating the number of strands that could be replaced with CFRP in typical sections.

Table 1.2. Damage Classification (ABC-UTC, 2020)

Damage Classification				
Minor	Moderate	Severe		
		I	II	III
Damage does not affect member capacity	Damage does not affect member capacity	Requires structural repair	Requires structural repair	Damage is too expensive to repair
Repairs are for aesthetic or preventative purposes	Repair is done to prevent further deterioration	Repair is done to restore ultimate limit state	Repair is done to restore both the ultimate limit state and the service limit state	The member must be replaced

In his influential work, Scheer (2010) identified that bridge failures often result from operators' failure to monitor the loading height. Notably, none of the 19 reported bridge failures referenced were associated with incidents during construction. Dunne et al. (2020) conducted a thorough review of state responses to collision impacts on bridge structures, revealing that between 2013 and 2018, there were between 13,000 and 18,000 collisions with bridges. Various states have published studies on the repair of impacted bridges, including research by Feldman et al. (1998), Erki and Meier (1999), Schiebel et al. (2001), Nanni (2001), Nanni et al. (2004), Miller (2006), Kim et al. (2008), Pantelides et al. (2010), Rizkalla et al. (2011), Kasan (2012), Kasan et al. (2012), Aimi and Sennah (2013), Cerullo et al. (2013), Gangi (2015), Gangi et al. (2018), Jones (2015), Cai and Xia (2015), Pino and Nanni (2015b), and Pino et al. (2017). The earliest studies on this topic were published in the early 1980s (Shanafelt and Horn, 1980). The most extensive research on the repair of collision-damaged prestressed girder bridges can be found in the works of Harries et al. (2009, 2012a, and 2012b). Harries et al. (2012a) presented a comprehensive flowchart to aid in decision-making for determining bridge repair strategies. Additionally, Ghaffary and Moustafa (2020) compiled an extensive list of damaged bridges from various states, though without clarification regarding whether the damage occurred during construction. While many studies concentrated on mid-section damage to girders, Pantelides et al. (2010), Hasenkamp et al. (2012), and Andrawes et al. (2018) specifically examined damage at the ends of girders. This focus is critical, as impacts may result in lateral displacement of girders, leading to damage at their ends.

1.2.3 Experimental research

Experimental testing of prestressed concrete bridge girders under lateral impact has been extremely limited, presumably due to the cost and logistical challenges associated with impact testing of girders under controlled conditions representative of overheight vehicular collisions. The only full-scale experiment known to the authors was conducted by Jing et al. (2016) uaing a single AASHTO Type I section with a narrow portion of composite slab that was subjected to a lateral impact to the bottom flange from an essentially rigid impactor with a 10 inch square steel plated head. Based on high-speed video observations, the authors described the failure of the girder occurring through the development of a diagonal cracks in the bottom flange of the girder adjacent to the supports, followed by a horizontal crack along the intersection of the bottom flange and web through the majority of the span, spalling of concrete from the bottom flange, and, ultimately, flexural failure about the major axis of the section characterized by the formation of a hinge at the midspan and large upward displacement. While the study provided this valuable direct observation of the response of a prestressed girder to lateral impact, several limitations of the published test program render the use of this case study for validation of numerical models challenging. First, the girder specimen had previously been subjected to a static load test resulting in shear failure and, although the girder was configured with a reduced span to exclude the damaged ends, the extent of damage, including visible section loss, or any prestress loss within the tested span from the prior static load test was not characterized. Additionally, the majority of the instrumentation failed to produce useful data, limiting the measurement of the girder response to only the vertical displacement at the midspan, strain adjacent to one support, and a sequence of still images of the girder response from a high-speed video recording (Jing, 2017). Lastly, it is notable that the type of failure observed in this experimental test program is not typical of those reported following overheight vehicle collisions to actual prestressed concrete girder bridges. The distinct mode of failure observed in this case study can be attributed to the nature of the experimental setup. Since the specimen was a single girder with only a narrow portion of composite slab representing the deck, the girder responded to the impact loading independently rather than interacting with the rest of the superstructure

components, as would occur in a complete bridge. Furthermore, the girder was configured with supports near the first and third quarterpoints rather than the ends, which produced a very short span of only 26 ft and significant negative flexural moments due to the nearly 15 ft long cantilever regions at each end created by the support locations.

Recently, a laboratory study was conducted to observe the effect of the presence of a bridge deck on the impact response of scale-model prestressed concrete bridge girders (ElGawady and Abdulazeez, 2024). This study provides additional insight into the different failure mechanisms that may be observed when a prestressed concrete girder is subjected to lateral impact as an isolated member, which may be the case for overheight collisions occurring during construction, or as a member of a complete superstructure, which would be the case for collisions occurring during service. In the study, two nominally identical girders were examined, with one of the girders tested as an isolated member and the other with a cast-in-place tributary section of composite deck slab. The girders were doubly symmetric I-shaped sections containing two prestressing strands, with a 12-inch total depth, 6-inch wide by 3-inch deep flanges, and a 3-inch wide web. The slab cast on the second specimen was 4-inch thick and 30-inch wide. A 660 lb rigid impactor with a steel plate at the contact interface. The impact force was measured using a load cell and the girder response was measured with an array of accelerometers, string potentiometers, and strain gauges. Despite subjecting each girder to the same impactor mass traveling at the same velocity, the peak force measured during impact to the girder featuring a portion of deck slab was approximately twice that developed for the impact to the isolated girder and the maximum lateral displacement at the midspan was one-fifth of that measured for the isolated girder. While these differences are indicative of the expectedly stiffer response of the girder with the connected portion of slab, the observed failure mechanisms were also significantly influenced by the presence of the deck slab. Figure 1.3 provides a depiction of the spalling and cracking across the specimens, approximated based on photographs provided within the referenced report. Damage in the isolated girder was characterized by localized spalling at the impact, visible flexure-shear cracks throughout the entire cross section and along a significant portion of the span on the impacted side of the girder, and significant localized shear cracks visible on the rear side of the girder. The authors of the report described the initiation of the failure as a localized punching shear mode of failure, as evidenced by the shear cracks on the rear side of the girder, followed by biaxial flexural failure with hinging about the damage region leading to significant residual deflection in both the lateral and vertical directions. In contrast, the girder with the portion of deck slab was reported to exhibit localized failure characterized by extensive spalling and predominantly shear cracks that were concentrated primarily within the girder web. The authors specifically noted the absence of damage to the top flange of the girder, which was attributed to the restraint provided by the attached portion of deck slab.

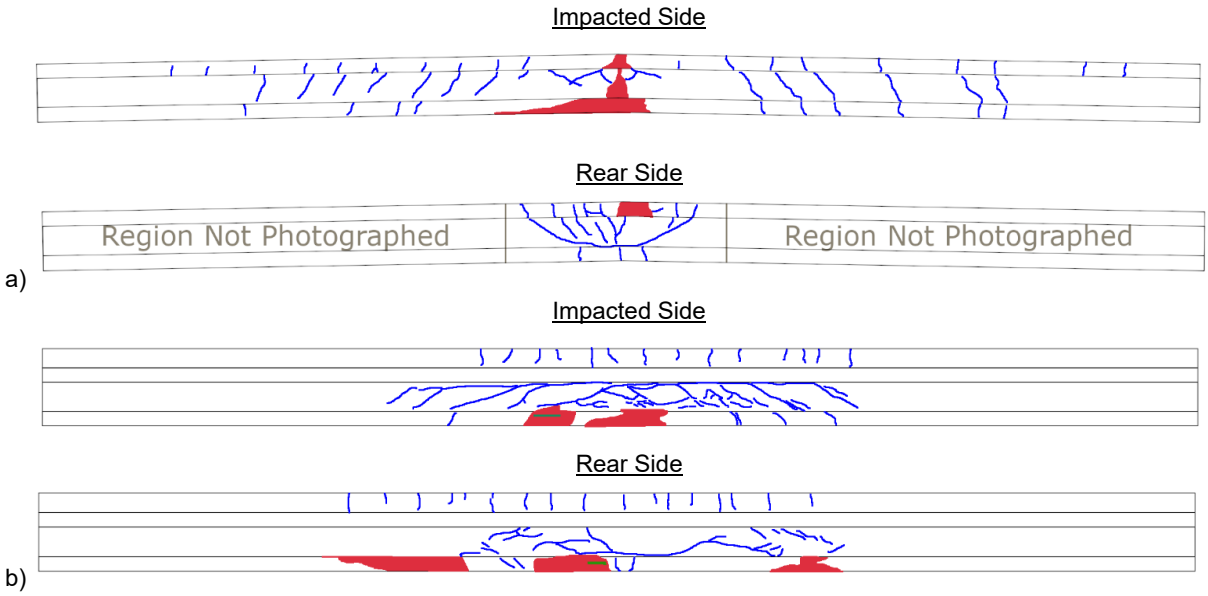

Figure 1.3. Depiction of observable damage in girder specimens reported in ElGawady and Abdulazeez (2024): a) isolated girder; b) girder with portion of deck slab

1.2.4 Numerical research

Due to the logistical challenges, risks, and significant costs associated with full-scale experimental impact testing of prestressed concrete girders, particularly given the necessity to either test a complete superstructure or realistically simulate the restraint provided by the bridge deck, diaphragms, and adjacent girders, much of the research on the behavior of bridges with prestressed concrete girders subjected to lateral impact has been performed using numerical simulation. Early numerical modeling efforts focused largely on the role of intermediate diaphragms on the resistance of bridges to lateral loads (Abendroh et al. 1995; Qiao et al. 2008). However, due to the technological limitations of the time of these studies, they were performed using coarse meshes, simplified constitutive models, idealized boundary conditions, reduced models, neglect of strain rate effects, and simplified modeling of the collision using prescribed force time histories rather than explicit modeling of contact with an impactor. A critical review of this earlier research recommended the pursuit of high-fidelity modeling to address the computational limitations (Cai et al. 2007).

Recently, several studies have utilized high-fidelity finite element analysis with advanced constitutive models to investigate the response of prestressed concrete girder bridges to overheight vehicle impacts. Xu et al. (2013) investigated damage mechanisms in prestressed concrete girder bridges by explicitly modeling the collision using finite element models of container, tipper, and tank trucks. The authors also presented a simplified model to predict the impact forces without requiring the use of a high-fidelity model of the vehicle. Oppong et al. (2021) predicted impact force characteristics associated with overheight impact from several objects by simulating collisions using finite element analysis. Specifically, the study included models of a hollow concrete pipe, a cylindrical steel tank with closed ends, a PVC pipe, a wooden box container, and a tractor trailer, all of which were modeled with nonlinear material models. Two bridge girder models were used, one with an AASHTO Type I girder and one with an AASHTO Type IV girder.

However, the girders were modeled as having only mild reinforcement and therefore were not modeled as prestressed concrete girders. The complete superstructure was not explicitly modeled, instead the nodes of the model along the top surface of the girder were restrained against translation in all directions to approximate the restraint provided by the bridge deck. The primary results discussed in the paper were developed with a 40 ft span length and translational restraint of all nodes at the girder ends to simulate an integral abutment, however the authors noted that span length and support boundary conditions were found to have little influence on the peak impact force and impulse. The steel tank model produced the largest peak and mean impact forces, followed by the concrete pipe, and consequently the most significant prediction of damage in the girder. The tractor trailer model introduced significantly lower impact forces on the girder and, likewise, lateral displacements an order of magnitude lower than those developed with the steel tank for each girder type. Empirical models to predict the peak and mean impact forces for concrete pipes and steel tanks were developed by performing nonlinear regression on databases of 24 simulations conducted for each object with different variations of diameter, wall thickness, and contact area. The study found that greater peak and mean impact forces developed on Type IV girders compared to Type I girders subject to impact from the same objects travelling at the same velocity. This was attributed by the authors to be a result of greater stiffness of the Type IV girder, however the empirical models were able to account for differences in girder type by accounting for the contact area, which differs between the two girders as a result of differences in the depth of the bottom flange. Collectively, the results from this paper suggest that differences in contact stiffness arising from bridge characteristics and location of impact produce only minor variations in the general characteristics of impact force time histories associated with overheight impacts from construction objects and vehicles. This result supports the development of empirical prediction models for representative construction vehicles to alleviate the need for computationally expensive simulation of impact using high-fidelity models of the vehicle.

ElGawady et al. (2024) used LS-DYNA to perform a limited parametric analysis of factors influencing the response of prestressed concrete girder bridges subject to overheight collisions from tractor-semitrailers. The study used the National Transportation Research Center (NTRCI) tractor-semitrailer model and the parametric analysis consisted of eight simulations with different girder types, truck speeds, and truck mass. As a component of the study, the authors compared simulation results obtained with a model of an entire 50 ft bridge span with six Missouri DOT Type II girders to those obtained with a reduced model featuring only a single girder and portion of bridge deck with a fixed boundary condition introduced along the edge of the deck to approximate the stiffness provided by the rest of the superstructure. The peak impact force was moderately higher and the contact duration and associated impulse were significantly greater for the full bridge model than for the simplified model. Furthermore, lower severity of damage was predicted when the full bridge superstructure was modeled, suggesting that the idealized restraint used to represent the contribution of the remaining superstructure to the response of the impacted girder was unrealistically stiff in the simplified model. Despite the noted differences, simplified single girder models were used to perform the parametric analysis due to the advantage offered by reduced computational cost.

Elshazli et al. (2025) investigated the behavior of prestressed concrete girder bridges under lateral impacts using high-fidelity finite element models developed in LS-DYNA. Specifically, the study used a numerical model of a 45 ft bridge span with three Missouri DOT Type II girders supporting an 8-inch thick reinforced concrete deck. In the study, a simplified rigid impactor model in the shape of a solid cylinder 3.2 ft in diameter and 3.9 ft in length was used. Due to the size and rigidity of the impactor, the majority of the

simulations presented resulted in prediction of significant damage to the impacted girder, even at lower initial impact velocities. The authors highlighted a transition from a global deformation response of the girder at low initial impact velocities to a localized failure mode as the impactor velocity increased. This observation is expected due to increased inertial forces and has been demonstrated in drop height impact testing of reinforced concrete beam specimens (Saati and Vecchio, 2009). A limited parametric analysis was also presented in the study to highlight the ability of intermediate diaphragms to reduce lateral displacement of the girder under lateral impact. Predicted displacement time histories presented in the paper suggest that girders with reinforced concrete intermediate diaphragms exhibit significantly less lateral displacement than those with steel channel intermediate diaphragms, but indicated that the reinforced concrete intermediate diaphragms may crack if impacts occur at highway speeds.

1.3 Identified Research Gaps

While recent studies have demonstrated the ability of high-fidelity finite element analysis to produce plausible predictions of the damage developed within prestressed concrete bridge girders when subject to lateral impact, the literature review identified several gaps needing to be addressed.

1. Foremost, bridge engineers are unlikely to perform high-fidelity finite element analysis in parallel with visual inspection to assess bridge condition after overheight vehicle collisions, so a simplified surrogate to case-specific finite element analysis is needed. Although some parametric analysis has been performed in recent studies, the influence of bridge characteristics and impactor characteristics on the response of prestressed concrete girders to lateral impacts has not been fully addressed. Consequently, a basis for simplified modeling of the problem is lacking.
2. Numerical research conducted to-date has relied on only rigid impactor models, pipe and tank models, and a tractor-semitrailer model. The development of finite element models of dump trucks with raised beds and excavators on flatbed trailers is needed to simulate the vehicles most frequently involved in overheight vehicle collisions. Prediction models are also needed to estimate key impact force characteristics for these vehicles.
3. Research on damage to prestressed concrete girder bridges from overheight vehicles has focused nearly exclusively on fully constructed, in-service bridges. The performance of prestressed concrete bridge girders during construction has not been studied.
4. The role of intermediate diaphragms and the effect of intermediate diaphragm material and design on the resistance of prestressed concrete bridge girders to impact damage received significant attention in the late 1990's and early 2000's (Andrawes, 2001; Abendroth et al. 2004; Qiao et al. 2008). However, the limited experimentation supporting this research was based on static load testing (Abendroth et al. 1995) and, as discussed in the prior section, numerical studies on this topic were hindered by computational limitations imposed by the technology available at the time. Furthermore, the effect of the presence and type of intermediate diaphragm has only been studied for fully constructed bridges.

2. HIGH-FIDELITY FINITE ELEMENT MODELING OF BRIDGES

One of the products of this research effort is the development of an extensive library of verified scripts to automatically generate high-fidelity finite element models of highway bridges with prestressed concrete girders. This library, referred to herein as the Collision Analysis Engine (CAE), enables the expedited development of detailed finite element models of complete bridge superstructures based on encoding a set of geometric dimensions and material properties that can be readily populated from bridge plans into a defined database structure. The CAE then reads this database structure and, without further manual intervention, generates all files necessary to initialize the finite element model and prepare simulations for collision analysis. The models generated by the CAE are highly detailed and include all girders, internal reinforcement, diaphragms, deck, sole plates, and utilize elastic boundary conditions to simulate the behavior of elastomeric bearings. Figure 2.1 depicts the workflow of the developed CAE. Figure 2.2 provides a wireframe rendering of a representative bridge model where the components included in the model are identified. Additional information on the elements, connectivity, meshing, constitutive models, and initialization of the models performed with the CAE is provided in this section of the report as well as in Samadzad et al. (2024).

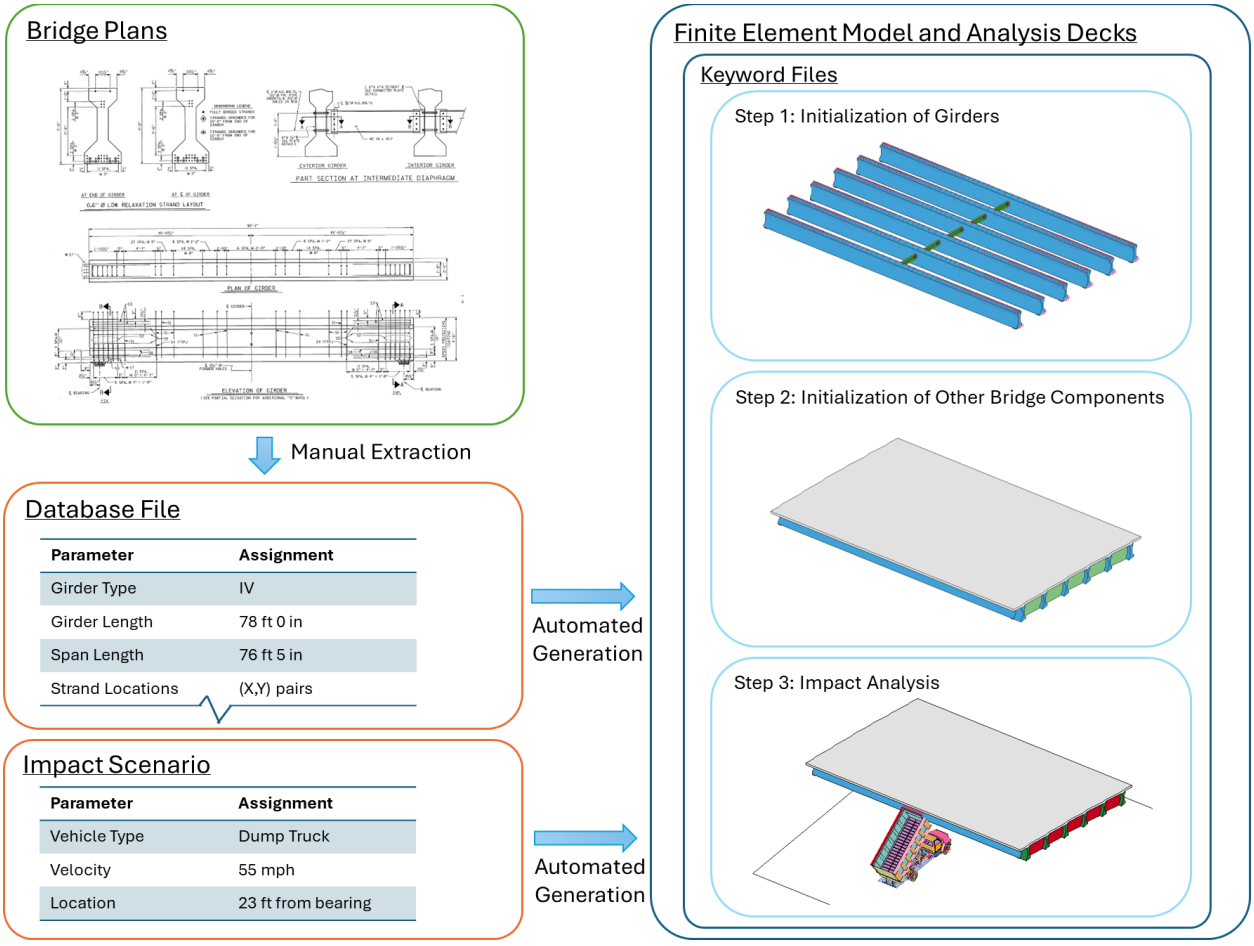

Figure 2.1. Schematic of developed Collision Analysis Engine (CAE)

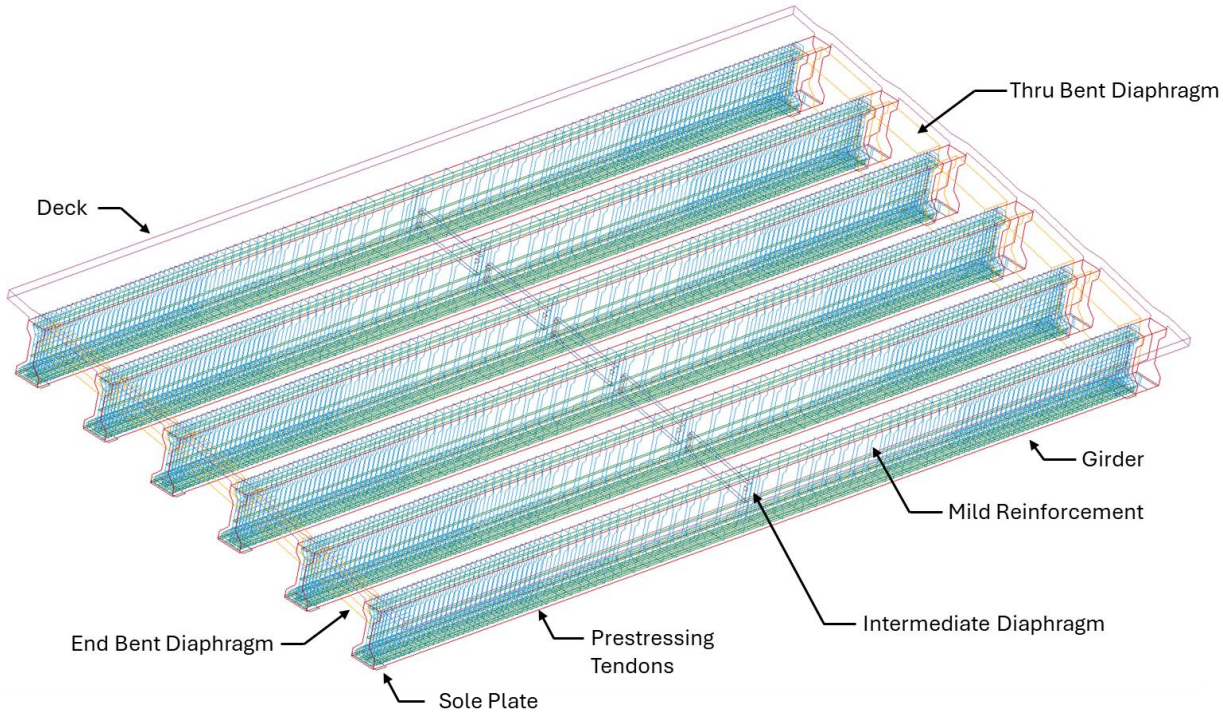

Figure 2.2. Wireframe rendering of a representative finite element model of a bridge span

Automated model generation can facilitate the rapid simulation of actual overheight collision incidents to provide physics-based insight into potential failure mechanisms and severity of internal damage that are not always readily ascertained by visual inspection. Furthermore, the automated model generation enabled the research conducted as part of this project to encompass a larger number of bridge models and impact scenarios than feasible if manual preparation of models was required, while also ensuring consistency in the modeling and assignment of critical material and contact parameters across the set of FE models, which is challenging when models are developed manually. The CAE was developed to generate keyword files for LS-DYNA, an advanced multi-physics finite element analysis solver. Version R15.0.2 in the shared memory processing (SMP) mode was used to conduct all of the numerical analyses contained in this final report. High Performance Computing (HPC) resources at UNC Charlotte were leveraged to expedite the simulations through parallel processing.

2.1. Elements and Connectivity

The CAE develops a high-fidelity three-dimensional finite element model of complete bridge superstructures to facilitate the simulation of collisions of representative overheight vehicles with bridge girders using advanced contact models. Constant stress hexahedral solid elements are used to model the concrete in the girders and bridge deck. The CAE accepts the skew angle and grade of the deck as inputs and automatically adjusts the girder positions and elevations to correctly model the geometry of the superstructure. The mesh for the girders is created by replicating a planar mesh at uniform increments along the length of the girder to produce a structured 3D mesh with aspect ratios close to unity and minimal distortion. A database of planar meshes for standard girder cross sections, including AASHTO, Modified Bulb-Tee, and Florida I-Beam (FIB) sections, was developed by the research team using HyperMesh to ensure high element quality while constraining the minimum edge size to prevent a small number of

elements from establishing an unnecessarily small required time step. Based on a convergence study, a maximum mesh edge size of 2 in was used in the generation of bridge models presented in this report, which was found to produce a reasonable balance between accuracy and computational time. The haunch is included in the model of the deck and connects the deck to the girders using shared nodes. Reinforced concrete end and thru bent diaphragms are likewise modeled with constant stress hexahedral elements and connected to the girders by merging nodes from the diaphragms to the girders and deck to create shared nodes. Merging of nodes in end diaphragms with the girders to introduce shared nodes for continuous, or monolithic, behavior between these components was performed in Elshazli et al. (2025). Figure 2.3 presents renderings of portions of a finite element model of a bridge with AASHTO Type IV girders generated by the CAE, where the discretization of the girders, deck, and bent diaphragms is visible. The sole plates at the girder bearing locations are modeled with shell elements. The inclusion of the sole plates in the model allows for the ability to prescribe boundary conditions at the locations of anchor bolts as well as introduces rotational degrees of freedom at the boundary that are not otherwise available when constant stress hexahedral solids are used to model the girder. This allows for the modeling of both the translational and rotational behavior of the elastomeric bearings using elastic springs, which is described in the "Initialization of Models" section. The shells representing the sole plates are connected to the solid elements of the girder using shared nodes.

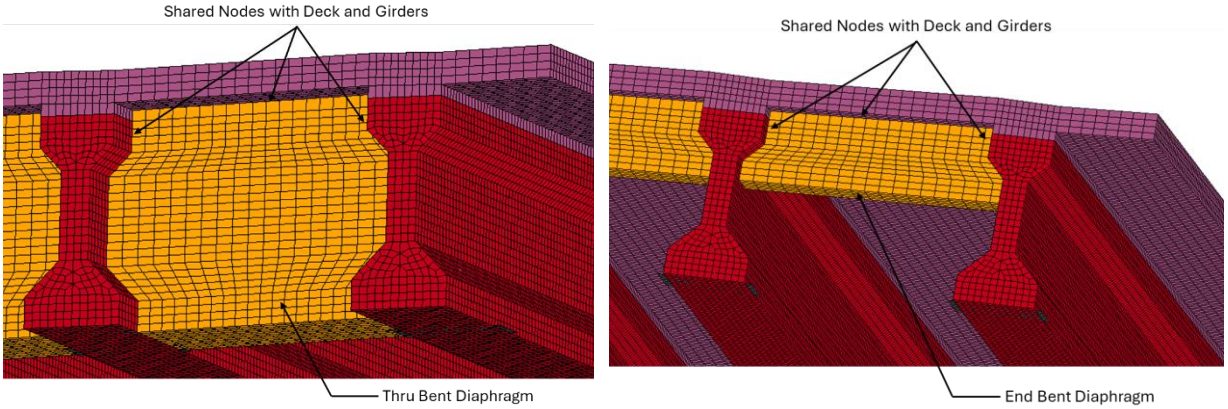

Figure 2.3. Representative meshing of the girders, deck, and bent diaphragms

The prestressing tendons were modeled using truss elements, while mild reinforcement was modeled with Hughes-Liu beam elements to ensure stability of any shear reinforcement that is not fully embedded in the concrete prior to the introduction of the deck. To simulate the bond between the internal reinforcement and the concrete, the constrained beam in solid constraint was used to couple the nodes of the respective elements. The approach assumes a perfect bond between the reinforcement and concrete, which is generally assumed valid for the impact response of reinforced concrete since the bond strength and development length have been experimentally observed to be significantly enhanced under higher strain rate loading (Weathersby, 2003).

The developed CAE provides capabilities to automatically generate intermediate diaphragms of the following types: steel channel, steel K-brace, and reinforced concrete. Steel channel diaphragms are modeled with 4-node Belytschko-Tsay shell elements, based on the depth of the channel, web thickness, flange width, and flange thickness. The Belytschko-Tsay shell includes membrane, bending, and shear response. Similarly, the angles connecting the steel channel to the girders are modeled with 4-node

Belytschko-Tsay shell elements. Tied surface-to-surface constraints are used to connect elements in the web of the channel to those in contact with elements defining the angles. Spot weld constraints are used to tie two nodes from the opposite leg of the angle to the girder. These spot weld constraints are intended to model the bolted connection of the angle to the girder. In addition, automatic surface-to-surface contacts are defined along this interface to model compression-only normal forces resulting from direct contact of the angle with the girder. Friction is defined along this interface using a static coefficient of 0.57 and dynamic coefficient of 0.456, which are consistent with experimental measurements of static friction between steel and dry concrete surfaces (Rabbat and Russell, 1985). Figure 2.4 provides a rendering of a representative steel channel intermediate diaphragm with the location of the spot weld constraints indicated. In related studies, steel channel diaphragms have been modeled with shell elements and the connectivity between diaphragms and connecting angles, as well as between connecting angles and girders, has been idealized as continuous using techniques such as shared or merged nodes (Elshazli et al., 2025). The use of a combination of spot welds at the location of bolts and automatic surface-to-surface contact at the girder interface is expected to improve the fidelity of the model by allowing for slip and eliminating the potential for any tensile forces to develop across the interface where no bolt exists.

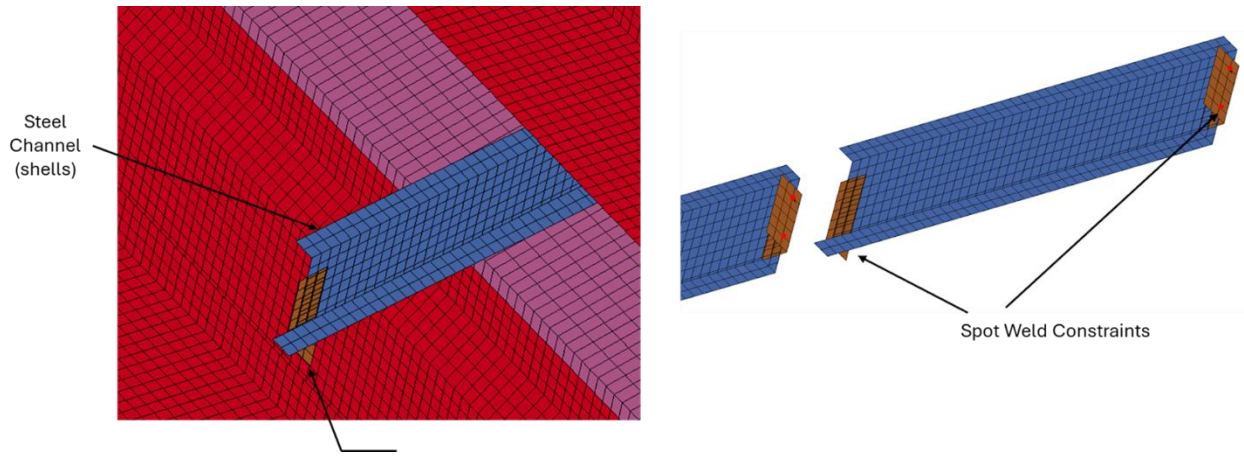

Figure 2.4. Modeling of steel channel intermediate diaphragms

Steel K-brace intermediate diaphragms are modeled similar to steel channel diaphragms, as shown in Figure 2.5, except that the bracing members are modeled with truss elements. Shared nodes are used to connect these elements to shell elements that model the angles connecting the diaphragm to the girder. As with the modeling of the steel channel diaphragm, the angle is connected to the girder with spot weld constraints at the location of bolts. An automatic surface-to-surface contact is also defined between the angle and the girder to model compression-only normal contact and friction using the same friction coefficients as prescribed for the steel channel diaphragm model.

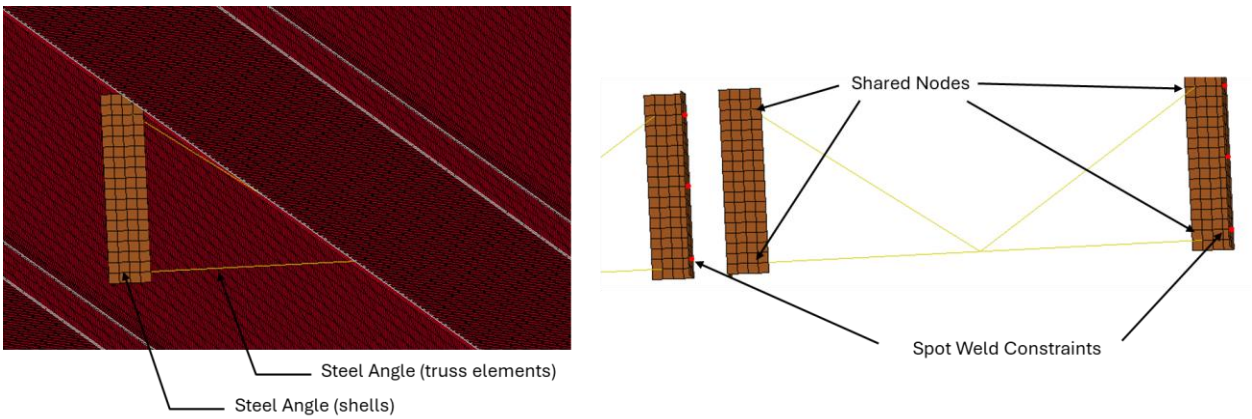

Figure 2.5. Modeling of steel K-brace intermediate diaphragms

Reinforced concrete intermediate diaphragms are modeled with constant stress hexahedral solid elements. The CAE constructs the mesh for the reinforced concrete diaphragm to follow the contour of the surface profile of the web of the girders, as shown in Figure 2.6. Reinforced concrete intermediate diaphragms are not cast monolithically with prestressed concrete girders, but rather supported by the girder through a combination of bearing and friction on the girder and a single tie rod passing through the diaphragm. To promote faithful replication of this interface, reinforced concrete intermediate diaphragms were modeled as separate parts with independent nodes from the girder along the contact interface. Automatic surface-to-surface contact is defined between the reinforced concrete intermediate diaphragms and the girders to enable compression-only normal forces along this interface. The frictional contact is also defined at this interface with a static coefficient of friction of 0.60 and dynamic coefficient of friction of 0.48. Since reinforced concrete diaphragms are secured to the girders with a tie rod that runs through hole in the midheight of the web, a spot weld constraint is included in the model to tie the node at the center of each end of the diaphragm to the corresponding node on the girder. Similar modeling of the interface between reinforced concrete diaphragms and girders was described in Andrawes (2001) and Abendroth et al. (2004).

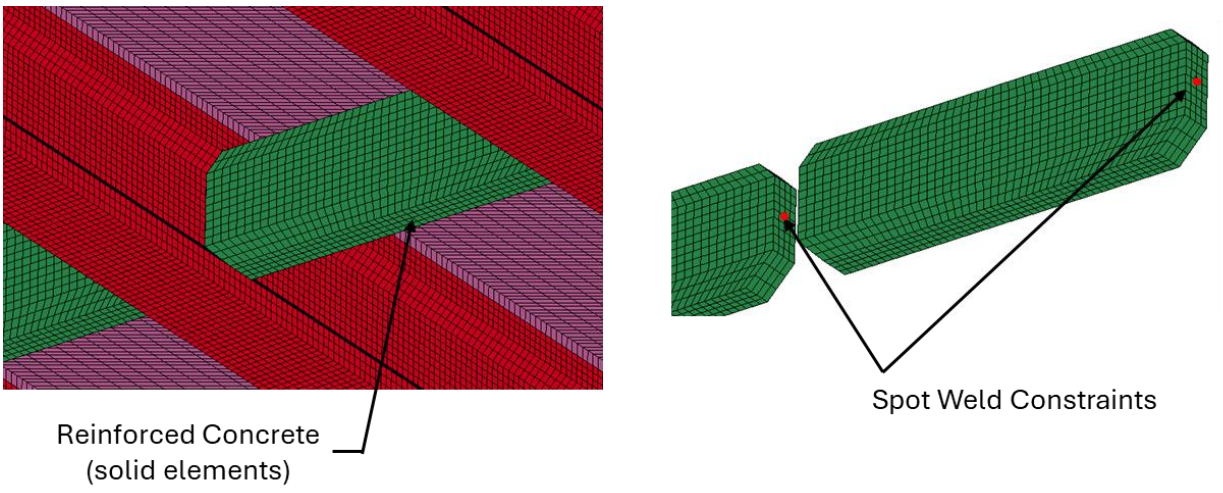

Figure 2.6. Modeling of reinforced concrete intermediate diaphragms

2.2. Initialization of Models

To accurately initialize the internal state of stress and initial camber in the complete bridge model, a staged development of the FE models that replicates aspects of the construction sequence is required. Since the bridge deck and bent diaphragms are placed or cast over prestressed girders that were previously prestressed and erected at the site, it is necessary to introduce the prestress force in a model that initially consists of the girders without the deck and bent diaphragms to ensure that the stress and camber in the model is accurately developed. The staged development of bridge models, which was accomplished using the full restart capability of LS-DYNA, is depicted in Figure 2.7. In this process, a complete bridge model is initialized in the first two steps. By leveraging the full restart capability, a finite element model of a specific bridge only needs to be initialized once. Multiple collision analyses (i.e., Step 3) can be performed on the initialized model by consistently restarting from the same d3dump file created at the conclusion of Step 2. This capability reduces the computational time associated with parametric analysis and ensures consistency in the model when parametric analysis is performed.

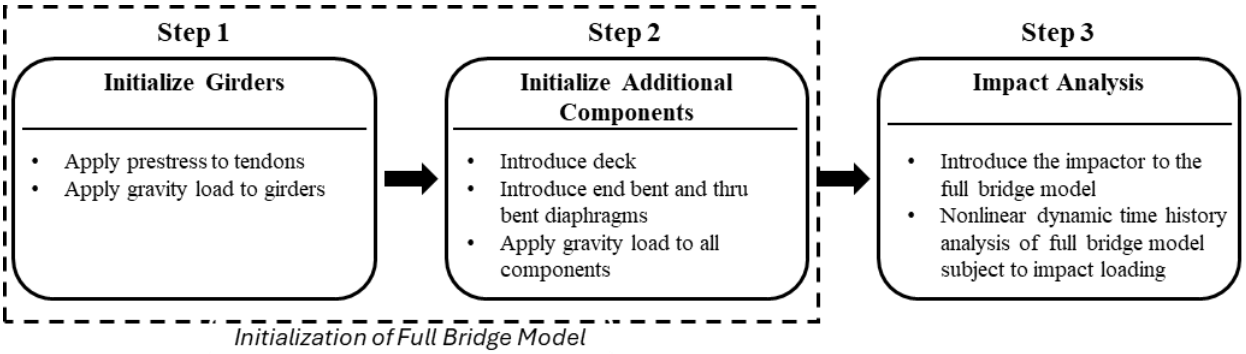

Figure 2.7. Staged development of bridge models to accurately replicate construction sequence and enable efficient parametric analysis

The prestressing forces in the model are introduced by applying an equivalent temperature-induced strain in the elements representing the prestressing tendons. This general approach was detailed in Jiang and Chorzepa (2015); however, the equation provided for the temperature change in this source does not account for elastic shortening. When elastic shortening is included in the strain compatibility, the temperature change, ΔT, associated with a desired prestress force, f, in the model is:

$$\Delta T = \frac{f}{\alpha}\left(\frac{1}{E_s A_s} + \frac{1}{E_c A_c} + \frac{e^2}{E_c I_c}\right) \qquad \text{(Eq. 2.1)}$$

where α is the temperature coefficient, E_s is the modulus of elasticity of the prestressing tendon, E_c is the modulus of elasticity of the concrete, A_s is the cross sectional area of the tendons, A_c is the cross sectional area of the concrete, I_c is the moment of inertia of the concrete, and e is the eccentricity of the strands. When using this approach, prestressing losses are first estimated, since the resulting prestress force introduced into the model equates to the desired prestress force. In other words, the analysis established by the CAE does not explicitly account for phenomena that lead to prestressing loss, aside from losses due to damage from the overheight vehicle impact. Gravity body forces are introduced simultaneously with the prestress. To avoid switching of the solver, the initialization of the models is performed through transient analysis with explicit time integration. The analysis extends over a multiple of the natural period of the fundamental major axis flexural mode of the girder and mass proportional damping is applied during the

initialization to suppress resonance of vibration modes during the introduction of the static loads. The mass proportional damping is removed from the model after the initialization so as to not influence the response of the bridge model during the simulation of overheight vehicle collisions.

During the application of prestressing and gravity loads, ideal pin and roller supports are prescribed to the node in the center of each sole plate, as shown in Figure 2.8(a). Following a full restart of the model, these idealized boundary conditions are removed from the model and replaced with linear elastic translational and rotational springs to approximate the behavior of the elastomeric bearings, as shown in Figure 2.8(b). These springs are introduced by applying the linear elastic discrete beam material model to zero-length beam elements connected between the node in the center of each sole plate and a ground node. The spring stiffnesses are calculated for compressive, shear, flexural, and torsional behavior of the steel-reinforced elastomeric bearings using guidance provided in AASHTO LRFD Bridge Design Specifications (2012). Whelan and Janoyan (2011) provided empirical evidence that the dynamic response of bridge superstructures supported by steel-reinforced elastomeric bearings can be accurately predicted with the use of such translational and rotational elastic springs.

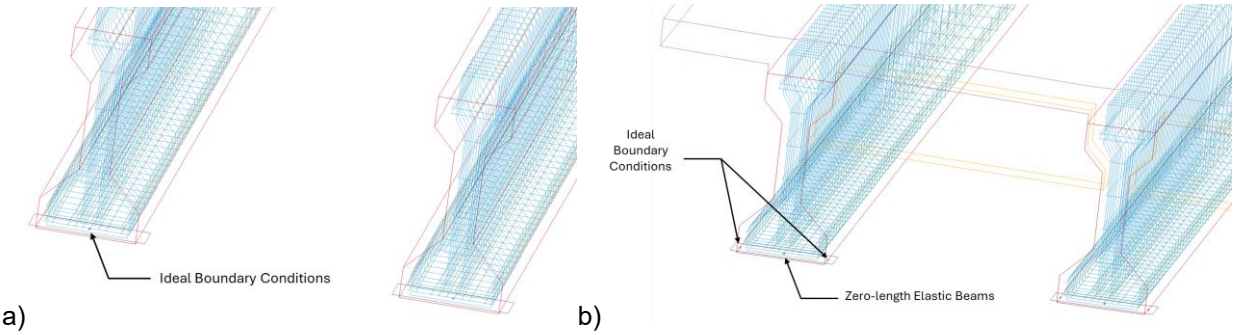

Figure 2.8. Boundary conditions applied to sole plates: a) during introduction of prestress force; b) during simulation of overheight vehicle collision

2.3. Constitutive Models

LS-DYNA offers an extensive library of advanced constitutive models capable of simulating the behavior of a wide variety of structural and non-structural materials. The choice of constitutive models adopted for different components of the bridge model was driven by a need to balance the fidelity of the model with the computational requirements. Since the concrete in the girders is subject to direct contact with the overheight vehicle and exhibits extensive fracture and spalling, significant attention was directed toward selection of the most suitable advanced constitutive model for the concrete. A comprehensive evaluation of available concrete constitutive models was performed as part of this research and is summarized at the end of this subsection of the report.

The nonlinear and strain-rate sensitive response of steel reinforcement was modeled using a bilinear elastic-plastic constitutive model with hardening (MAT_PLASTIC_KINEMATIC). For the prestressing tendons, an elastic modulus of 29000 ksi, yield stress of 256.5 ksi, and tangent modulus after yield of 124.7 ksi were assigned. To allow for the simulation of rupture, a failure strain of 0.057 in/in was prescribed, which enables erosion of elements from the model when strains exceed this threshold. For the reinforcing steel, a similar bilinear elastic-plastic constitutive model with hardening was used, except the yield stress was prescribed as 60 ksi, the tangent modulus after yielding was set to 217.6 ksi and the failure strain was set

to 0.20 in/in. For any steel intermediate diaphragms, a yield stress, tangent modulus after yielding, and failure strain of 50 ksi, 217.6 ksi, and 0.20 in/in, respectively, were prescribed. To account for strain rate effects on the yield stress of all steel components, the Cowper and Symonds model was implemented with parameters $C = 40.4$ and $p = 5.0$. The assignment of these parameters was based on empirical results presented in Cowper and Symonds (1957).

None of the incidents reviewed by the research team, either sourced from the literature, NCDOT supplemental inspection reports, or site investigations, indicated any damage to the bridge deck following collision of overheight vehicles with prestressed concrete girders (aside from cases involving collapse). Consequently, the elements associated with the deck were assigned a linear elastic constitutive model for computational efficiency. Likewise, the end bent and thru bent diaphragms and sole plates at the bearing locations were assigned linear elastic material properties consistent with concrete and steel, respectively.

The capabilities of available concrete constitutive models were reviewed to identify those within LS-DYNA that are both suitable for simulating responses at high strain rates and offer either automatic parameter generation or initialization with a minimal set of mechanical properties that can be readily estimated from the compressive strength. Five constitutive models were identified: Continuous Surface Cap Model (CSCM); Karagozian-Case Concrete Model (KCC); Riedel-Hiermaier-Thoma (RHT), Concrete Damage Plasticity Model (CDPM); and Winfrith concrete model. Each of these constitutive models differs in theoretical foundation, replication of phenomenological behaviors under different types of loading, and empirical calibration of settings when automatic parameter generation is employed. Subsets of these constitutive models have been previously evaluated for their ability to accurately predict the behavior of reinforced concrete under impact loading (Saini and Shafei, 2019), but the comparisons to experimental data presented in these studies have been limited to a single beam specimen. Furthermore, no comparison of the ability of these constitutive models to simulate post-impact response of damaged reinforced concrete to subsequent static loading was identified in the existing literature.

To address these gaps in the current knowledgebase and inform the selection of an appropriate constitutive model for the CAE, a comprehensive evaluation of these five concrete constitutive models was performed using a set of experimental drop weight impact tests encompassing a range of different span-to-depth, longitudinal reinforcement, and transverse reinforcement ratios published in Adhikary (2014) as well as an extensively studied experimental benchmark in Fujikake et al. (2009). In both of these studies, instrumented simply supported beam specimens were subject to midspan impact from a mass dropped from fixed elevations. The Adhikary (2014) test program additionally provided experimental measurement of the residual capacity of the damaged specimens through three-point bending static load tests performed after each impact. The dimensions and reinforcement details for all of the beam specimens included in the comparison are presented in Figure 2.9. The beam specimens in the Adhikary (2014) study were each subjected to impact loading from a 660 lb impactor dropped from three different elevations, while the beams in the S1616 set of the Fujikake et al. (2009) study were subject to impact loading from 880 lb impactor dropped from heights of 5.9 in, 11.8 in, 23.6 in, and 47.2 in. All of the specimens were conventional reinforced concrete beams. A literature review was conducted to identify published data for impact response of prestressed concrete beams, but this review largely identified a few case studies of isolated tests of single prestressed beams with insufficient detail to sufficiently model the experiments. The few experimental studies that included a range of prestressed concrete beam specimens subject to multiple

impact intensities were performed using model-scale beams (Hughes and Mahmood, 1984; Chan, 1986), which would be unsuitable for evaluating the performance of the available concrete constitutive models due to issues associated with scaling effects and automatic parameter generation for microconcretes. The beams in Adhikary (2014) study were cast with normal weight concrete with a compressive strength of 5570 psi and a maximum aggregate size of 0.4 inch, while the concrete used in the beam specimen from the Fujikake et al. (2009) had a reported compressive strength of 6092 psi and a maximum aggregate size of 0.4 inch. All of the specimens are flexure-controlled, but the ratio of the shear-to-flexural resistance varied significantly across the specimens. The shear-to-flexural resistance ratio for the DR5.7-1.6-0.15 specimen was 1.19, for DR5.7-1.6-0.20 was 1.33, for DR3.8-0.8-0.11 was 1.38, for DR3.8-0.8-0.15 was 1.51, and for the S1616 specimen was 2.55. This is significant because reinforced concrete beams that are flexure controlled can fail in shear under impact loading (Saatci and Vecchio, 2009), especially if the shear-to-flexural resistance ratio to static loading is close to unity. The likelihood of shear failure is also more significant as the impact velocity increases, with higher velocity impacts typically tending to result in the formation of a local shear plug.

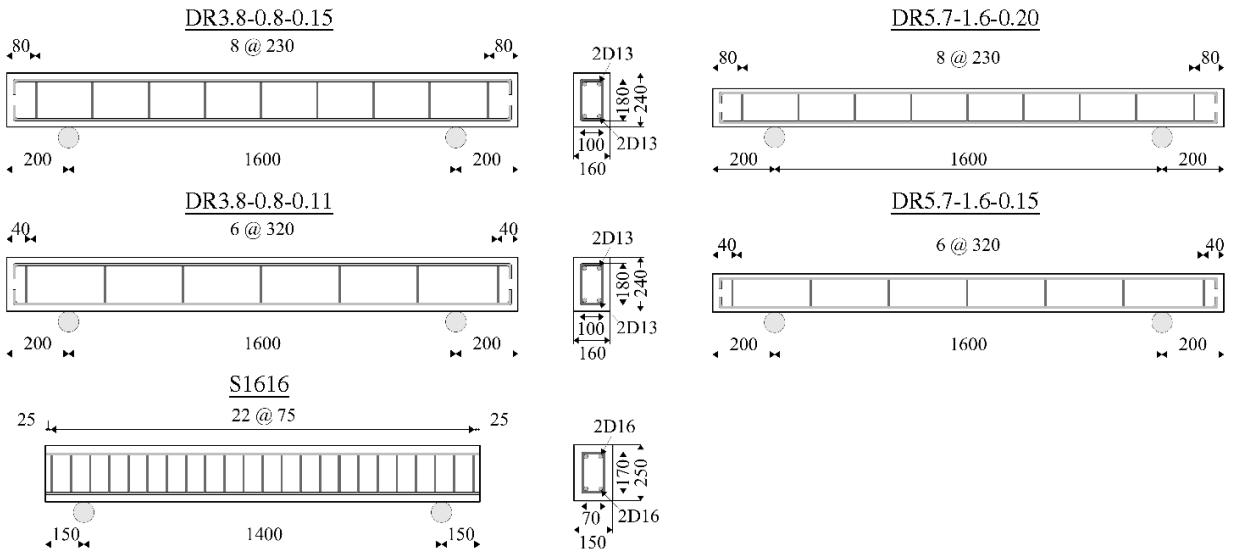

Figure 2.9. Dimensions and details for reinforced concrete beams subject to impact loading in Adhikary (2014) and Fujikake (2009) and included in model comparisons (all dimensions provided in mm units)

Finite element models were developed for all five of the beam specimens and analyses were conducted for all drop heights for each series (a total of 16 different combinations of beam specimen and impact intensity) using the explicit solver of LS-DYNA with all simulations performed using release 13.0.0. The beam specimens were modeled consistent with the modeling techniques previously described for the modeling bridge girders within the CAE (i.e. constant stress hexahedral solid elements for the concrete and Hughes-Liu beam elements for the internal reinforcement with a beam-in-solid constraint used to enforce connectivity of these beam elements representing the reinforcement to the solid elements representing the concrete). Likewise, the same strain-rate enhancement models were utilized. Based on a mesh convergence study and consistent with prior studies (Saini and Shafei, 2019), a uniform edge size of 0.4 in (10 mm) was used to mesh the concrete in the S1616 beam specimen, which corresponds to 25 rows of elements through the depth of the beam. To maintain consistent discretization, an element size of 0.38 in x 0.39 in x 0.39 in

(9.6 mm x 10 mm x 10 mm) was used to model the DR3.8-0.8-0.11 and DR3.8-0.8-0.15 beam specimens and an element size of 0.27 in x 0.30 in x 0.29 in (6.8 mm x 7.5 mm x 7.27 mm) was used to model the DR5.7-1.6-0.15 and DR5.7-1.6-0.20 beam specimens. Figure 2.10 presents a rendering of the finite element model developed for the DR3.8-0.8-0.11 beam, where the solid elements representing the concrete are hidden across one half of the beam length to permit visualization of the internal reinforcement. In this figure, the model is shown for both stages of analysis: the transient analysis of the beam response to impact from dropped spherical mass, and static analysis of the beam residual capacity following the simulation of the impact. The impactor and cylindrical supports were modeled with constant stress hexahedral elements and both parts were assigned a rigid material model. Similarly, for the analysis of the residual static capacity, the loading bar was modeled with constant stress hexahedral elements that were treated as a rigid material. The automatic surface-to-surface contact algorithm was employed to model contact between the impactor, supports, loading bar, and the beam. Static and dynamic friction were included in these contacts using Coulomb friction coefficients of 0.3, based on assumptions utilized in prior research (Saini and Shafei, 2019).

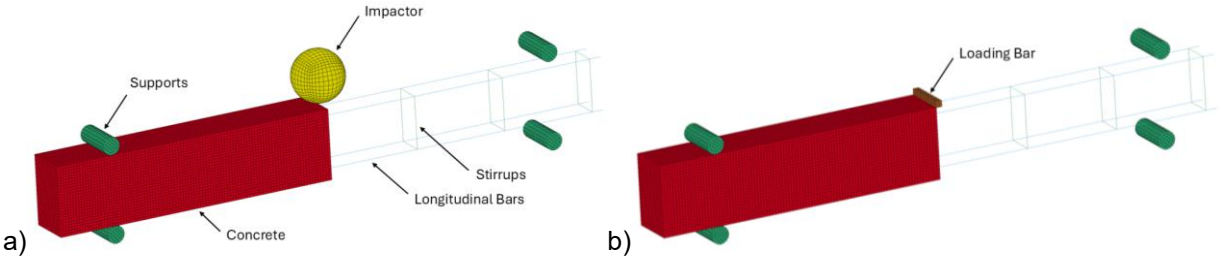

Figure 2.10. Representative finite element models of reinforced concrete beam specimens to simulate drop weight impact and residual capacity experiments

Simulation of the impact response and post-impact static response to concentrated loading at the midspan was performed across all five of the concrete constitutive models for all 16 combinations of beam series and impact intensity. The reported unconfined compressive strength of the concrete and maximum aggregate size were used to automatically generate parameters for the CSCM, KCC, and RHT constitutive models. The CDPM and Winfrith constitutive models were initialized using mechanical properties estimated from the unconfined compressive strength and maximum aggregate size using empirical models provided in the CEB-FIB Model Code 2010 (Comite Euro-International du Beton, 2013). These estimated mechanical properties included the tensile strength of the concrete, elastic modulus, fracture energy, and tensile threshold value. For the CDPM constitutive model, the bi-linear damage formulation was used with the default assignments for the threshold values at the transition between the two linear portions of the damage law. For all of the constitutive models, element erosion was not enabled to avoid introducing a dependency of the results on the erosion criteria and thresholds used. Since the drop weight impactor did not penetrate into the beam specimens, the beam response and damage mechanisms should be able to be predicted without erosion of elements. It should be noted that the comprehensive assessment of the available constitutive models performed for this study was limited to evaluating the performance of these constitutive models with automatic parameter generation and default options. It is plausible that any of these constitutive models could be calibrated using extensive materials characterization and produce strong correlations to the experimentally measured displacement time histories and observed damages. However,

since the mechanical test results necessary to calibrate these models is not typically available in either design or in post-impact forensic analysis, the performance of the constitutive models with automatic parameter generation is often of greatest significance from a practical standpoint.

An hourglass coefficient sensitivity analysis was conducted for each of the constitutive models. Hourglass stabilization is a technique used with under-integrated solid elements, such as the constant stress hexahedral solid element, to suppress nonphysical hourglass modes of deformation that may arise. In this sensitivity analysis, both the Flanagan-Belytschko stiffness and viscous forms of hourglass control with exact volume integration were evaluated for all drop heights and all beam series using a set of eight hourglass coefficients ranging from 0.0001 to 0.1. The hourglass energy relative to the internal energy was assessed for each simulation, as well as the principal strain distributions, to examine the effect of the hourglass coefficient on the predicted response of each beam. Ultimately, the hourglass coefficients for each constitutive model were established by identifying the lowest coefficient required to suppress any visual instabilities across all of the models. This resulted in the use of the stiffness form of Flanagan-Belytschko hourglass control with exact volume integration and hourglass coefficients of 0.01 for CSCM, 0.001 for KCC, 0.0025 for RHT, 0.0075 for CDPM, and 0.001 for Winfrith. Additional information, results, and discussion of this sensitivity analysis can be found in Samadzad and Whelan (2024).

For every model, dynamic relaxation was first performed to introduce initial stress and deflection due to self-weight. Explicit dynamic analysis was then conducted to simulate the response of each beam to the associated drop weight impact. Subsequently, the impactor was removed from the model and mass proportional damping was temporarily introduced for a period of time to attenuate oscillations and restore the beam to static equilibrium. Lastly, the loading bar was introduced to each model and loading of the beam in a three-point bend configuration was simulated by prescribing vertical displacement of the loading bar at a constant rate of 0.5 inch per second. This loading rate was determined to be sufficiently slow to avoid exciting the modal response of the beam and strain rate enhancement was removed from all of the constitutive models prior to restarting the analysis for the residual static capability determination. The use of full restart analysis to modify the parts within the model and assignment of parameters is similar to the staged construction of the prestressed girder bridge models previously discussed in the development of the CAE; the simulation of the reinforced concrete beam experiments assisted in establishing familiarity and competence in using full restart analysis.

Assessment of the five different constitutive models included comparisons with experimentally measured midspan displacement time histories, failure modes as evidenced by maximum principal strain distributions, computational time, and residual static capacity estimates. Figure 2.11 presents representative comparisons between the experimentally measured displacement time histories and those predicted by each of the five constitutive models for a subset of the beam series included in the investigation. The CSCM, RHT, and Winfrith models produced the strongest correlation with the experimentally measured peak displacement, with each predicting the peak displacement with an accuracy of 3% on average. However, the CSCM constitutive model consistently predicted the peak displacement with high accuracy regardless of the impact intensity, while the RHT and Winfrith models tended to overpredict the peak displacement for lower intensity impacts and underpredict the peak displacement for higher intensity impacts. The CDPM model consistently underpredicted the peak displacement, especially for beams with higher shear-to-flexural resistance ratios. Conversely, the KCC model exhibited strong accuracy in predicting the peak

displacement for beams with high shear-to-flexural resistance ratios, but significantly overestimated the peak displacement when the shear-to-flexural resistance ratio fell below 1.5. Computationally, the RHT and KCC models required the least processor run time, followed closely by the CSCM model which required only 9% more time. Use of the Winfrith and CDPM models was found to require 27% and 79% more processor run time, respectively.

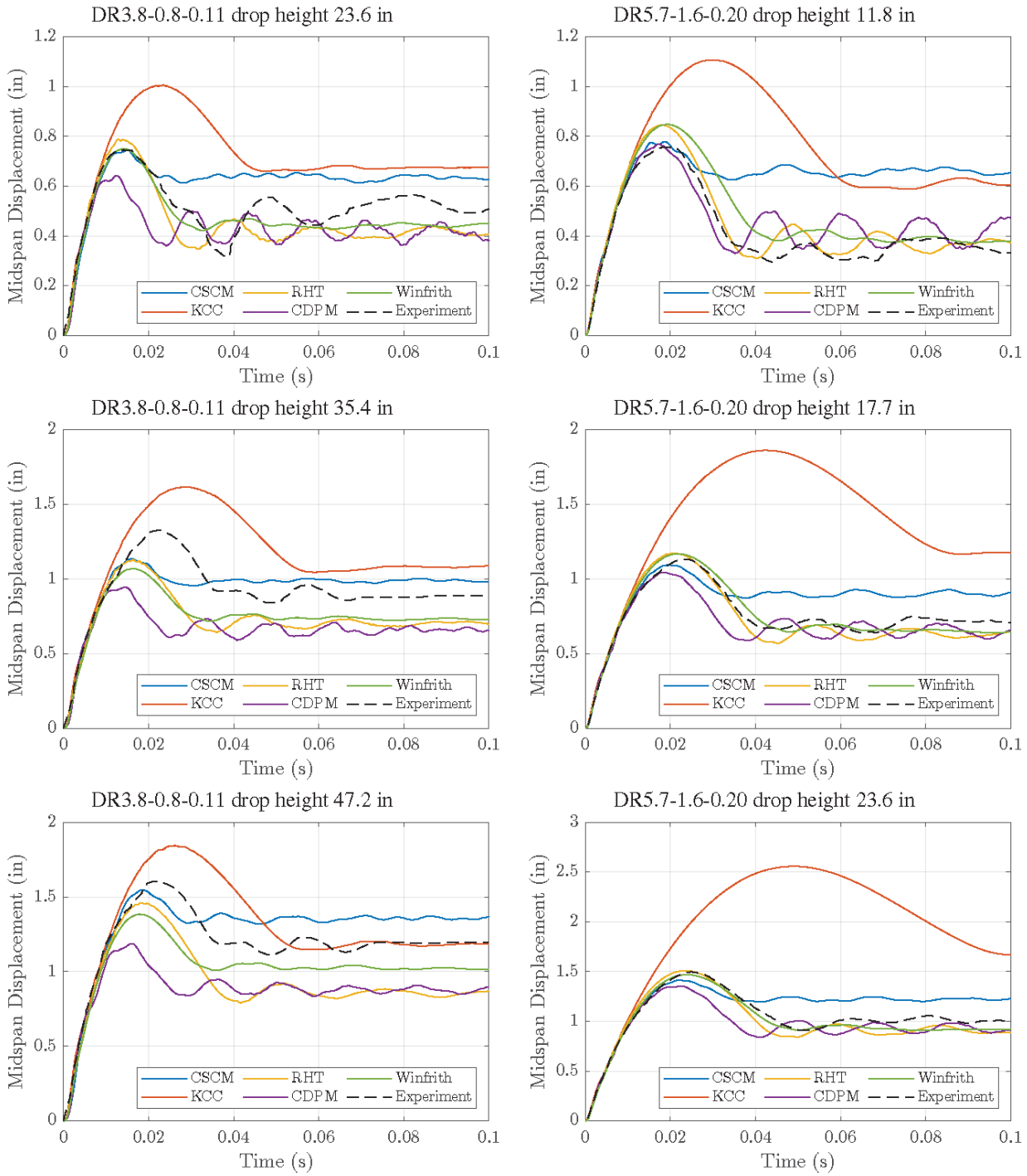

Figure 2.11. Displacement time histories predicted by different concrete constitutive models for drop weight experiments performed on reinforced concrete beams

Although the concrete constitutive models, with the exception of the Winfrith model, do not directly predict the location or orientation of cracking, the maximum principal strain distributions can serve as a surrogate to indicate the nature and likelihood of cracking. Figure 2.12 presents a comparison between profiles of visible surface cracks and spalls in select specimens (as obtained by superimposing a layer over published photographs of each specimen) and the maximum principal strain distributions following the transient analysis of the beam response to the impact using each constitutive model. As observed in this figure, there is a wide variation in the nature and severity of damage predicted by each constitutive model, despite the often similar midspan displacement time history predictions. Overall, CSCM produced damage estimates that were most similar to the experimental observations. The maximum principal strain distributions developed with the CSCM model reflect flexure and flexure-shear cracks within the same general portion of the span as observed experimentally and significant strain in the region of localized concrete crushing around the impact location. Consistently, the correct failure mode was predicted when using the CSCM constitutive model and the severity of the damage increased with impact intensity. The Winfrith concrete model also produced damage estimates similar to CSCM, however damage in the region of localized concrete crushing was absent when using the Winfrith model due to the absence of compression softening in this constitutive model. The RHT constitutive model failed to predict flexure-shear cracking and routinely limited the flexure cracking to a small concentrated region around the midspan of the beam. Furthermore, at increased impact intensities, the RHT model suggested the formation of a local shear plug that was not reflected in the experimental results. The KCC model similarly predicted the formation of a local shear plug, except a greater severity of damage is reflected in the maximum principal strain distributions. The deformed shape of the beam and maximum principal strain distributions for the beam series with low shear-to-flexural resistance ratios where KCC significantly overpredicted the peak displacement reveal that the reason for the overprediction was the occurrence of localized shear failure of the beam within the simulation. Lastly, the CDPM model predicted only flexure cracks at the midspan of the beam for all beam series and impact intensities.

While several of the concrete constitutive models achieved strong correlation with the experimental observations for the drop weight impact simulations, the prediction of residual capacities of the reinforced concrete beam specimens proved to be particularly challenging. The beam specimens included in the comprehensive assessment were flexure-controlled designs and therefore should not experience significant reductions in load capacity when the damage is limited to flexure or flexure-shear cracking, although the ductility will be reduced. However, the beam specimens subjected to higher intensity impacts experienced crushing of concrete in the compression zone around the impact location. As a result, many of the impact-damaged specimens exhibited lower stiffness, load capacity, and ductility than that exhibited by undamaged reference beam specimens. Figure 2.13 presents the experimental results for the DR3.8-0.8-0.11 beam series alongside the applied load versus midspan displacement response predicted using each of the five concrete constitutive models. Likewise, Figure 2.14 presents similar results for the DR5.7-1.5-0.20 beam series. While the constitutive models were generally able to predict the stiffness and load capacity of the undamaged beam specimens, none of the models replicated the experimentally measured results for the impact-damaged beams with high accuracy. As a result of this difficulty to reliably predict the post-impact residual capacity of simple reinforced concrete beam specimens as well as the significant computation demand associated with this analysis, a decision was made to forgo determination of the severity of damage in the bridge models developed with the CAE using simulation of static loading and instead rely on

alternative measures for classification of damage severity, such as loss of prestress, that can be readily obtained during the simulation of overheight collisions.

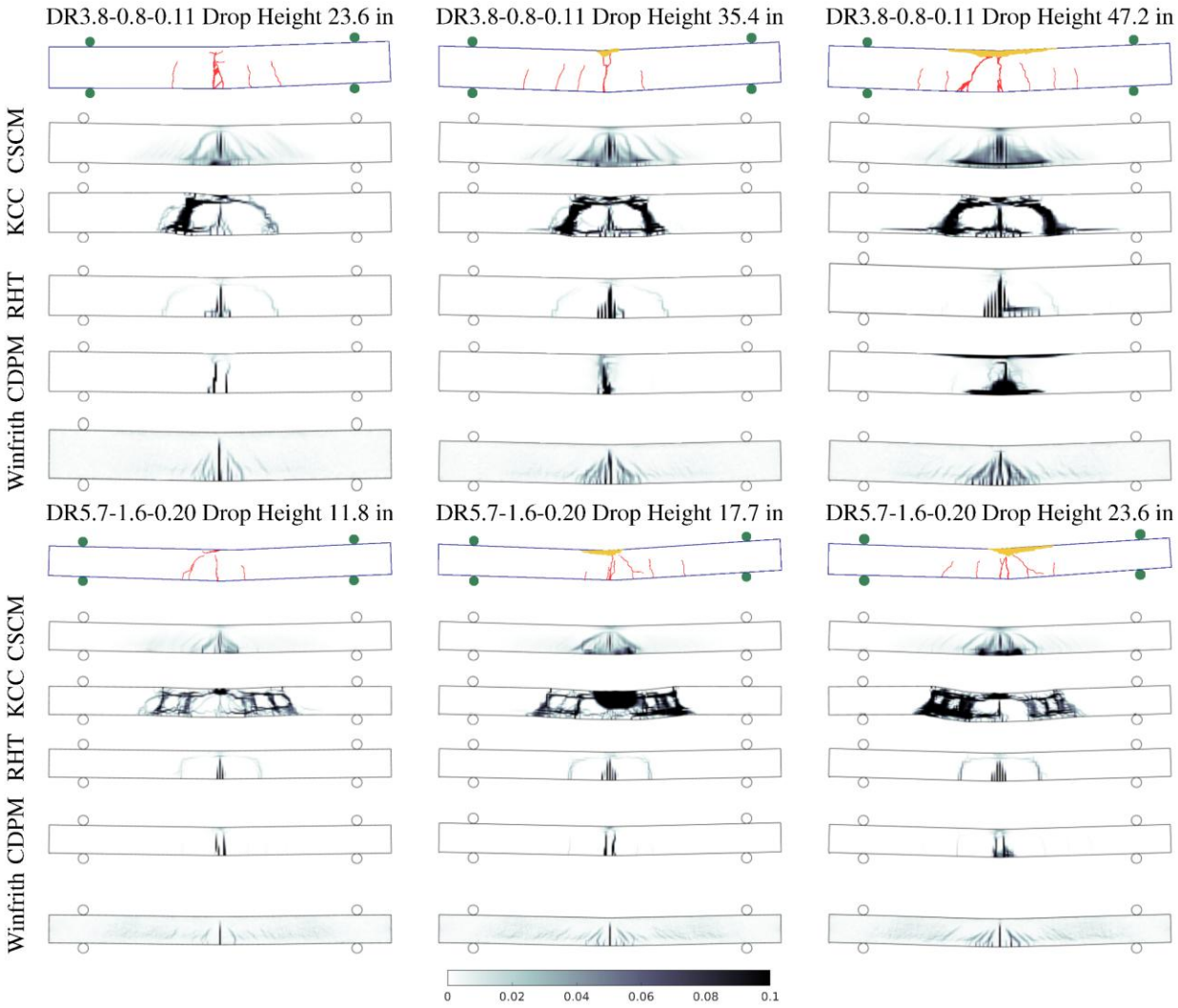

Figure 2.12. Comparison between crack and spall maps from experimental test and maximum principal strain distributions predicted for reinforced concrete beam specimens with different concrete constitutive models

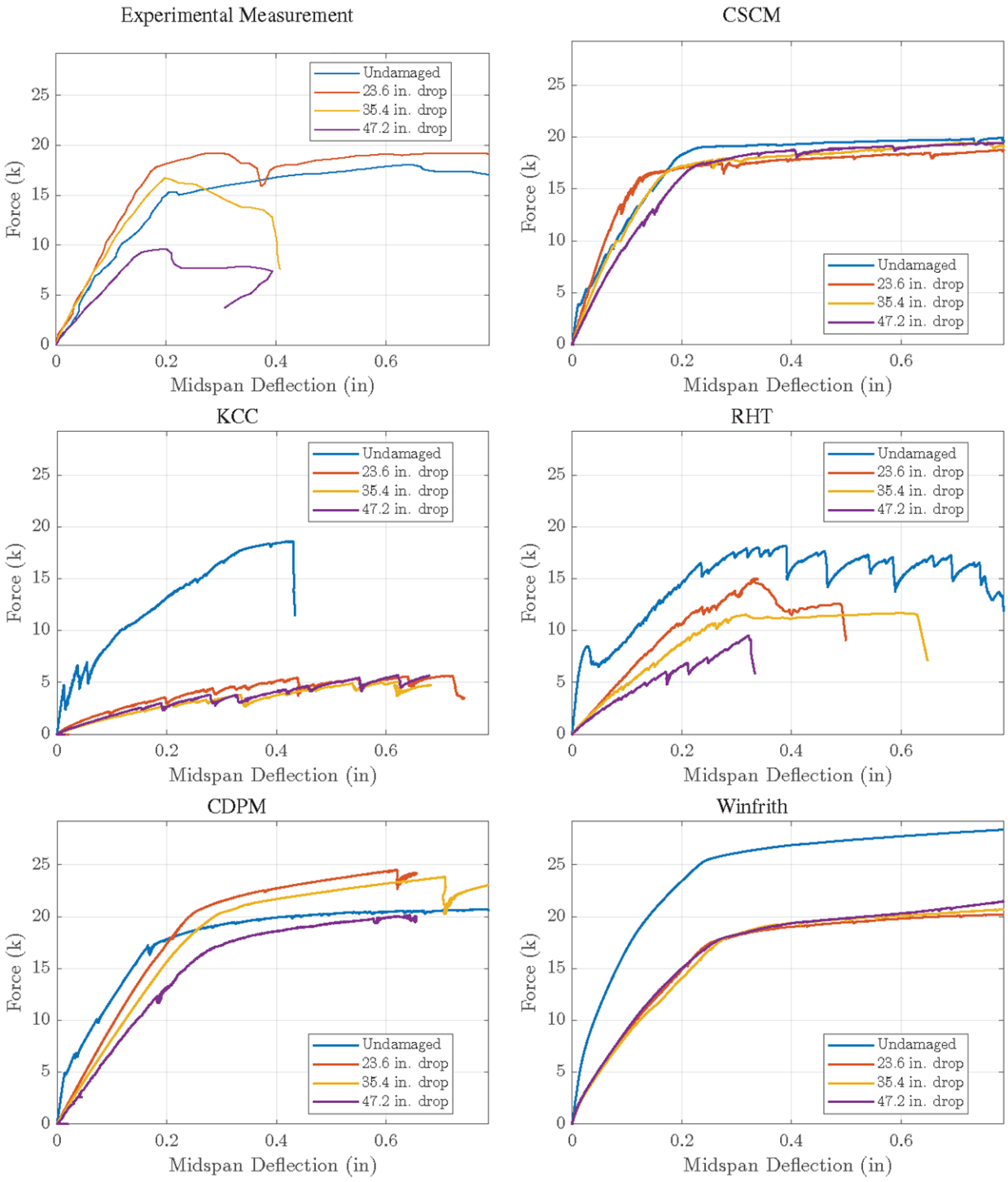

Figure 2.13. Quasi-static load versus midspan displacement for DR3.8-0.8-0.11 beam series

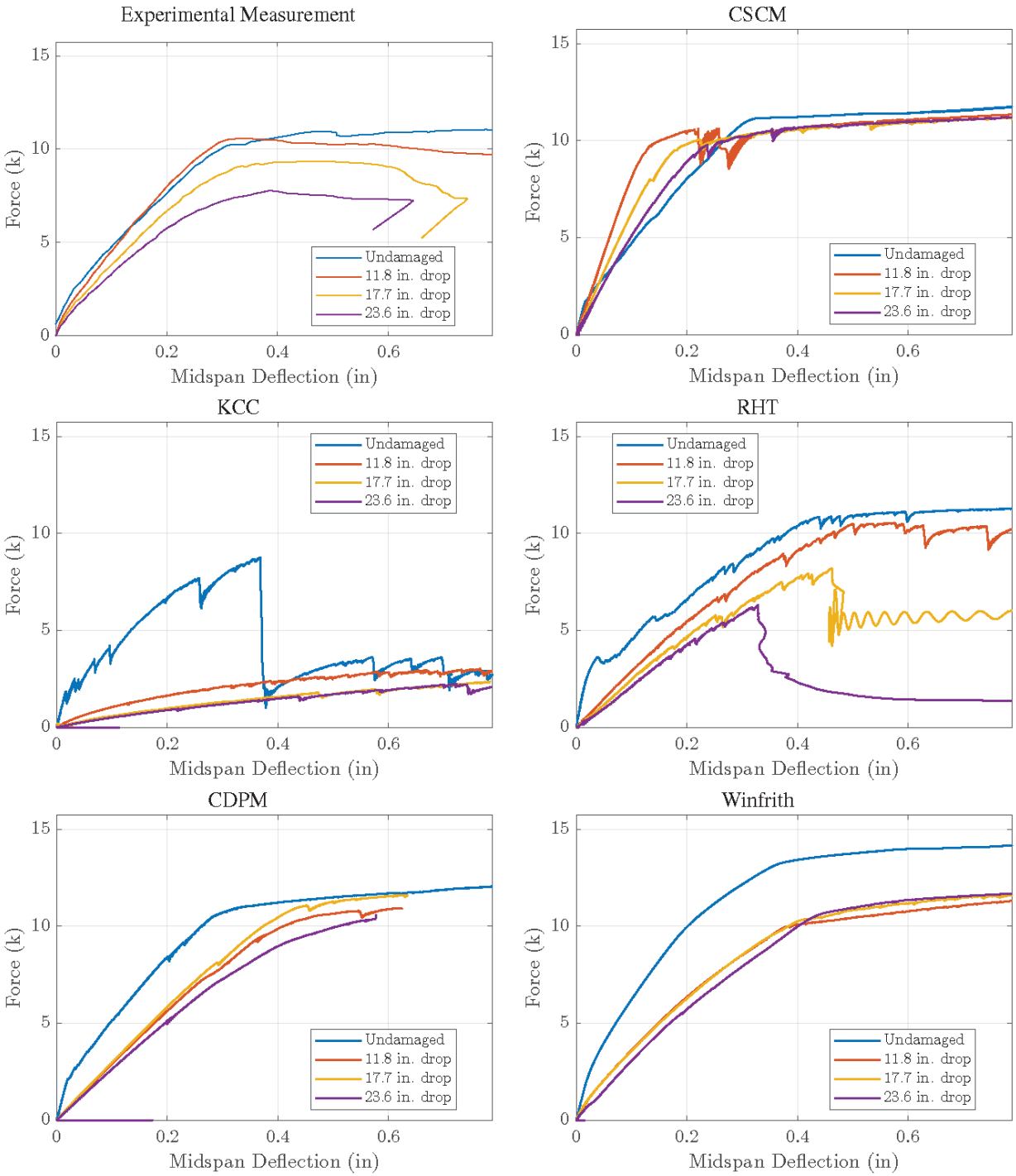

Figure 2.14. Quasi-static load versus midspan displacement for DR5.7-1.6-0.20 beam series

An expanded evaluation of the concrete constitutive models can be found in Samadzad et al. (2025). Collectively, the CSCM model produced the strongest correlation with the experimental observations across all of the five concrete constitutive models evaluated with automatic parameter generation. As a result of the strong performance of the CSCM concrete constitutive model across all beam series and impact intensities included in the comprehensive assessment, it was selected as the default concrete constitutive

model for the CAE and was used when modeling all prestressed concrete girders in the results presented subsequently in this report. To support the validation of the modeling technique and selection of the constitutive model, Figure 2.15 is presented with comparisons between the experimentally observed cracks and regions of localized concrete crushing and the maximum principal strain distributions obtained with the CSCM model.

Figure 2.15. Comparison between crack and spall maps from experimental test and maximum principal strain distributions predicted for all reinforced concrete beam specimens with CSCM constitutive model

2.4. Verification of Collision Simulations through Benchmark Comparison

A literature review conducted during the development of the proposed research plan identified guidance for constructing high-fidelity finite element models of construction objects to investigate overheight vehicle impacts to bridge girders in the work of Oppong et al. (2021). This reference presented descriptions of concrete conduit pipe, steel tank, PVC pipe, and wooden container models representative of cargo objects that might be involved in overheight collisions. The impact force characteristics, namely peak force and mean force, were investigated for different velocities and girder profiles and empirical equations were proposed by the authors to predict the peak and mean forces associated with overheight collisions involving concrete conduit pipes and steel tanks of arbitrary dimension and vertical underclearance violation.

Consistent with the research scope of work, an effort was undertaken to replicate impact force time histories presented in this paper to verify the implementation of modeling techniques and contact algorithms within the developed CAE. However, one significant difference between the modeling strategy used in the CAE and adopted within Oppong et al. (2021) is that the CAE develops models of the complete bridge superstructure, including the girders, deck, diaphragms, and bearings, while the Oppong et al. (2021) study modeled only single girders. In an attempt to account for the contributions of other components in the superstructure, the authors of this prior study introduced translational restraints in all directions along the entire top flange of the girder to mimic stiffness provided by a deck and translational restraints in all directions along both ends of the girder to mimic stiffness provided by abutments. Consistent with the models used to develop the published results, two girder models were developed to verify the modeling technique: a 40 ft long AASHTO Type I girder and a 40 ft long AASHTO Type IV girder. The published paper did not consider these girders to be prestressed and included mild reinforcement at all of the typical locations where prestressing tendons might be placed within these AASHTO sections. Shear reinforcement was also included in the models. The concrete for the girders was represented with the CSCM constitutive model using automatic parameter generation assuming an unconfined compressive strength of 5.8 ksi and maximum aggregate size of 0.4 in. The concrete pipe, steel tank, and tractor-semitrailer models described in the paper were replicated. Renderings of these objects are provided in Figure 2.16 alongside the girder model to provide a reference for the relative scale. The concrete pipe model is an open-ended hollow cylinder with an outside diameter of 7 ft 2 in, a wall thickness of 7 in, and a length of 7 ft 6 in. The total weight of the concrete pipe model is 13605 lb. Constant stress hexahedral solid elements were used to model the concrete pipe and the CSCM concrete constitutive model with erosion enabled was used to model the concrete behavior. The steel tank model is a closed ended hollow cylinder with a wall thickness of 1 in and the same outside diameter and length as the concrete pipe. The total weight of the steel tank model is 6162 lb. A plastic kinematic material model consistent with the material model used for mild reinforcing steel in the CAE was used to model the nonlinear and strain-rate dependent behavior of the steel in the steel tank model. Lastly, the tractor-semitrailer model was the National Transportation Research Center (NTRCI) model developed and enhanced by Battelle, Oak Ridge National Laboratory, and the University of Tennessee at Knoxville over several project phases (Miele et al. 2010). It was sourced from an Oak Ridge National Laboratory website (Oak Ridge National Laboratories, 2025). For all simulations, automatic surface-to-surface contact was used to model the interaction between the girder and the respective impacting object.

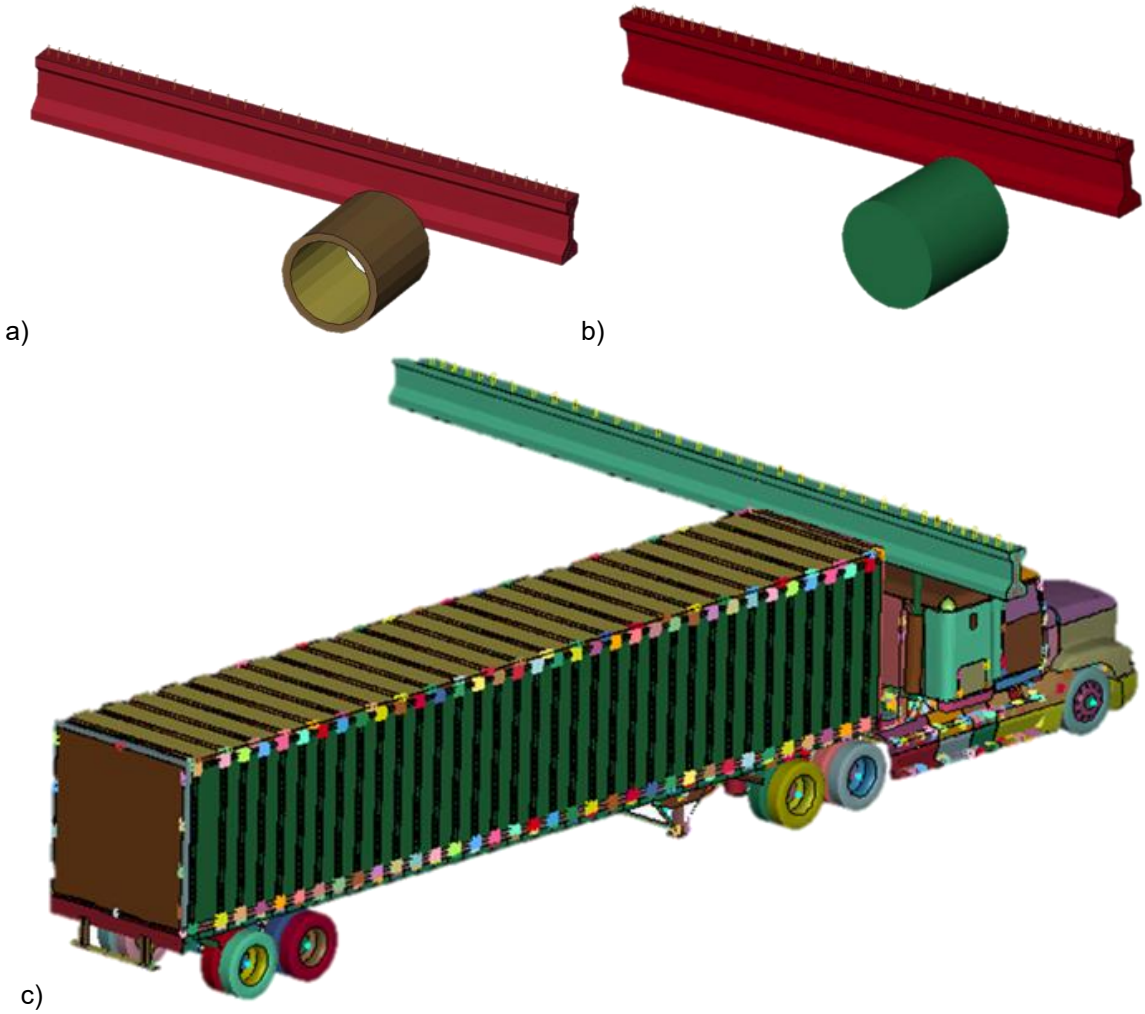

Figure 2.16. Overheight impact object and vehicle models replicated from Oppong et al. (2021) study: a) steel tank; b) concrete pipe; c) tractor-semitrailer

LS-DYNA was used to simulate impacts for each object striking the bottom flange of the girder models with an underclearance violation of 13 inches. The location of the impact was assumed to be at the quarterpoint of the span and simulations were performed for impactor velocities of 45 mph and 75 mph to allow for direct comparison with impact force time histories presented in the published study. Table 2.1 presents comparisons between the peak impact force recorded during each simulation with the values reported in the published study.

Table 2.1. Comparison between peak impact forces obtained from simulation and reported in Oppong et al. (2021)

		Impacting Object					
		Concrete Pipe		Steel Tank		Tractor-Semitrailer	
Velocity	Type	Peak Force (k)	Oppong et al. (2021)	Peak Force (k)	Oppong et al. (2021)	Peak Force (k)	Oppong et al. (2021)
45 mph	I	1945	1945	4512	4690	1266	1079
	IV	2880	3436	7102	7588	1620	1274
75 mph	I	2825	2584	7088	7423	3197	2582
	IV	4351	4690	11577	12606	3327	2898

In addition to using the Oppong et al. (2021) study to verify the modeling techniques incorporated in the CAE, an extended analysis was conducted to evaluate the influence of simplified modeling techniques that were employed in the Oppong et al. (2021) study. Specifically, as previously discussed, the finite element models used in this prior study consisted of only a single girder with translational restraints incorporated along the entire top surface of the girder and across the ends to represent the presence of the bridge deck and supports in a simplified manner. These simplified models offer the advantage of significantly reduced computational time and memory requirements compared to modeling a complete superstructure, so the research team sought empirical evidence to justify the extent of modeling required to conduct the parametric analysis presented later in this report. To provide a comparison, a finite element model of a complete bridge superstructure was developed in the CAE using design details sourced from bridge plans provided by the Steering and Implementation Committee. The bridge span was 76 ft 5 in and consisted of six AASHTO Type IV girders spaced at 8 ft 1 in on center. The girders were prestressed with 26 low relaxation tendons of 0.6 in diameter, which were all straight and bonded over the full length of the span. The specified compressive strength of the concrete for the girders was 6 ksi, which was similar to the assumed concrete strength utilized in the Oppong et al. (2021) study. The developed model included the steel channel intermediate diaphragms located at the midspan, as well as the reinforced concrete partial depth end bent diaphragm and full depth continuous bent diaphragm. Since the bridge girders are prestressed, the model was initialized using the staged technique previously described in section 2.1 and depicted in Figure 2.7.

For the complete bridge model, impact simulations were performed using both the concrete pipe and steel tank impactor models with collisions occurring at a quarterpoint, third point, and midspan. Simulations were performed for initial velocities of 45 mph, 55 mph, 65 mph, and 75 mph. Analysis of the impact force time histories revealed that the longitudinal location of the impact along the length of the girder did not have a significant effect on the impact force time history, peak force, or impulse. A similar finding was reported in the Oppong et al. (2021) study. Similarly, the severity of damage was observed to be less sensitive to the location of the impact along the span of the girder than to the velocity of the impact. However, the duration of the impact force when performing the simulation with the full bridge model was approximately twice as long as presented in the published results for the simplified single girder models. Likewise, the mean impact force, and consequently the impulse, was found to be significantly

underestimated by the empirical prediction models developed in Oppong et al. (2021) using the simplified single girder models. The significantly shorter contact durations reported for the simplified single girder models reflect an overly stiff response of the girder resulting from the application of the idealized translational restraint boundary conditions along the top of the girder model to represent the presence of a bridge deck. These findings are consistent with similar results obtained by ElGawady et al. (2024), where impact force time history characteristics were compared for a 50 ft bridge span comprising six Missouri DOT Type II girders against a simplified model consisting of a single girder with simplified boundary conditions. This study further reported that the single girder model resulted in prediction of greater severity of damage due to the unrealistically stiff conditions produced by the simplified boundary conditions. Given the numerical results generated as part of the current research effort and the supporting evidence in the published literature, the research team chose to perform all finite element analyses reported in subsequent chapters of this report with detailed finite element models that included the entire bridge superstructure rather than adopting a simplified modeling technique. The additional computational time and memory requirements were deemed to be justified by the advantage provided by full bridge models in assuring that the fidelity of the predictions for impact force characteristics and girder response to the impact loading are not compromised by simplifications and idealizations required for the creation of single girder models.

3. DEVELOPMENT OF MODELS FOR CONSTRUCTION VEHICLES

As referenced earlier in this report, prior studies have analyzed the rates of overheight vehicle collisions with highway overpasses and have determined that overheight construction vehicles account for the majority of incidents. However, there is a lack of information in the published literature regarding the relative incidence rates for specific types of construction vehicles. To better inform the development of relevant models of construction vehicles for this research effort, news articles reporting collisions of vehicles with bridges in the United States and Canada were sourced and reviewed. A total of 93 reported incidents were collected over a three and a half year period from January 2020 to July 2023. A complete list of the identified incidents is provided in Appendix B of this report. The majority of the incident reports came from 2022 and 2023, which is attributed to greater accessibility to the archived news articles and should not be interpreted as a trend toward greater actual incident rates. Furthermore, it should be acknowledged that actual incident rates will always be under-reported in news articles since minor impacts that do not impact traffic or that occur on low-volume roads are typically not newsworthy. Figure 3.1 presents a pie chart depicting the relative frequency of incidents involving different categories of vehicles. As shown in the figure, nearly 80% of all of the incidents involved either a dump truck with an accidentally raised bed or the boom of an excavator being hauled on a trailer, with each of these vehicle types having nearly equal rates of occurrence. Trucks with raised booms but no cargo on the boom, trucks carrying overheight objects, and tractor trailers accounted for the remaining incidents. Typically, the incidents involving a truck carrying an overheight object were garbage trucks with objects that extended beyond the vertical dimension of the truck. Notably, collisions of tractor trailers with overpasses accounted for only 4% of the discovered cases and in nearly half of those cases the tractor trailer was carrying an "over-dimensioned" load. The few discovered incidents involving a typical tractor trailer resulted in extensive damage to the trailer, but no noted damage to the structure. Early in the research, the authors considered using a high-fidelity model of a tractor trailer for simulation of overheight vehicle impact due to the availability of the existing model and the use of the model in a prior paper investigating overheight collisions with overpasses (Oppong et al., 2021). However, due to the infrequent occurrence of tractor trailer overheight collisions with bridges and low probability of damage to the structure, the use of the tractor trailer model was limited only to verification of the general modeling technique through comparison to the referenced published literature.

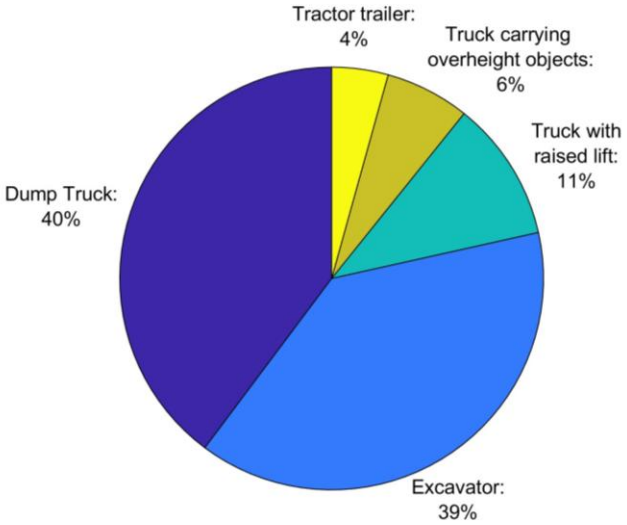

Figure 3.1. Vehicle type reported for overheight vehicles collisions in discovered news articles

Prior to developing a finite element model of a dump truck to facilitate the research, the existing literature and open-source model databases were reviewed to determine whether an existing model could be sourced and, if not, the modeling strategies used in prior research to explicitly model overheight vehicle collisions. Xu et al. (2013) presented finite element models for a double-axle truck, container truck, tipper truck, and tank truck, however results from simulations involving the double-axle truck were the primary focus of the paper. In a study focused on collisions of large trucks with bridge piers, Buth et al. (2010) developed a finite element model of a dump truck by first modifying the NCAC tractor-trailer model to produce a single-unit truck and then introducing a model of a dump truck bed. A detailed description of the modeling technique was not provided in the report, but renderings suggest that shell elements were used to produce the walls of the bed, stiffeners, and shield. Since this study was focused on collisions with bridge piers, the bed was not raised in the model.

3.1 Description of Dump Truck Model

A high-fidelity finite element model of a dump truck with raised bed was developed to enable the research, since no existing model could be sourced. To expedite the development of the model and to ensure accurate modeling of the mass and stiffness of the truck portion of the model, a strategy similar to that employed by Buth et al. (2010) was adopted. However, instead of modifying the NCAC tractor-trailer model, a detailed finite element model of a Ford F800 single-unit truck developed by FHWA at NCAC was modified to develop a dump truck model. This approach was taken since the F800 is regularly configured as a dump truck. The F800 model was freely sourced from a web site hosted by Oak Ridge National Laboratory and has undergone extensive development and evaluation (Simunovic and Zisi, 2005). It has been also validated against experimental data collected from impacts with roadside safety hardware (Mohan et al. 2007) and bridge piers (Gomez and Alipour, 2014). Figure 3.2 shows the original F800 model, which was configured as a box truck, and this model with the box, internal cargo, and supporting steel structure removed from the model.

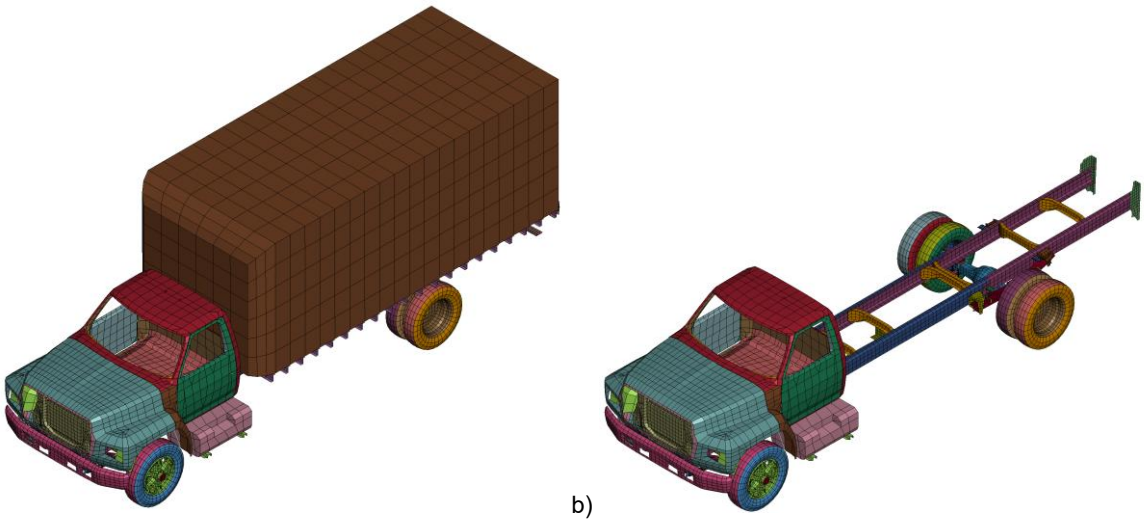

Figure 3.2. NCAC model of F800 single-unit truck: a) complete truck model; b) with box and cargo removed from the model

To develop the dump truck model, a finite element model for a representative dump body was created. The geometry of the dump body, thickness of individual components, and material properties were informed by a product brochure published by a dump bed manufacturer. The developed dump body has a length of 20

ft, width of 9 ft, and height of 6 ft. The developed finite element model of the dump body with individual components labeled is presented in Figure 3.3 alongside a rendering of the complete dump truck model developed by coupling this dump body to the modified NCAC F800 single-unit truck model. Since all components of a dump body are manufactured from either plate steel or rolled steel shapes, shell elements were used to model each component. The floor, walls, and gate of the dump truck were assumed to have a plate thickness of 0.25 in. The sides of the dump bed were stiffened with 9 in by 9 in by 0.25 in top and bottom rails as well as 15 in by 9 in by 0.25 in ribs. The subframe of the dump body included 3 in by 2 in by 0.25 in cross members supported by a pair of 8 in by 2.5 in by 0.25 in longsill beams. A representative cab shield design was modeled as a 21.25 in long and 4.75 in deep hollow section formed from 0.25 in steel. A single 0.25 in thick stiffener plate was included along the centerline of the shield. All steel components of the dump body were assigned a plastic kinematic constitutive law with mechanical properties consistent with AR450 steel, an abrasion resistant steel typically used in the fabrication of dump trucks. A yield stress of 180 ksi, tangent modulus of 145 ksi, isotropic hardening, and strain rate sensitivity were included in the material definition. The total weight of the dump truck model was 20,340 lb (10.17 US ton), with the dump body accounting for approximately 56% of the total weight.

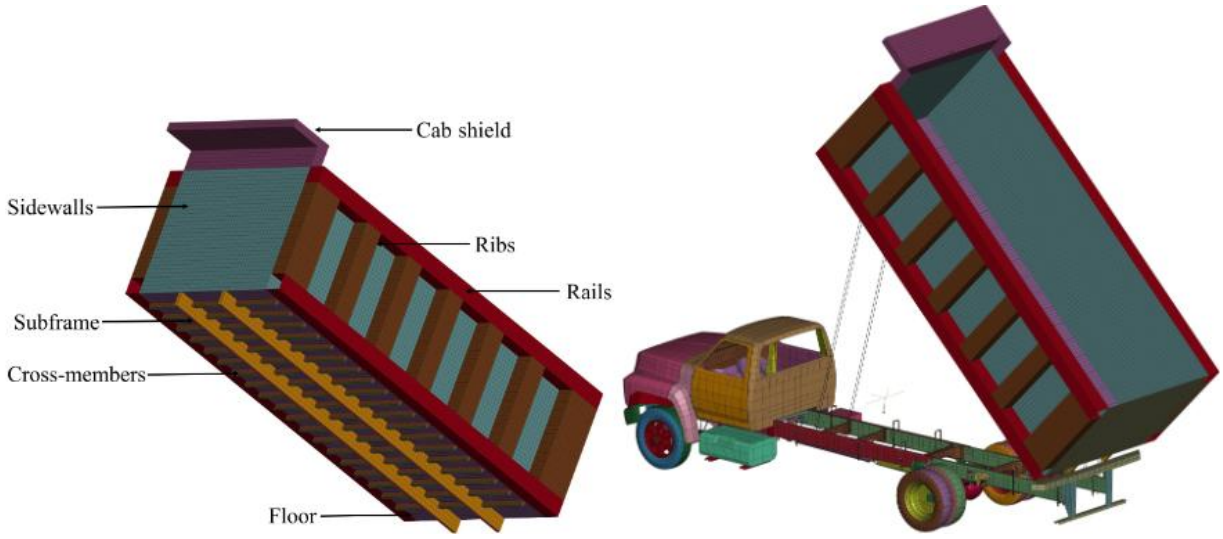

Figure 3.3. Developed model of dump body and assembled model of dump truck with raised bed

The dump body model was connected to the modified NCAC F800 single-unit truck model using spot weld constraints between the longsill beams of the dump body and the two primary frame members of the truck. These spot weld constraints enforce connectivity to both frame members near the gate end of the dump body. Likewise, instead of explicitly modeling the hydraulic cylinder that raises the bed of the truck, spot weld constraints were used to connect the frame of the truck to the longsill beams of the dump body where this hydraulic cylinder would be located. A benefit of modeling the connection between the dump body and the truck with only constraints between nodes of the dump body and nodes of the truck is that the inclination of the raised bed can be easily modified without having to remesh any explicitly modeled components connecting these objects together. A MATLAB script was written to perform coordinate transformations on the nodes within the dump body model to allow for the angle of the raised bed to be prescribed according to any user assigned value. Likewise, a script was developed to adjust the elevation,

longitudinal position, and angle of incidence of the truck to enable parametric analysis of different overheight collision scenarios without manual intervention. These scripts enable the automated generation of different impact scenarios, which provides for rapid replication of actual reported incidents as well as generation of large parametric analyses with assurance of consistent modeling.

3.2 Validation of Plausibility of Model Based on Case Study Comparison

In March 2024, a dump truck with raised bed impacted a bridge under construction in Raleigh. At the time of the incident, all five 45-inch Florida I-Beams (FIBs) were placed and connected together with intermediate steel channel diaphragms at the midspan. Fillet welding of the girder embedded plates to the sole plates of the elastomeric bearings at each end had also been completed. During the accidental collision, the exterior girder was impacted by the dump truck, but the underclearance violation at this girder must have been relatively mild, as damage to this girder was limited to two shallow spalls on the bottom flange of the girder and hairline cracking adjacent to the sole plate connection. However, three of the interior girders, girders 2, 3, and 4, exhibited deeper spalling across a wider surface area at the locations of the impacts and severe damage adjacent to the sole plate connections. The supplemental inspection report noted that no damage to the sole plate welds was visible and, furthermore, that ultrasonic testing of the anchor bolts found no indication of anchor bolt rupture. For girders 2 and 3, the bottom surface of the flange showed significant scraping, indicating that the dump truck maintained contact with the underside of the girders as it passed underneath them, and shallow spalling was also present on the rear side of the bottom flange. The spalling and scraping damage to the girders appeared to be cosmetic or superficial in severity, but the damage adjacent to the sole plate connections at both ends of the girders was severe and ultimately required the replacement of all of the girders in the span. Figure 3.4 provides photographs of the bridge that the research team collected shortly after the incident, which document the status of the bridge completion at the time of the incident and representative visible damage to the girders that was observed.

Newscast footage of the dump truck following the incident revealed significant damage to the shield of the dump body and overturning of the entire dump truck, but no evidence that the bed separated from the truck during the impact. While difficult to confirm from the post-incident state of the truck, the angle of the raised bed appeared to be relatively shallow based on the images contained in the news broadcast. Based on the research team's on-site observations of damage, the damages documented in the inspection report, and the nature of the damage to the dump truck, it appears most probable that the shield of the dump truck struck the girders during this incident and, furthermore, the underclearance violation of the raised bed was such that the dump truck made only mild contact with the exterior girder. From the perspective of validating the developed dump truck finite element model, this specific incident provided a very valuable case study for the research effort, since photographic evidence of the dump truck was available, the damages resulting from the impact were visible and consisted of both localized damage at the impact and connection damage, and the elevation of the raised bed could be estimated with relatively high confidence.

The bridge span consisted of five 45-inch FIB sections, each 85 ft 11 in in total length. Figure 3.5 presents a drawing of the cross section of the partially constructed bridge. The girders were prestressed with 32 fully bonded, 12 partially debonded, and 2 slack strands, each being 0.6 in diameter low relaxation Gr 270 strands. The specified 28-day compressive strength of the concrete for these girders was 8500 psi. The girders were spaced 8 ft 8 in on center, the span had a skew of 22 degrees (skew angle of the bent line of 112 degrees), and the grade of the deck and elevation of the girders sloped in one direction. The intermediate

diaphragms, which were present at the time of the incident, were steel MC12x31 channels bolted to L6x6x1/2 angles that were connected to the girders with through-bolts. These diaphragms were oriented perpendicular to the girders, rather than aligned with the skew of the bridge, which is standard NCDOT practice for bridges with skew angles exceeding 20 degrees.

Figure 3.4. Photographs of partially constructed bridge subject to accidental overheight vehicle collision: a) status of bridge construction at time of incident; b) spalling of impacted side of bottom flanges; c) scraping of underside of girder and spalling on rear side of flanges; d) severe damage adjacent to sole plate connections

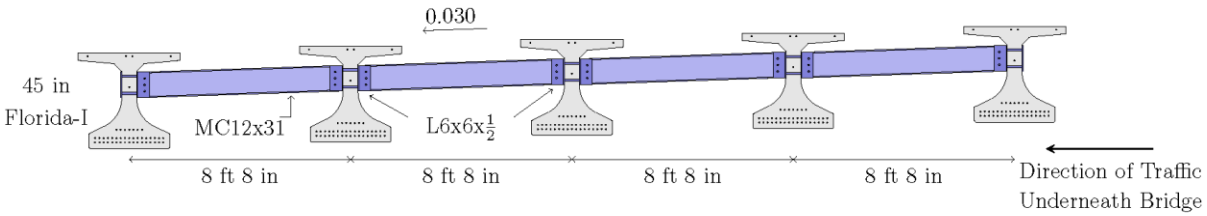

Figure 3.5. Dimensions and design details for under construction bridge impacted by dump truck with raised bed

A finite element model of the partially constructed bridge was created using the developed CAE. A model consisting of only the components present at the time of the incident was created by simply suppressing the

subroutines responsible for creating the meshes for the deck, end bent diaphragms, and thru bent diaphragms. During the field visit to the bridge, the research team collected LiDAR scans of the bridge and the roadway underneath the bridge (Figure 3.6). The point cloud data generated from this scanning was analyzed to determine the precise difference in elevation between the surface of the roadway and the underside of the girders at the longitudinal location of the impact. Figure 3.7 presents an image of a slice of the actual point cloud data that has been annotated to indicate the measured elevation of each girder relative to the roadway. In this image, the point cloud is limited to the bottom flange for all but one exterior girder due to line-of-sight restrictions from the scan used. The rightmost girder in the image corresponds to the exterior girder that was first impacted by the raised bed of the dump truck. As can be seen in the elevation difference measurements, the vertical underclearance reduces for each girder, which explains why the shield of the dump truck would have struck multiple girders with significant force even if the impact force from each collision was significant enough to damage the shield. The vertical underclearance measurements obtained from the LiDAR scan were used to prescribe a ground plane in the finite element model to represent the roadway in a way that would be consistent with the actual relative differences in grade. Additionally, the LiDAR scan was used to determine the longitudinal location of the dump truck impact to the bridge girders. Spalling of the interior impacted girders was clearly visible in the point cloud data and was used to establish the location of the impact relative to the end of the girder (Figure 3.8). Furthermore, the location of spalls on the individual girders confirmed that the collision of the dump truck with the bridge girder was an oblique impact with an angle of impact corresponding to the direction of the roadway underneath the structure. The angle between the direction normal to the face of the girder and the direction of travel was approximately 20 degrees and was included in the finite element analysis by orienting the truck for oblique impact at this angle.

Figure 3.6. Point cloud generated from LiDAR scanning of bridge after incident

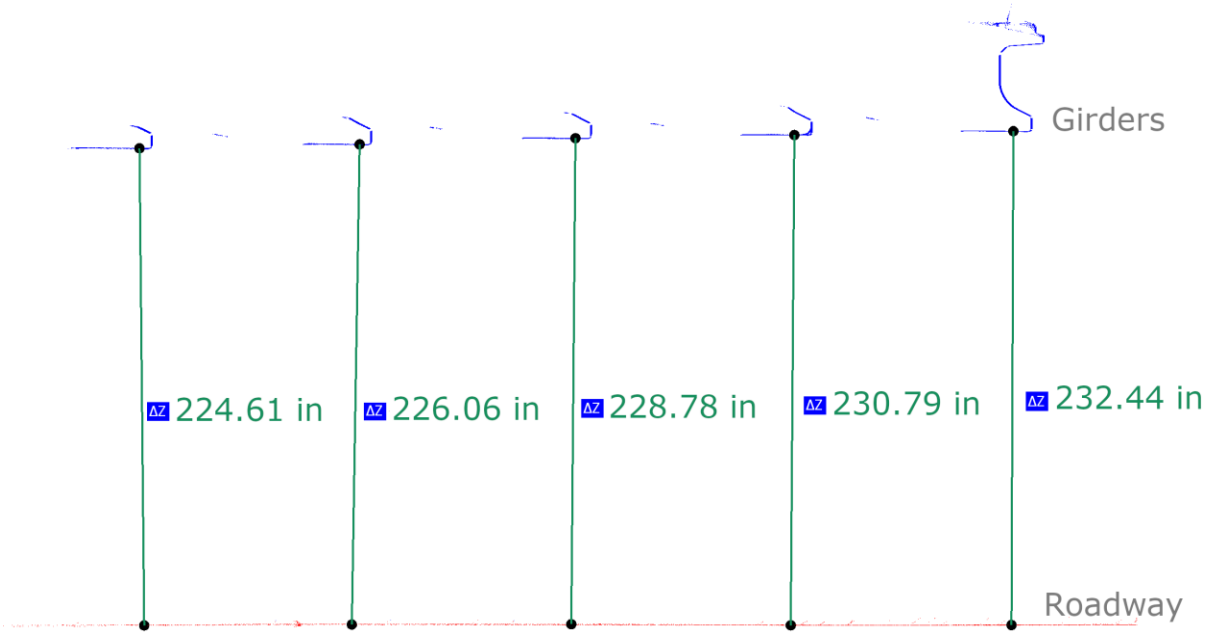

Figure 3.7. Measurement of girder vertical underclearances from LiDAR point cloud to accurately model the slope of the roadway under the superstructure

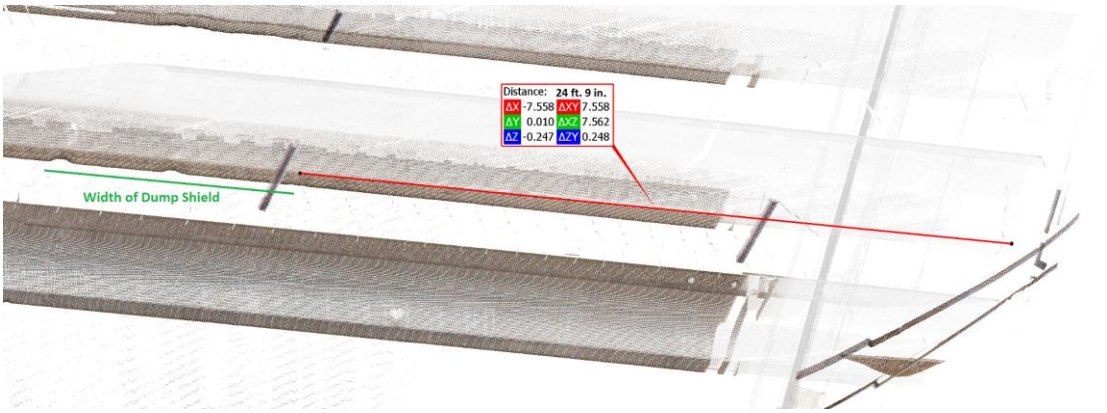

Figure 3.8. Measurement of distance from end of girder to edge of dump truck impact location

A rendering of the finite element model developed to simulate the case study incident is presented in Figure 3.9. This rendering depicts the components in the finite element model as well as the orientation of the raised bed dump truck relative to the bridge girders. Since the empirical evidence collected by the field visit and supported by the inspection report suggests that the dump truck likely grazed the exterior girder before impacting the first interior girder, the dump truck was positioned in the finite element model with an elevation corresponding to the elevation of the bottom surface of the exterior girder. It was also positioned just ahead of the first interior girder, thereby assuming that the impact to the exterior girder was insignificant. Given the vertical underclearance measured from the point cloud data, the angle of the bed in the developed dump truck model corresponds to 22.8 degrees for the simulated scenario. As previously stated, images of the overturned dump truck shown in a newscast of the incident suggest that the bed was raised at a shallow angle, but it is impossible to confirm the exact configuration of the dump truck at the time of the incident. Furthermore, the speed of the dump truck at the time of the incident was unknown. Since the interstate that the dump truck was travelling on was posted with a speed limit of 65 mph, simulations were performed for speeds of 55 mph, 60 mph, and 65 mph. All three simulations resulted in similar results for the prediction of damage to the impacted girders, with the exception of the damage predicted in the last girder of the bridge. The reason for the difference is that the finite element analysis predicted that the dump truck would overturn for all three velocities, but the rate of overturning varied across the models resulting. In all cases the last girder was at least partially impacted by the bed of the dump truck rather than the shield. It should be noted that simulating impacts to four consecutive girders is exceptionally challenging and the confidence in the prediction results decreases with each subsequent impacted girder.

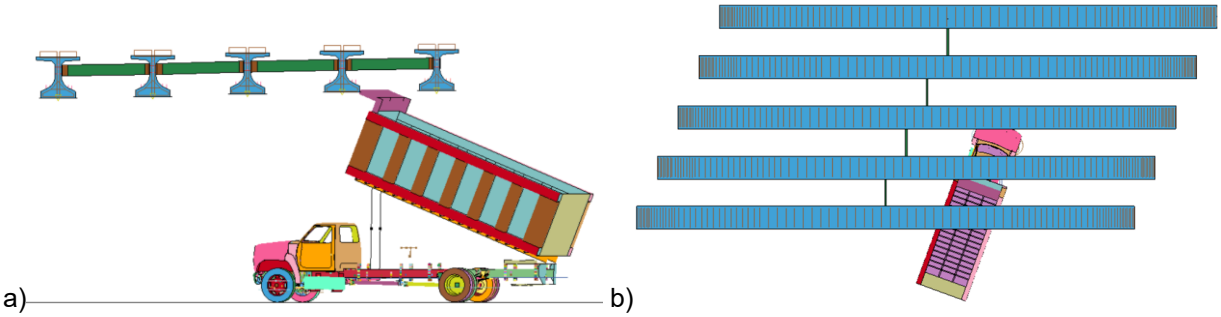

Figure 3.9. Renderings of finite element model for case study structure: a) elevation view; b) plan view

The finite element analysis simulations generated predictions for damage to the prestressed concrete girders that were consistent with the visible observations of damage. For all of the impacted girders, localized spalling of the concrete was predicted where the shield of the dump truck struck the girders (Figure 3.10a) and, furthermore, evidence of damage to the underside and rear side of the bottom flange from the shield scraping the girder as the truck passed underneath were also present in the simulation result (Figure 3.10b). Importantly, the finite element simulation also predicted the damage observed adjacent to the sole plate connections (Figure 3.10c). Although some discrepancies between the model predictions and the actual damages are expected due to modeling uncertainties, particularly those related to the geometry of the dump truck shield, the plausibility of the finite element model predictions for the nature and severity of damage supports the predictive fidelity of the developed CAE and modeling techniques.

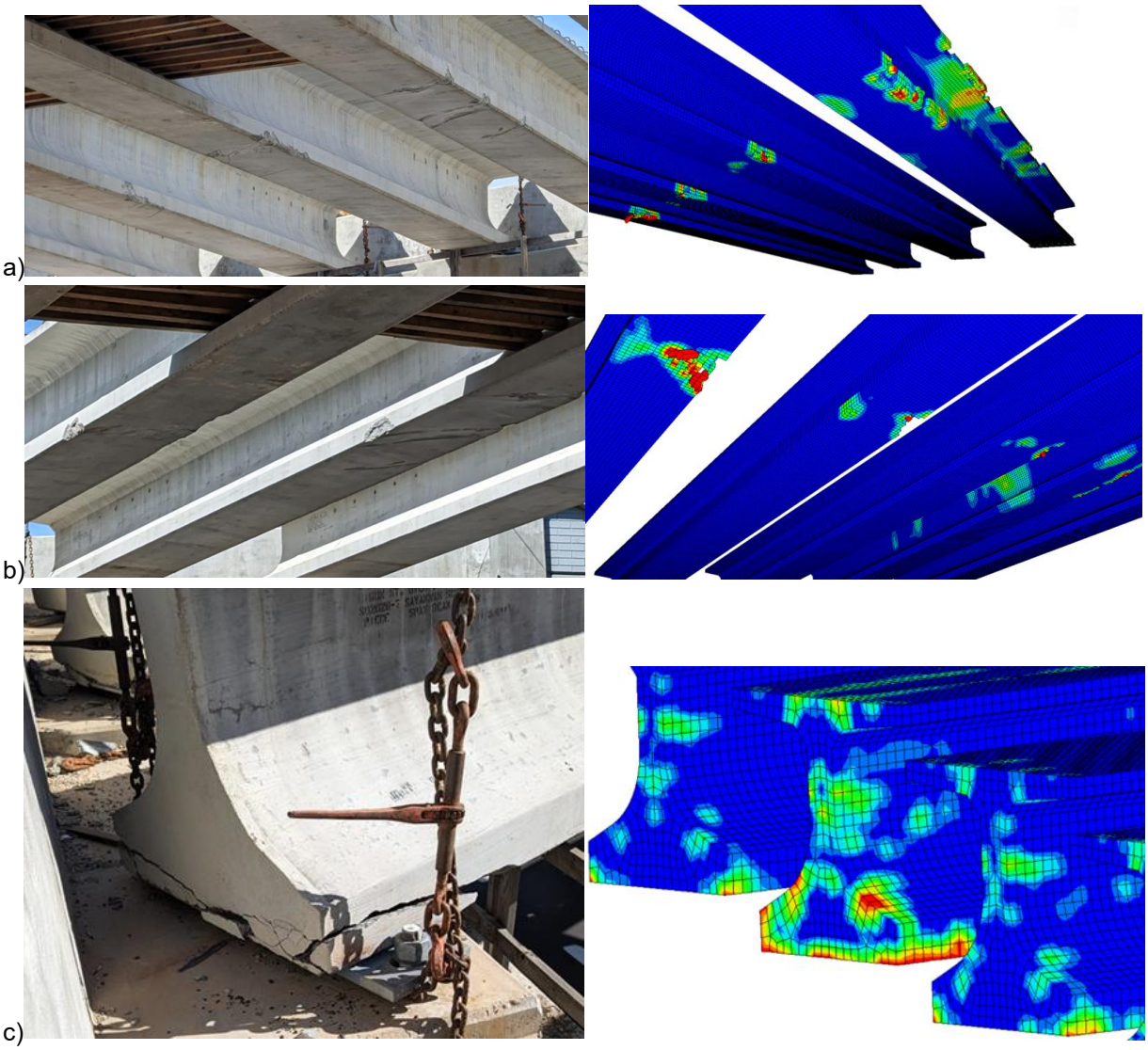

Figure 3.10. Comparison between damages predicted by finite element analysis and photographs of visible evidence of damage: a) localized spalling of bottom flange at location of impacts; b) scraping on bottom and spalling on back side of bottom flange; c) damage adjacent to sole plate connections

One of the capabilities introduced by the utilization of high-fidelity finite element analysis for simulating the response of prestressed concrete girders to overheight vehicle impacts is the ability to predict internal damages that may not be readily apparent from visual inspection. Of particular importance for prestressed concrete is the effect of the impact forces on the prestress force in the strands. Figure 3.11 provides a plan view rendering of the distribution of prestressing forces in all of the strands within the bottom flange of the girders in the model. In this figure, yellow corresponds to the normal level of prestressing force in the strand, red indicates an increase in prestressing force, green indicates a reduction in prestress force, and blue indicates total loss of prestress. Arrows are superimposed on the figure to indicate the direction of the dump truck travel and the width of the dump shield. Solid arrows are used to indicate the edge of the shield that struck the girder in the simulation, while dashed arrows indicate that the corresponding edge of the shield did not make contact with the girder. The simulation results suggest partial localized loss of prestress in several strands at the location of the impact in all of the girders. Furthermore, localized total loss of prestress is predicted for some strands in the first impacted girder (girder 2) as well as the last girder (girder 5) where the back wall of the overturning dump truck struck the girder in the simulation. Additionally, for these girders, the reduction in prestress forces at the ends of the girders extend beyond the transfer length predicted for the undamaged girder. Given the severity of the observed damage adjacent to the sole plates in the case study, this further supports the plausibility of the modeling technique and simulation result.

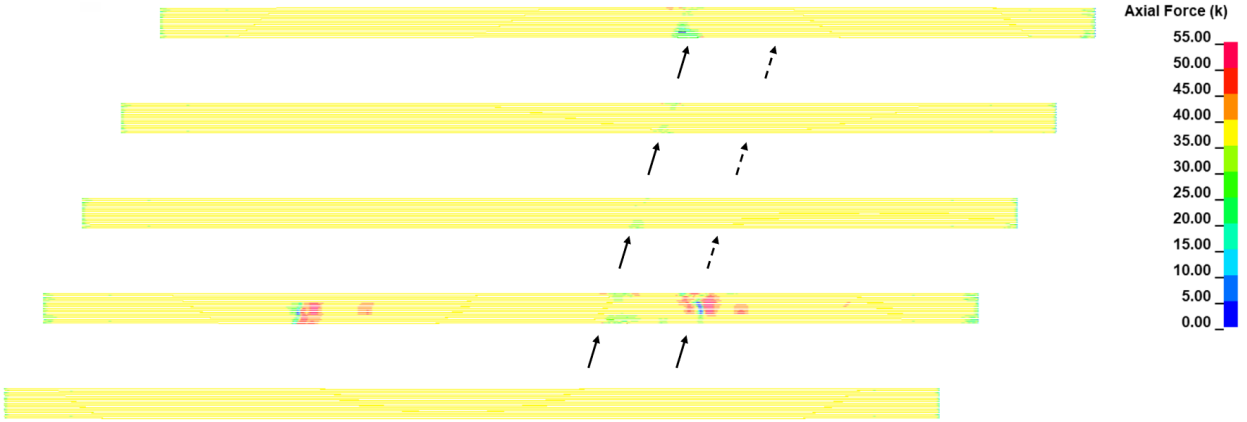

Figure 3.11. Finite element prediction of prestress loss in impacted girders

Figure 3.12 presents the maximum principal strain distributions predicted across the front, bottom, and rear surfaces of the impacted girders. In this figure, the maximum extent of the colormap is fixed to 0.1, or 10% strain. In doing so, regions of the girder that are predicted to have visible signs of distress, such as cracking, are identified in blue. Furthermore, eroded elements are colored in red to depict the location and extent of spalling predicted by the finite element analysis. The maximum principal strain distributions and eroded elements in the bottom flange of the girders exhibit similar spalling from direct impact and damage from the shield scraping the underside of the girder that was observed in the actual incident. Furthermore, damage adjacent to the sole plate connections at both ends of the girder were predicted for all of the impacted girders. Although the maximum principal strains are lower in amplitude adjacent to the sole plate connections in girder 3 and 4, the ductile and brittle damage predicted by the concrete constitutive model (Figure 3.13) clearly identifies localized damage adjacent to all sole plate connections. The finite element model does predict damage to the top flange of girder 2 that was not observed by the research team or noted in the supplemental inspection report. Since the renderings provided in Figures 3.12 and 3.13 are limited to

the front, bottom, and rear views, the extent of damage predicted in the flanges appears more extreme than actually reflected by the model. The actual predicted extent of spalling in the flanges was limited exclusively to the flange tips. The prediction of this damage may be a result of incorrect assumptions for the length or thickness of the shield of the dump truck, which may have resulted in the prediction of moderately larger impact forces. However, the predicted damage in the flange may have been caused by modeling the sole plate as bonded across the entire surface of the bottom flange instead of connected only along the edges where the bearing plate is welded to the sole plate. This modeling assumption may have inhibited the model from predicting the uplift of the girder that likely occurred at the supports, thereby leading to a prediction of greater negative moments in the girder during the positive (upward) response of the girder following impact. Another discrepancy between the simulation and field observations are the damages predicted in girder 5. This girder did not exhibit evidence of damage from impact, but the simulation predicted that the raised bed would strike the girder during overturning of the truck. However, accurately predicting the response of the dump truck after impacts to three prior girders is an unrealistic expectation, especially in a situation where the dump truck overturns.

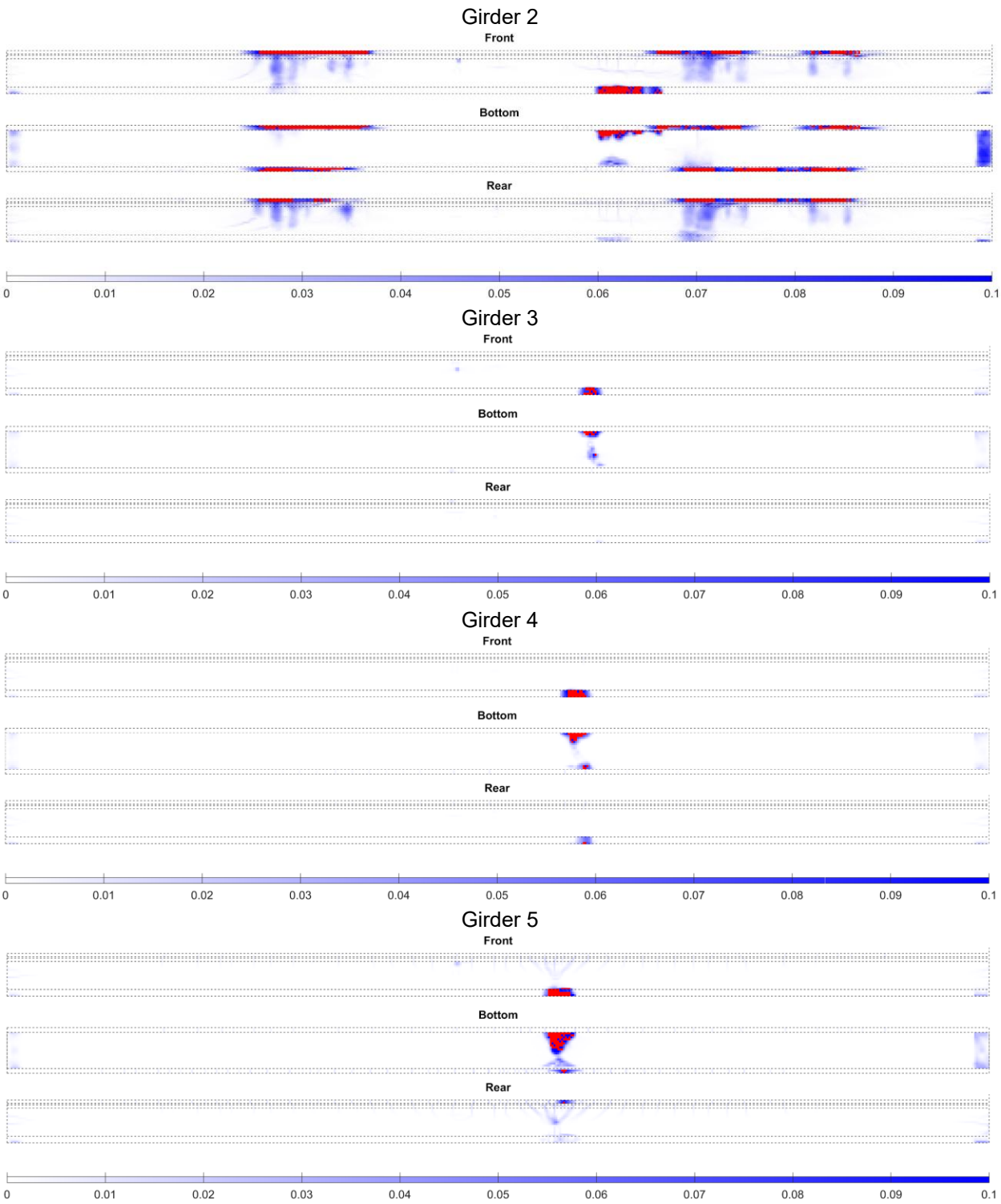

Figure 3.12. Maximum principal strain distributions predicted for each impacted girder by finite element analysis (eroded elements shown in red)

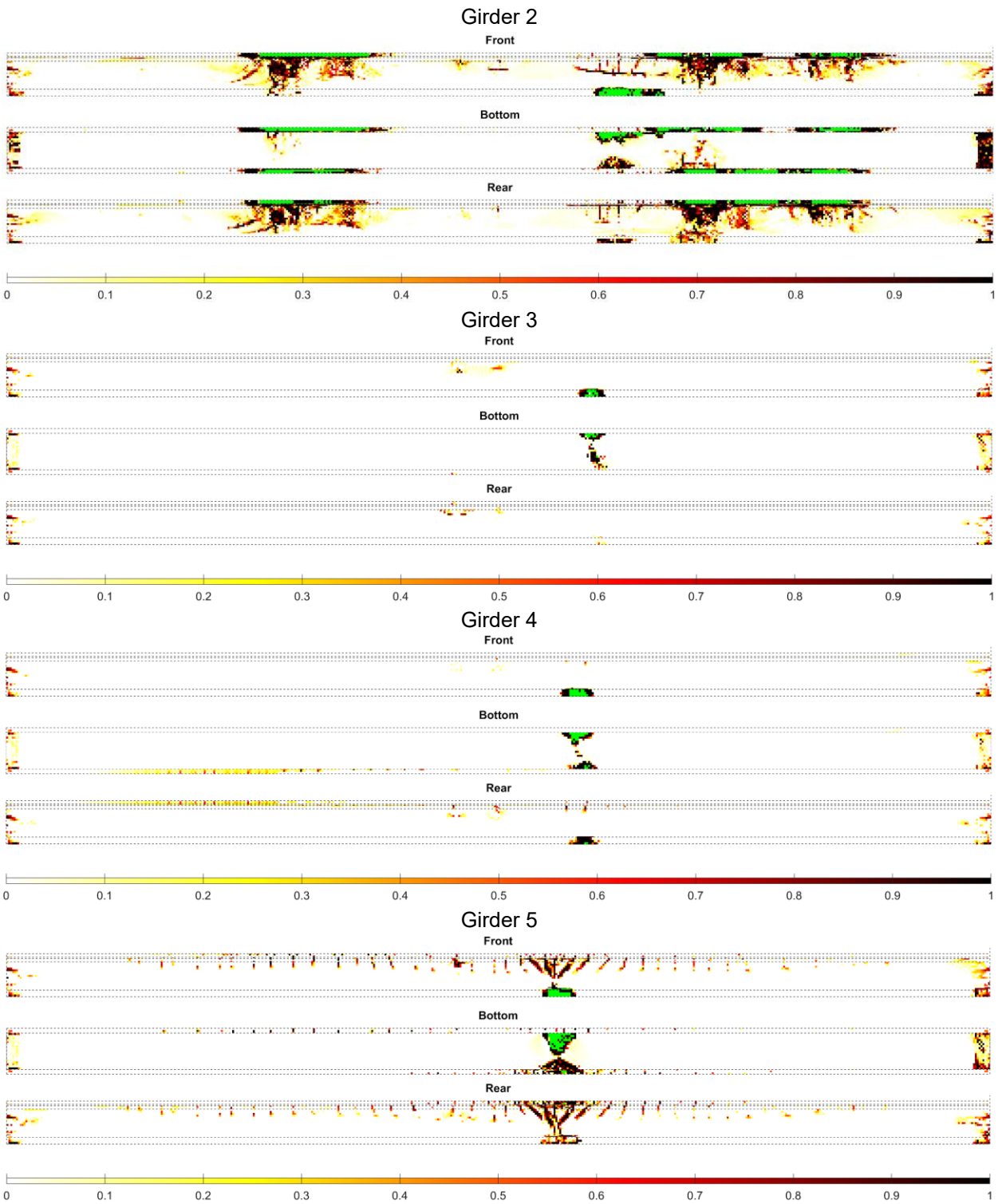

Figure 3.13. Maximum brittle and ductile damage distributions predicted for each impacted girder by finite element analysis (eroded elements shown in red)

4. VULNERABILITY OF PRESTRESSED GIRDERS IN BRIDGES UNDER CONSTRUCTION

The literature review conducted for this study revealed that previous studies on the damage to, and repair of, prestressed concrete girder bridges subject to overheight vehicle impacts have focused primarily on in-service bridges. The vulnerability of prestressed concrete bridges to damage from overheight vehicle impacts during construction, particularly when some components are not yet installed or placed, has not been investigated. However, as summarized in the literature review, recent experimental research anticipates significant differences in the failure mechanisms of laterally impacted girders when the deck is present or not (ElGawady and Abdulazeez, 2024). Furthermore, severe damage adjacent to the sole plate connections observed in the case study presented in the previous chapter of this report suggests unique vulnerability of prestressed concrete girder bridges under construction to damage from uplift forces from overheight vehicle impacts that has not been observed in completed bridges following similar incidences.

In this chapter of the report, girder responses to overheight vehicle impacts are compared for sets of identical overheight vehicle collisions to bridge models representing several stages of construction completion. The parametric analysis includes two different vertical underclearance violations for the dump truck model and a range of different vehicle speeds. Furthermore, this study explores how the presence, location, and type of intermediate diaphragms can influence the response of partially constructed prestressed concrete girder bridges under vehicle impact and the nature and severity of resulting damage.

4.1 Description of Structure

In an effort to explore whether the damages observed in the case study presented in the prior chapter were unique to that particular incident or reflect damages that would be typical for most prestressed concrete girder bridges under construction, the investigation presented in this chapter was performed using a model of a different bridge. To provide variation from the case study, a bridge with a different girder type, different span length, and without skew was selected from the set of bridge plans provided to the research team by the Steering and Implementation Committee. This bridge was a two-span structure with each span constructed using five (5) AASHTO Type IV girders spaced at 8 ft 2 in on center. The girders support an 8-inch reinforced concrete deck with an out-to-out width of 38 ft 9 in. Each span is nominally identical in design, with girder spans of 98 ft 4.5 in measured from the center of the bearings and mono-sloped at 0.020 ft/ft. Each girder is prestressed using 26 low relaxation Grade 270 strands of 0.6 in diameter. Six of the strands are draped with hold-down points at 5 ft from the midspan. Intermediate diaphragms located at the midspan are constructed from MC18x42.7 channels that are bolted to L6x6x1/2 angles connected to the girders. Figure 4.1 presents the cross section of the superstructure at the midspan and an elevation view that indicates the location of the intermediate diaphragms. This bridge model was specifically selected because it has no skew. Since steel channel intermediate diaphragms follow the skew for moderate skew angles, while reinforced concrete diaphragms are oriented normal to the girder web, this bridge model allows for comparison between the behavior exhibited by each intermediate diaphragm type without introducing the diaphragm orientation as an additional variable. This bridge model was utilized for additional analysis in Chapter 5 of this report, wherein it is referred to as Bridge A.

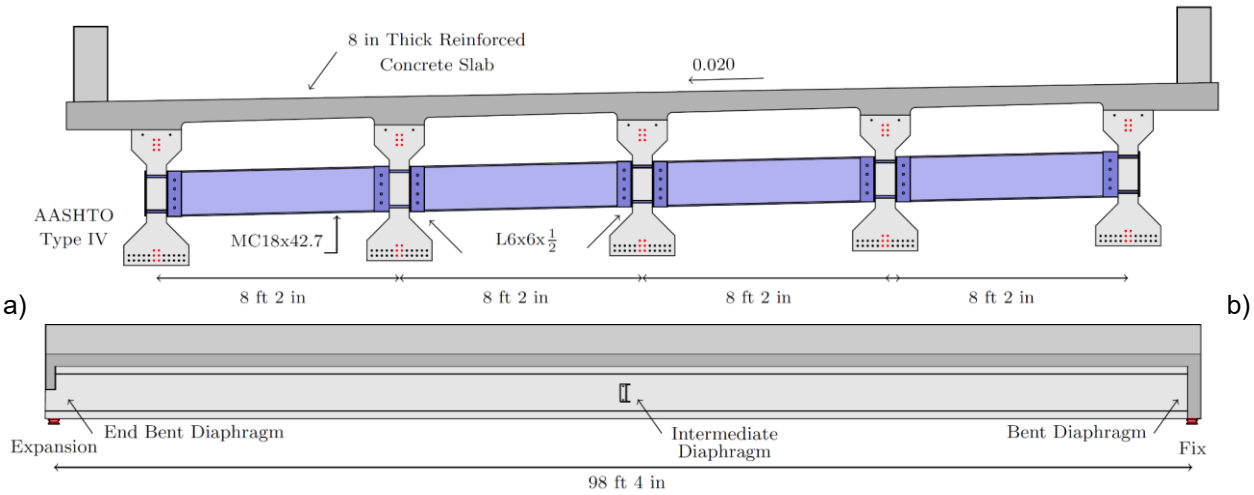

Figure 4.1. Dimensions and details for bridge span (Bridge A) modeled to investigate vulnerability of prestressed concrete bridge girders during construction: a) cross section (draped strands shown in red); b) elevation view

4.2 Parametric Modeling

In total, four bridge models were developed to represent the bridge during three different phases of construction and to contrast the performance of reinforced concrete intermediate diaphragms with steel channel intermediate diaphragms. The first model represents the complete bridge as designed, incorporating all components, including steel channel intermediate diaphragms, concrete deck, and reinforced concrete end bent and thru-bent diaphragms. The second bridge model includes the steel channel intermediate diaphragms indicated in the bridge plans, but does not include the concrete deck, end bent diaphragms, or thru-bent diaphragms. This model represents a partially constructed bridge at the same stage of construction as the case study structure discussed in the previous chapter. The third model mirrors the second one in producing a scenario of an under construction bridge prior to placement of the deck but includes 8 in thick reinforced concrete intermediate diaphragms in place of the steel channel intermediate diaphragms. The final model features the bridge girders without any diaphragms or concrete deck and corresponds to the short period of time after the girders have been placed but prior to the installation of the diaphragms. This model is also useful for producing predictions of the response of prestressed concrete girders in bridges without intermediate diaphragms that are under construction. The NCDOT Structures Management Unit Manual requires the placement of an intermediate diaphragm at the midspan for prestressed concrete girder bridges with a span length between 40 ft and 100 ft, but this practice varies by state. Figure 4.2 presents renderings of the four different bridge models included in this investigation. All models were developed with the CAE with the same staged introduction of prestressing and gravity forces as well as identical boundary conditions.

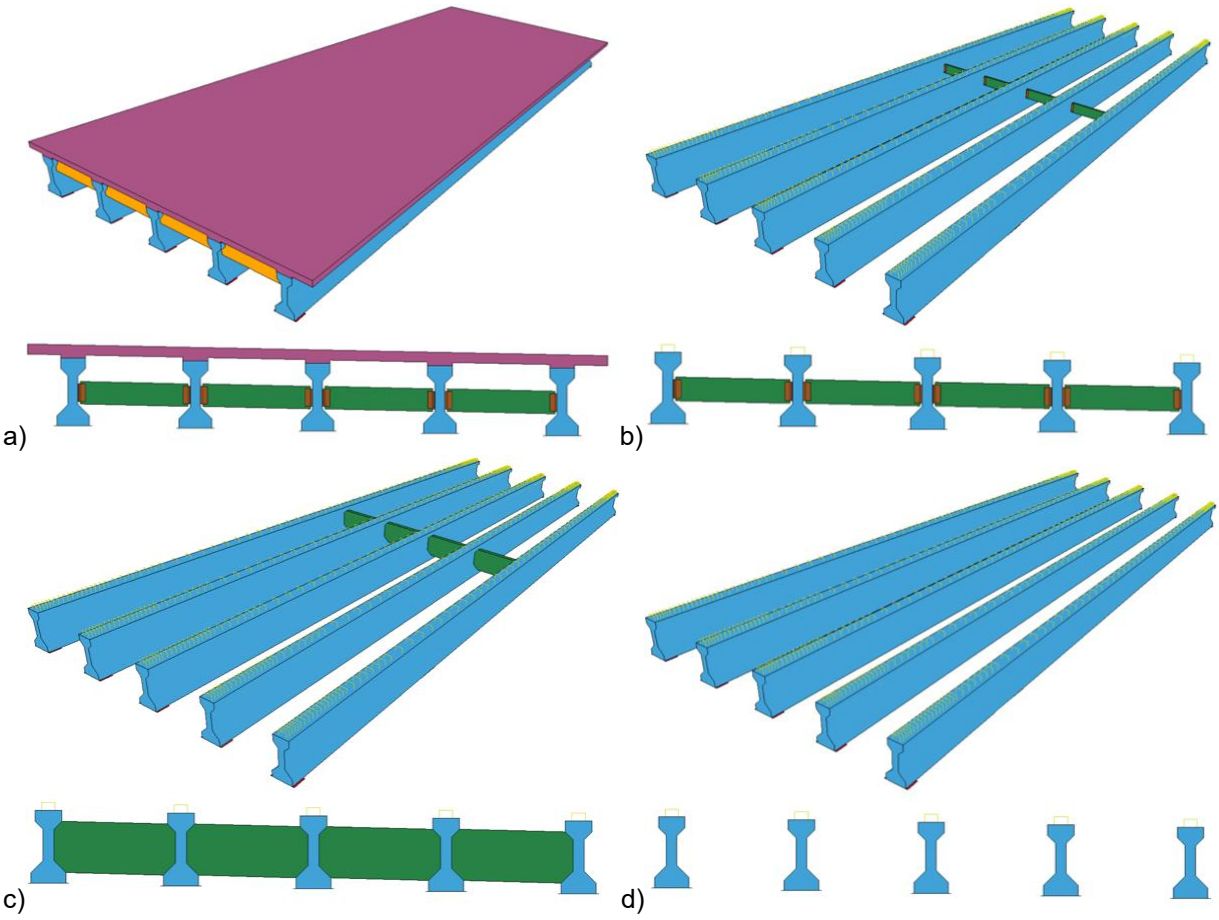

Figure 4.2. Bridge models included in parametric analysis: (a) completed bridge with deck; (b) without deck but with steel intermediate diaphragms; (c) with reinforced concrete intermediate diaphragms; (d) without deck or intermediate diaphragms

The dump truck model introduced in the prior chapter of this report was used to simulate overheight vehicle impacts to each of the four bridge models. Two different vertical underclearance violation scenarios were considered. The first, referred to as a "shield impact," corresponds to an overheight underclearance violation of approximately 4 inches, which results in the exterior girder of the bridge being impacted at the midheight of its bottom flange by the protective extension of the dump bed that overhangs above the cab. The second scenario, referred to as a "back wall impact," corresponds to a significantly greater vertical underclearance violation resulting in the back wall of the dump bed directly impacting the bottom flange of the exterior girder. For both impact scenarios, the dump truck was aligned normal to the bridge girders and centered at the midspan of the bridge, which corresponds to the location of the intermediate diaphragms. Figure 4.3 provides renderings of the position and orientation of the dump truck for each of the two vertical underclearance violation scenarios considered. Since the camber of the bridge is affected by the presence of the bridge deck, the elevation of the dump truck was adjusted correspondingly so that the initial location of contact with the girder was consistent for bridge models with and without the deck present. For each bridge model and for each of these two vertical underclearance violation scenarios, simulations were performed for initial dump truck velocities of 15 mph, 20 mph, 25 mph, 30 mph, 35 mph, 40 mph, 45 mph,

50 mph, and 55 mph. Consequently, the parametric analysis described in this chapter of the report consisted of a total of 72 different finite element analyses.

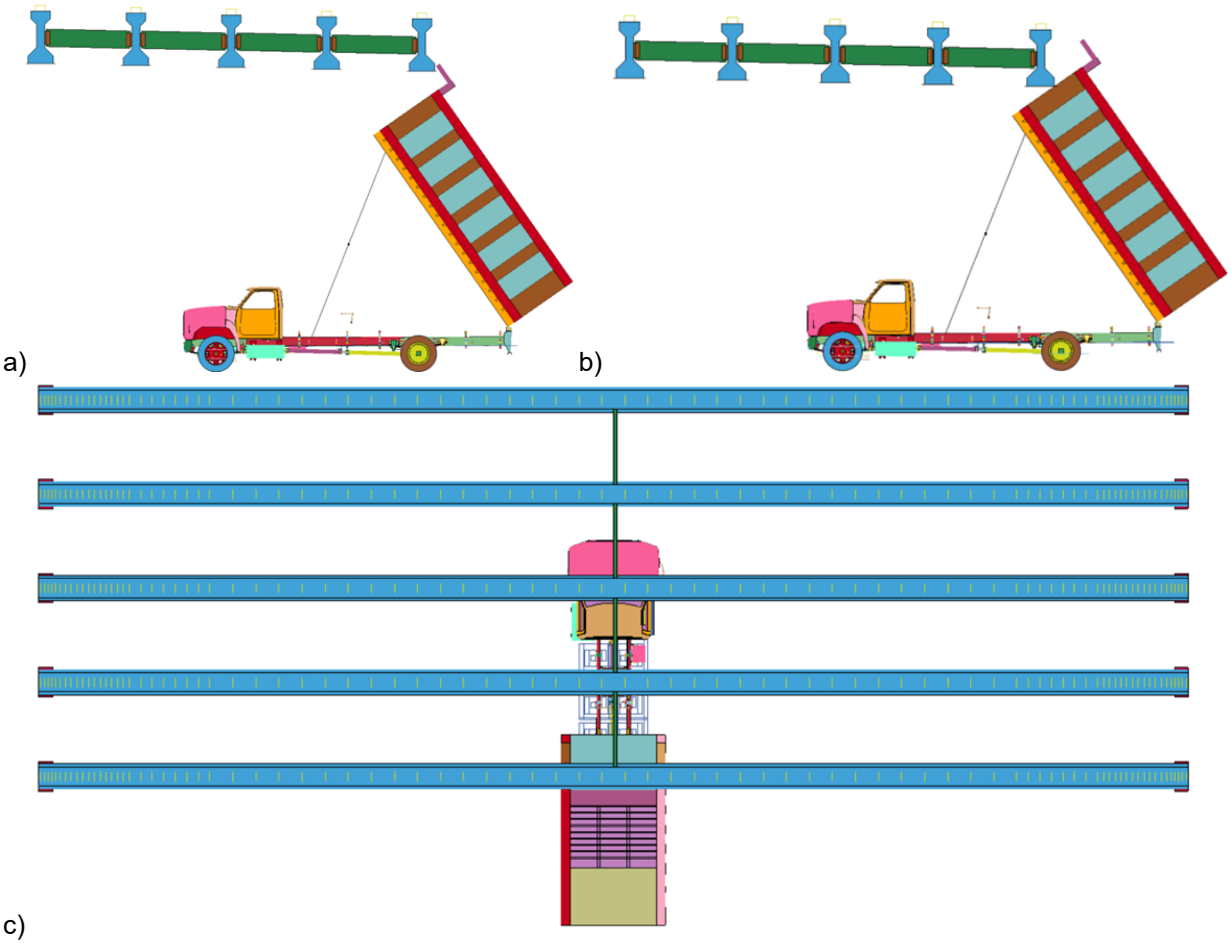

Figure 4.3. Vehicular impact scenarios evaluated for parametric analysis; a) shield impact; b) back wall impact; c) position and alignment of dump truck for both impact scenarios

For all bridge models without the deck present, the higher intensity impact involving collision of the back wall of the dump truck with the exterior girder of the bridge caused girder collapse at all initial truck velocities included in the parametric analysis. In contrast, the simulations forecast that the bridge model with the deck present was able to resist the impact forces from the back wall impacts for all initial truck velocities, albeit while sustaining severe damage at the higher initial truck velocities. Figure 4.4 presents a subset of the results for the damage predicted to the exterior girder of the complete bridge model from collision of the back wall of the raised bed of the dump truck. For lower truck velocities, the predicted damage is limited to spalling and longitudinal cracking along the web-to-flange transition (Figure 4.4a). As the initial velocity of the truck was increased, the severity of the damage increased significantly and the damage began to include the D-shaped cracking that has been widely reported in prior case studies of prestressed concrete girder bridges severely damaged by overheight vehicle impacts, as detailed in the literature review. Shear push-out failure was also indicated by the simulations run with the complete bridge model for the highest initial truck velocities. The consistency of the predicted damage mechanisms

produced in the simulations for different impact velocities with case studies from the literature further supports the plausibility of the simulation results. The bridge models replicating the condition of bridges under construction prior to the placement of the deck all predicted girder collapse followingimpacts from the back wall of the raised bed of the dump truck at all of the speeds investigated. Consequently, the remainder of this chapter of the report will focus on the simulations involving collision of the shield of the dump truck with the girders. However, the significant difference in the resistance of the girders predicted when the deck was present compared to when the deck was absent emphasizes the vulnerability of prestressed concrete girders to severe damage if subjected to overheight vehicle impacts while under construction.

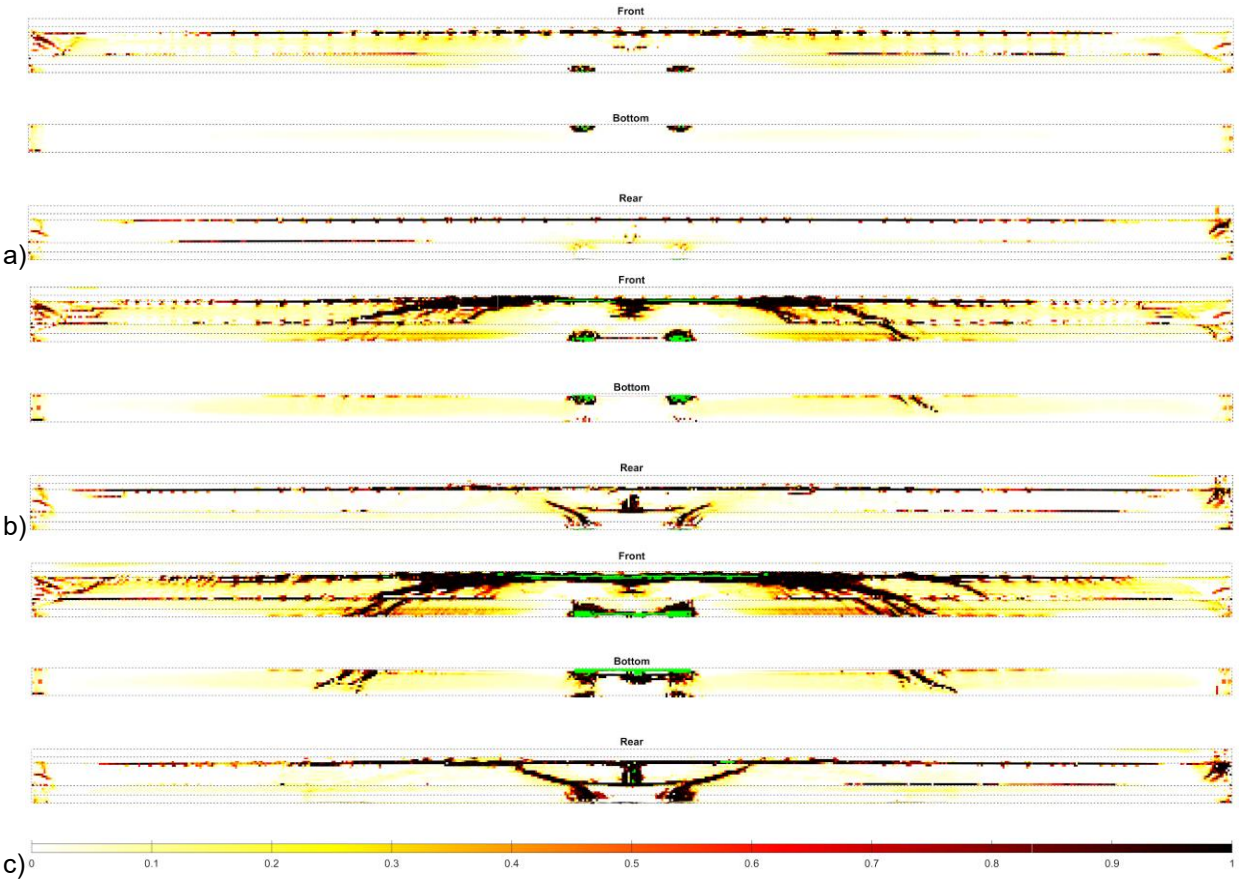

Figure 4.4. Predicted damage to exterior girder of complete bridge model with deck from back wall impact from raised bed of dump truck: a) 15 mph; b) 35 mph; c) 55 mph

Prior to investigating how the different bridge models responded to the simulated impacts from the shield of the raised bed dump truck, the contact force time histories were evaluated to examine whether the presence of the deck or type of intermediate diaphragm significantly influenced the collision forces. Figure 4.5a and 4.5b present a comparison of contact force time histories obtained for the four different bridge models when the shield impact was simulated for an initial truck velocity of 45 mph. In general, the contact force time history is shown to be largely unaffected by the presence of the concrete deck or the presence and type of intermediate diaphragm. Figure 4.5c presents the peak lateral impact force predicted by the finite element analysis for each bridge model and each initial truck velocity. As expected, the peak impact

force increases with velocity and the results indicate that there is no significant difference in peak impact force across the three bridge models without a bridge deck for each velocity examined. When the bridge deck is present, the peak impact force tends to slightly reduce, especially for higher initial truck velocities. However, when the deck was present in the model, the duration of the contact was slightly longer, resulting in a total impulse that was very similar to the total impulse of the contact forces for the three bridge models without the deck (Figure 4.5d). It was somewhat unexpected that the total impulse increased with initial truck velocity up to 35 mph and then decreased. However, a careful examination of the simulations revealed that the reason for the change in the trend is that at velocities at or below 35 mph the shield of the dump truck remains in contact with the girder for a longer period of time, pushing on the girder as the truck slides under the bridge. At higher velocities, the shield yields or buckles in flexure after some period of contact, resulting in a reduced total duration of contact. This behavior would be dependent on the characteristics of the dump truck shield. Longer, thinner, or otherwise more flexible shields will likely exhibit this change in response at lower velocities, while shorter or stronger shields will sustain increases in impulse to higher initial velocities. Tabular peak lateral force and impulse values for all of the shield impact simulations are provided in Table 4.1.

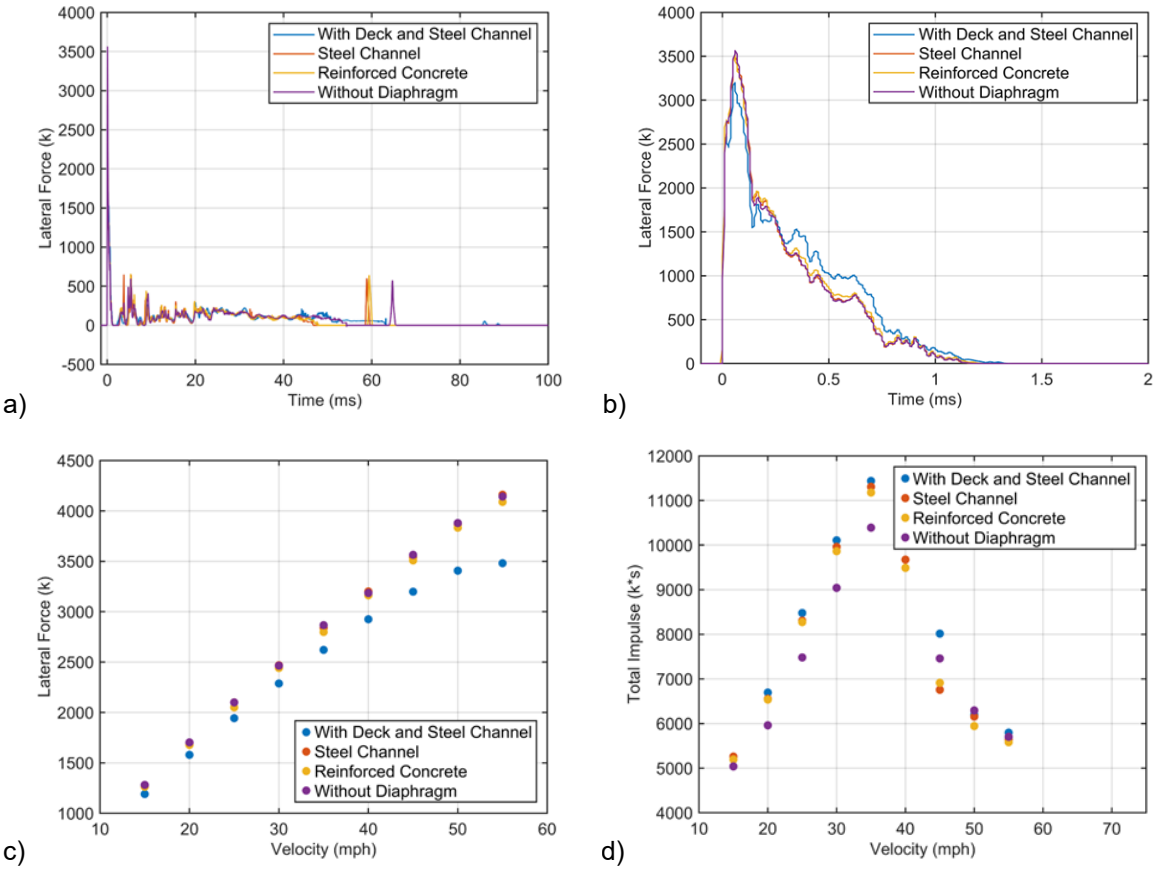

Figure 4.5. Comparison of lateral impact forces for shield impact: a) force time histories for 45mph impact; b) initial 2 ms of force time histories for 45 mph; c) peak lateral forces for different initial dump truck velocities; d) total impulse for different initial dump truck velocities

Table 4.1. Peak lateral force and total impulse for shield impact models

Shield Impact								
mph	Peak Lateral Force (k)				Total Impulse (k·ms)			
	With Deck and Steel Channel	Steel Channel	Reinforced Concrete	Without Diaphragm	With Deck and Steel Channel	Steel Channel	Reinforced Concrete	Without Diaphragm
15	1,191	1,266	1,263	1,282	5,194	5,259	5,193	5,039
20	1,580	1,697	1,678	1,704	6,695	6,554	6,537	5,961
25	1,944	2,101	2,051	2,100	8,478	8,306	8,273	7,481
30	2,288	2,469	2,442	2,465	10,107	9,960	9,863	9,041
35	2,621	2,841	2,799	2,867	11,438	11,307	11,178	10,391
40	2,925	3,201	3,163	3,185	10,125	9,674	9,489	11,541
45	3,198	3,541	3,509	3,564	8,015	6,757	6,913	7,459
50	3,407	3,869	3,833	3,879	6,194	6,157	5,944	6,294
55	3,481	4,160	4,089	4,143	5,796	5,641	5,582	5,704

The lateral displacement of the impacted girder was found to be significantly influenced by the presence of the deck and presence of the intermediate diaphragm. Figure 4.6a presents a comparison of displacement time histories for the case of shield impact for the initial truck velocity of 45 mph. The displacement time histories presented in this figure are for a node centrally located on the bottom flange of the exterior girder at the midspan. As expected, the configuration without a deck or intermediate diaphragms exhibited the greatest peak lateral displacement under the impact. Additionally, the period of the dynamic response of the girder for this model was notably longer than that of the models with intermediate diaphragms. The significantly reduced lateral displacement and period of the response when the intermediate diaphragm was present indicates that the intermediate diaphragms transfer significant force to the interior girders and result in a stiffer overall response to the impact. When the deck was also present, the peak lateral displacement following the impact from the shield of the dump truck was further reduced. The period of the response was also significantly reduced because minor axis flexure of the girder was largely suppressed by the presence of the deck, with the girder response to the lateral impact force being dominated by lateral-torsional behavior. Figure 4.6b presents the predicted peak lateral displacement for each model against the initial truck velocity. The results demonstrate that the noted observations regarding the effects of the deck and intermediate diaphragms were not limited to the case of 45 mph initial truck velocity. Furthermore, the peak displacement results indicate that the maximum dynamic response was predicted for an initial truck velocity of 35 mph, which corresponds to the velocity at which the maximum impulse of the contact force was observed. As previously noted, at higher velocities, the contact duration was shortened by failure of the shield in yielding or buckling. The fact that the peak dynamic displacement follows the trend in the impulse rather than the peak force suggests that the girder response to the impact from the shield of the dump truck falls within the dynamic region of response rather than exhibiting characteristics of structural response to highly impulsive loadings. Table 4.2 provides the data presented in Figure 4.6b in tabular format to allow for a clearer comparison between the results obtained for the models with intermediate diaphragms. With the exception of the 15 mph initial velocity, the peak inward lateral displacement was greater for the models without the deck when the intermediate diaphragm was a steel channel compared to a reinforced concrete intermediate diaphragm.

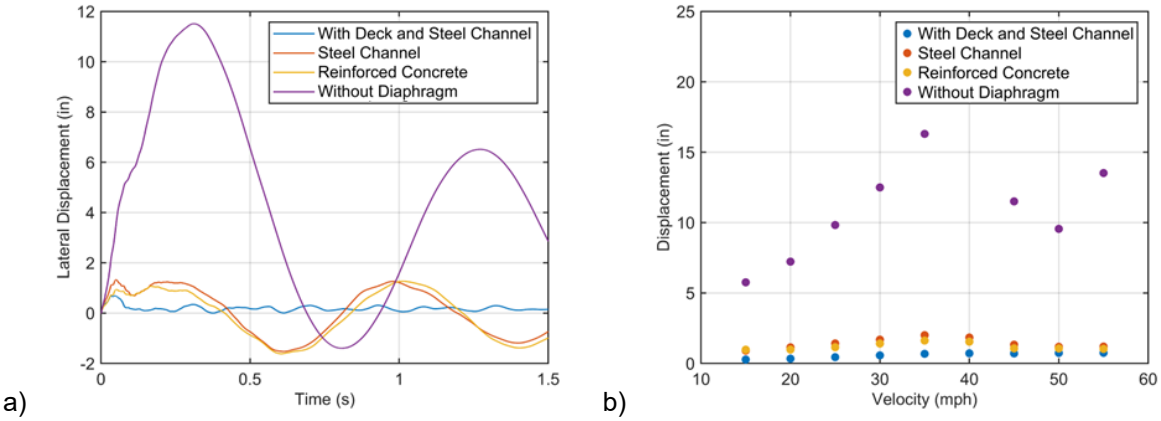

Figure 4.6. Comparison of lateral displacement for shield impacts: a) displacement time histories for 45 mph initial velocity; b) peak inward displacement against initial velocity

Table 4.2. Peak inward lateral displacement during first period of response for shield impact

Peak Inward Displacement (in)				
mph	With Deck and Steel Channel	Steel Channel	Reinforced Concrete	Without Diaphragm
15	0.28	0.91	0.97	5.76
20	0.34	1.14	0.98	7.23
25	0.44	1.42	1.15	9.83
30	0.57	1.69	1.41	12.50
35	0.68	2.01	1.62	16.30
40	0.72	1.84	1.54	30.55
45	0.71	1.33	1.07	11.51
50	0.74	1.18	1.07	9.56
55	0.75	1.20	1.03	13.52

The damage predicted by the concrete constitutive model provides evidence of both the extent of predicted damage from the impact as well as the nature of the failure mechanisms. Figure 4.7 presents the brittle and ductile damage distributions for each bridge model following impact from the shield with an initial truck velocity of 45 mph. When the deck was present, the predicted damage was limited to spalling of the bottom flange across the surface directly impacted by the dump truck and longitudinal cracking at the web-to-flange interface. Notably, the presence of the deck suppressed the development of any significant damage adjacent to the sole plate connections. In contrast, when the deck was not present in the models, significant damage was predicted adjacent to the sole plate connections. It is expected that a combination of the additional mass of the deck and stiffness contributed by the deck enhances the resistance to uplift forces developed during the dynamic response of the girder to the impact. Similar to the complete bridge model, the bridge models without a deck but with intermediate diaphragms at the midspan exhibited erosion indicative of spalling across the surface directly impacted by the dump truck. However, in the absence of the deck, the models with only intermediate diaphragms exhibited damage patterns consistent with significant major axis flexural response. In both models, damage consistent with flexural cracking was produced in the top flange at the midspan. The extent of longitudinal cracking at the web-to-flange interface was reduced relative to the complete bridge model as a result of the response being a combination of both

major axis flexure and lateral-torsional response. The model without a deck or diaphragms exhibited damages consistent with biaxial flexure of the girder. The damage distributions suggest significant flexural cracking along the top flange, with the cracking being more pronounced and extending over a longer region of the rear side of the girder. This cracking resulted from a combination of both minor axis and major axis flexural response observed in the simulation result.

The simulations predicted that all four bridge models would provide sufficient resistance to the lateral impact from the shield of the dump truck to avoid collapse of the girder, with the exception of the case of a 55 mph impact to the bridge without deck or diaphragms and the case of a 35 mph impact to the bridge without a deck but with steel channel intermediate diaphragms. However, damage adjacent to the sole plate connections was predicted for all of the models without the concrete deck present, even for the simulations involving initial truck speeds as low as 15 mph. This result highlights the particular vulnerability of prestressed concrete girders to damage from overheight vehicle impacts. Figure 4.8 presents the brittle and ductile damage distributions for the models without a deck following impact from the shield of the dump truck travelling at 15 mph. The result is particularly noteworthy not only because of the presence of predicted damage adjacent to the sole plate connections at low truck velocities, but also because damage elsewhere in the girder is largely absent. This result suggests that damage adjacent to the sole plate connection may be the first failure mechanism to occur if prestressed concrete bridge girders are impacted by overheight vehicles prior to construction of the deck. Furthermore, the simulations suggest that it is possible that damage may be present at the sole plate connection even if there are no or only superficial visible signs of distress, such as spalling and cracking, at the impact location. The parametric analysis conducted for this research effort is not conclusive enough on its own to definitively conclude that prestressed concrete girders subjected to lateral impacts of any speed prior to the placement of the deck will require repair or replacement, but the research suggests that supplemental inspections performed following accidental overheight collisions of vehicles to bridges under construction should place particular emphasis on evaluating the condition of the girder adjacent to the sole plate connection.

In addition to highlighting the vulnerability of prestressed concrete girders prior to construction of the deck to damage adjacent to the sole plate connection, the parametric analysis revealed the important role that intermediate diaphragms provide in promoting load sharing between the girders when subject to overheight vehicle impacts. Furthermore, the results suggest that reinforced concrete diaphragms promote greater load sharing, suppress the maximum dynamic displacement, and may increase the resistance of the girder to damage relative to steel channel intermediate diaphragms. The modest improvement in impact resistance offered by reinforced concrete intermediate diaphragms is expected to be the result of greater rotational stiffness introduced to the girder by the deeper reinforced concrete diaphragms, which extend completely from the top flange to the bottom flange. This result is supported by previous finite element analysis conducted in Qiao et al. (2008), which found that full depth reinforced concrete intermediate diaphragms were preferable to partial depth reinforced concrete intermediate diaphragms with respect to lateral force resistance. Brice (2013) reported that WSDOT adopted a requirement that full depth intermediate diaphragms be utilized for all overpasses constructed over routes that carry average daily traffic greater than 50,000 on the basis of that research.

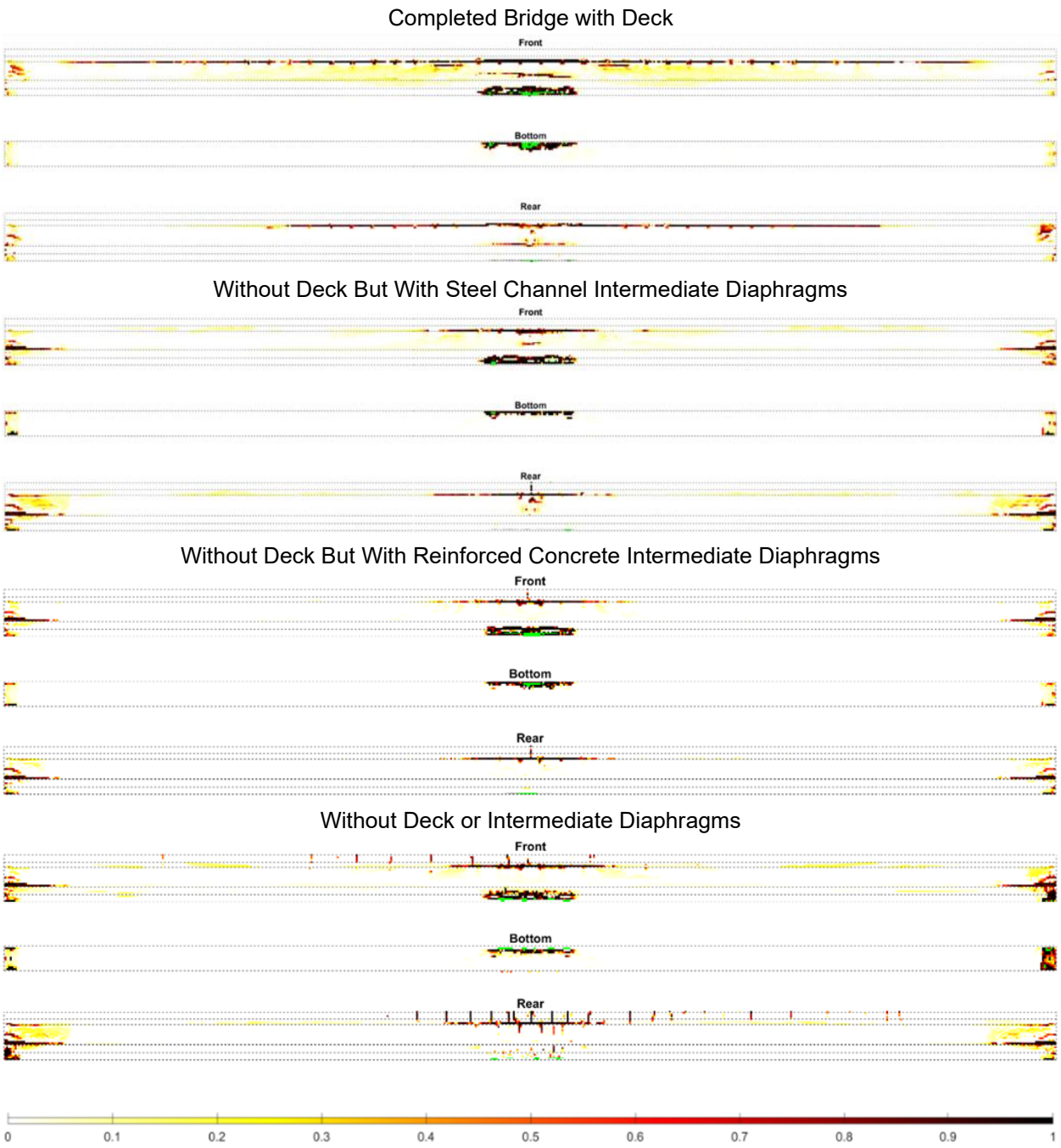

Figure 4.7. Damage predicted for each bridge model following impact from the shield of the dump truck travelling at an initial velocity of 45 mph

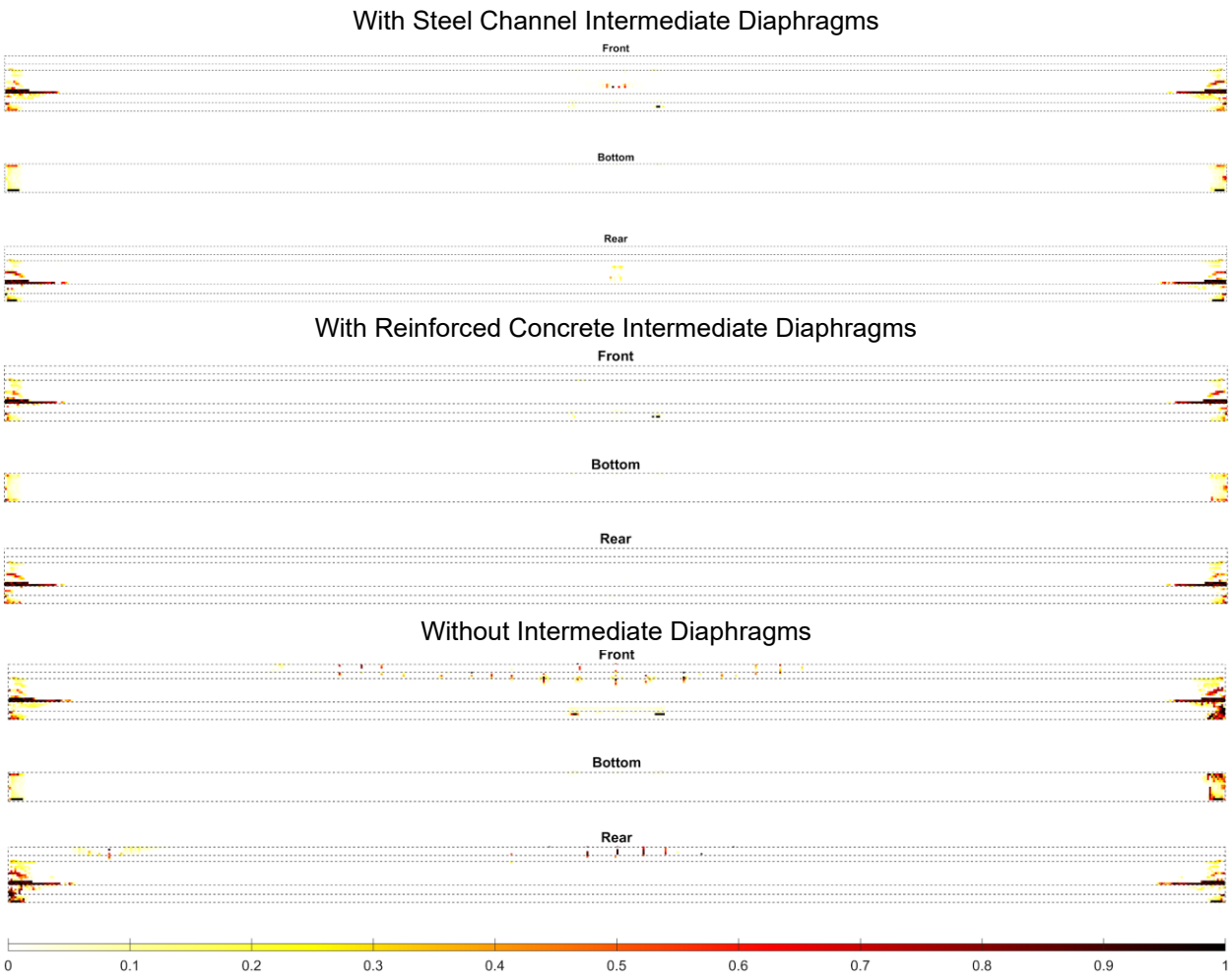

Figure 4.8. Damage predicted for bridge models without a deck following impact from the shield of the dump truck travelling at an initial velocity of 15 mph

5. DEVELOPMENT OF SIMPLIFIED MODEL FOR PREDICTING DAMAGE TO PRESTRESSED CONCRETE GIRDER BRIDGES FROM OVERHEIGHT VEHICLE COLLISIONS

One of the primary objectives of the research effort is to develop a simplified prediction tool for assessing the severity of overheight vehicle impacts to bridges constructed of prestressed concrete girders. The literature review conducted for this study revealed no existing simplified prediction tools for overheight vehicle impacts, but did identify several studies that produced iso-damage curves to provide a means for assessing severity of damage to reinforced concrete bridge columns from vehicular collisions. Iso-damage curves are simply functions that delineate different levels of damage severity using characteristics of the applied loading that influence the structural response and, consequently, the damage. They can be developed for a range of different types of loads and are regularly utilized in blast resistant design and fatigue life assessments, as they offer a simplified alternative to rigorous computational analysis. In the context of assessing structural damage due to impact loading, the iso-damage curves are developed as a function of peak impact force and impulse. Figure 5.1 depicts these impact force characteristics and the concept of iso-damage curves. The impulse associated with a collision is the integral of the contact force over time, which equates to the area under the force time history. Collectively, the peak force and impulse provide insight into the nature of the loading. Impact forces that are highly impulsive are short in duration and generally have high peak force and low impulse, which produce structural response characterized by stress wave propagation. Conversely, if the loading duration is long, the impulse will generally be higher in amplitude and the structural response may approach quasi-static behavior. Between these extrema, the lower-order vibration modes of the structure will be excited and the behavior will be governed by dynamic response. Based on the simulation results presented in Chapter 4 of this report, the predominant behavior of prestressed concrete girders when subjected to overheight vehicle collision from dump trucks with raised beds is expected to be dynamic response.

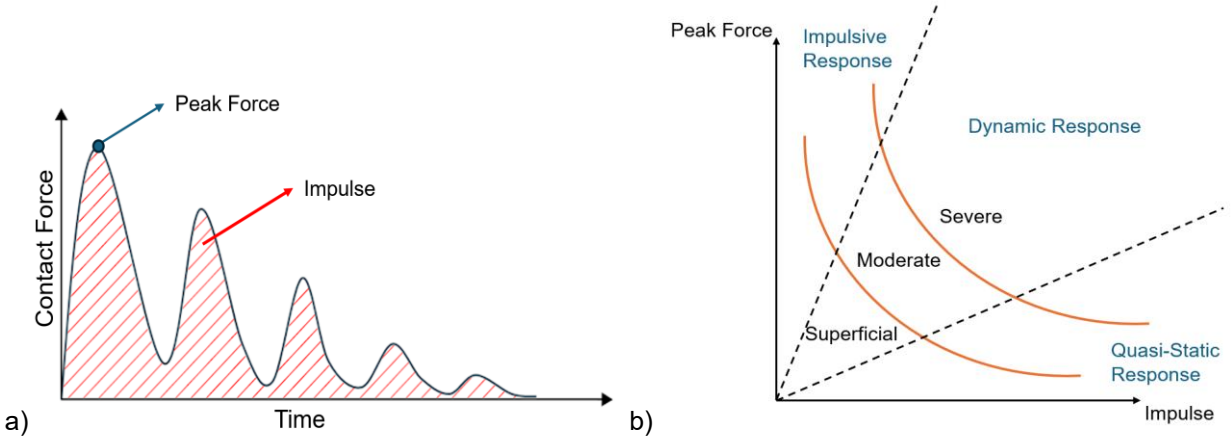

Figure 5.1. Concept of iso-damage curves for simplified assessment of damage severity: a) an impact force time history and its characteristics; b) iso-damage curves that delineate regions of superficial, moderate, and severe damage based on peak impact force and impulse

With iso-damage curves established for a given structure, only a prediction of the peak impact force and impulse associated with the specific impact event are required to arrive at the predicted damage severity.

Since empirical models can be developed to predict the peak impact force and impulse for a given object, iso-damage curves could enable a risk-based assessment of whether damage to an impacted prestressed girder would result in superficial, moderate, or severe damage without having to perform a time consuming case-specific finite element simulation of the incident. In this chapter of the report, a parametric analysis is first conducted to examine the influence of the impact location, velocity, vertical underclearance violation, and angle of the raised bed of the dump truck on the severity of damage to a prestressed concrete girder bridge. The plausibility of a simplified methodology for predicting damage from overheight vehicle collisions based on iso-damage curves is then assessed. Additionally, empirical prediction models are developed to enable estimation of peak impact force and impulse for collisions from a representative dump truck based on truck velocity, bed angle, and overheight underclearance violation.

5.1 Parametric Analysis of Impact Force Characteristics on Damage Severity

To further expand the range of bridge models included in the research effort, the parametric analysis presented in this Chapter of the report involved the development of an additional bridge model based on a set of actual bridge plans provided by the Steering and Implementation Committee. The modeled bridge is a two-span structure, with each span constructed of six AASHTO Type IV girders spaced at 8 ft 1 in on center supporting an 8.25-inch reinforced concrete deck with an out-to-out width of 47 ft 7 in and symmetrically crowned at a slope of 0.020 ft/ft. The modeled span has a length of 77 ft 10 in and the girders are prestressed using 26 low relaxation Grade 270 strands of 0.6 in diameter. Intermediate diaphragms constructed from MC18x42.7 channels are present at the midspan and are bolted to L6x6x1/2 angles connected to the girders. The bridge has a skew angle of 10 degrees (skew of 100 degrees from the bent line), so the intermediate diaphragms are oriented parallel to the bent lines consistent with NCDOT Structures Management Unit Manual. Figure 5.2 presents the cross section of the superstructure at midspan and a plan view to indicate the location and orientation of the intermediate diaphragms. The finite element model of the case study bridge was automatically generated using the Collision Analysis Engine script library described in Chapter 2 of this report. Furthermore, the parametric analyses performed with different impactor characteristics were automatically generated to eliminate the possibility of errors introduced by manual manipulation of the models. This bridge model is referred to throughout this report as Bridge B.

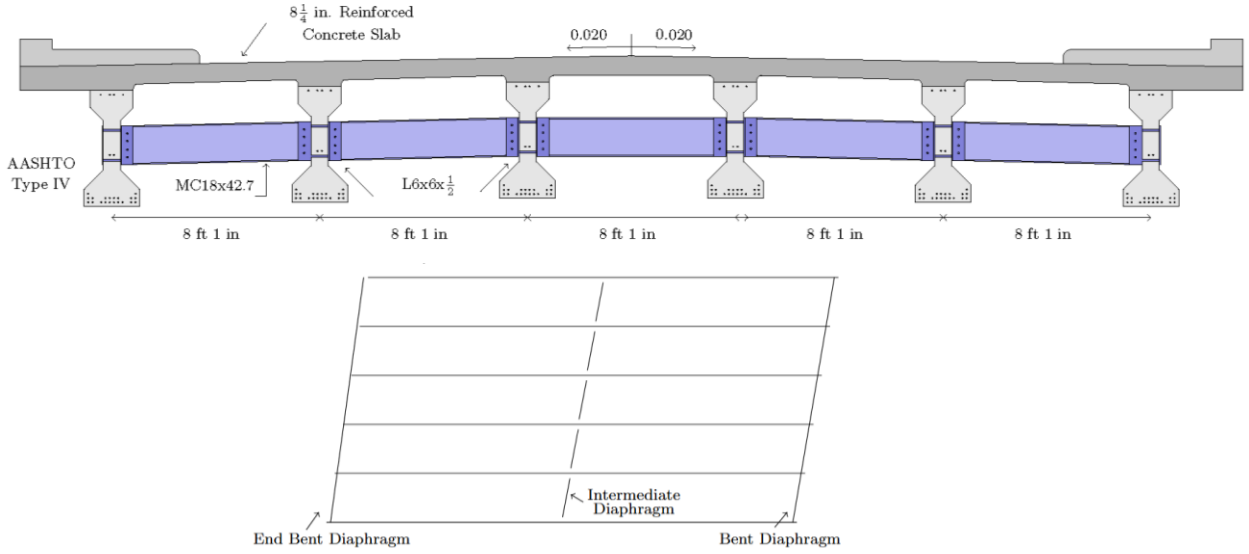

Figure 5.2. Dimensions and details for bridge span (Bridge B) used to formulate simplified damage prediction model

A matrix of cases was established to examine the influence of the characteristics of the dump truck, including vertical underclearance violation, velocity, and angle of the raised bed, on the severity of damage to prestressed concrete girder bridges. Furthermore, a total of three different locations of impact along the length of the girder were included in the parametric analysis to explore the influence of impact location on the predicted damage. The first parameter, the vertical underclearance violation, was discretized into four cases, referred to herein as the "impact scenario". The four scenarios are shown in Figure 5.3. The first two scenarios involve collisions resulting in impact of the back wall of the truck bed with the bottom flange of the girder and last two scenarios result in impact of the dump shield with the bottom flange. In Scenario 3, the initial contact between the shield and the bottom flange occurs at the top of the vertical surface of the bottom flange, while in Scenario 4 the initial contact occurs at the bottom corner of the flange. These two scenarios are expected to be representative of the minimum and maximum bounds of damage expected for overheight impact from the shield of the modeled dump truck. Since the velocity of the dump truck will have a significant influence on the impact force characteristics and resulting damage to the impacted girder, simulations were performed for each of the four scenarios with six different initial truck velocities: 15, 25, 35, 45, 55, and 65 mph. In addition, since the angle of the raised bed is variable, four discrete values (35°, 45°, 55°, and 65°) were included in the parametric analysis. These different bed angles are shown for Scenario 1 in Figure 5.4. Lastly, to investigate the effect of the location of the impact along the span, the longitudinal location of impact was varied to include three positions: midspan, third point, and quarterpoint of the exterior girder. Collectively, the parametric analysis described in this section of the report consisted of 288 different analyses with unique combinations of vertical underclearance violation, initial truck velocity, bed angle, and longitudinal location of impact.

Each of the 288 different analyses were performed by restarting the same finite element model, which was first initialized to introduce prestressing and gravity forces following the staged construction of the model described in Chapter 2. Each impact simulation was performed as an explicit dynamic analysis over a total time increment of 500 milliseconds. Following the simulations, the reported global energy components of each model were examined to ensure that the ratio of hourglass energy to internal energy was reasonable and that the internal and kinetic energy components did not exhibit unexpected behavior. By predefining analysis outputs for components of interest for the key quantities of interest from the finite element analysis, including the strain components for the solid elements that model the girders, the axial force in the beam elements that model the strands, and the contact force time histories, output files were generated that could be parsed in an automated way to expedite the processing of the parametric analysis results and ensure consistent calculation of performance indicators.

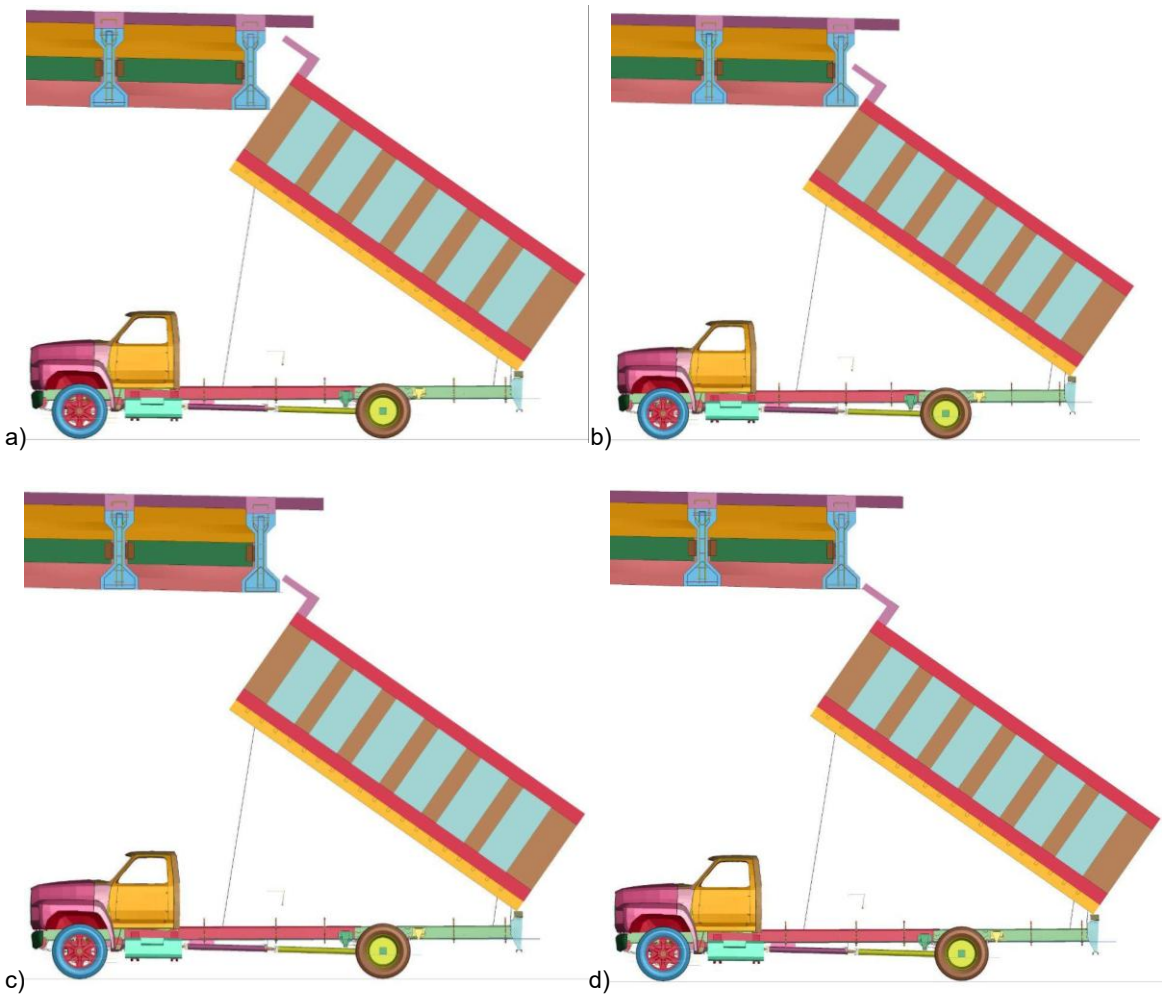

Figure 5.3. Vehicular impact scenarios included in parametric analysis for formulation of simplified damage prediction model: a) Scenario 1; b) Scenario 2; c) Scenario 3; d) Scenario 4

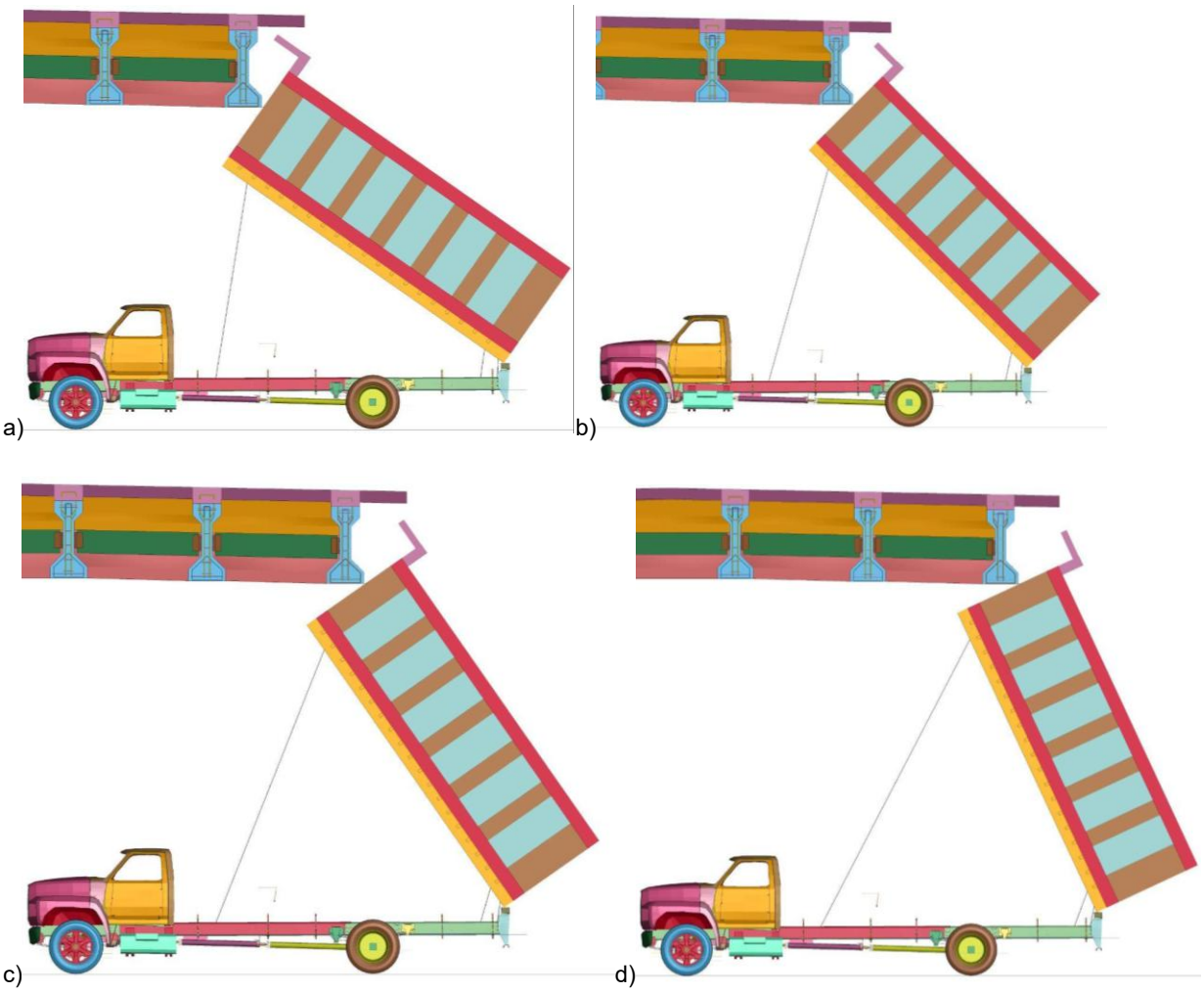

Figure 5.4. Vehicular different angles included in parametric analysis for formulation of simplified damage prediction model: a) 35° 1; b) 45° 2; c) 55° 3; d) 65°

5.2 Classification of Damage Severity

Following an accidental overheight collision, a critical determination that needs to be made is whether the incident requires immediate partial or full closure and subsequent structural repair or replacement of the affected girders, requires only repairs to remediate concerns related to the long-term durability of the girder, or is superficial in nature and can be accepted without repair. Since the envisioned simplified model relies on iso-damage curves that are associated with specific definitions of damage thresholds, a classification of damage was established in an effort to categorize impact events falling into each of these categories of likely maintenance action. Classification of damage severity based on visual inspection has been the topic of several studies focused on repair strategies for prestressed concrete girders subjected to overheight vehicle impact. Synthesis of the indicators for the threshold at which repair actions are recommended revealed that damage is typically considered superficial (i.e. repairs would only be undertaken for aesthetic reasons) if limited to "shallow spalls, nicks and cracks, scrapes and some efflorescence, rust or water stains" (Harries et al. 2012). Damage is classified as moderate if repair is required to address durability-related issues, such as larger cracks and spalling significant enough to expose, but not significant enough to require structural repairs to address reduction in strength limit state capacities. The threshold at which damage is

considered severe is typically when structural repairs are required. Visual damage indicators are this damage threshold are rupture of strands and loss of camber due to the associated loss of prestress (Harries et al. 2012).

A key aspect of processing the results from the parametric analysis was to establish criteria for classifying the predicted severity of damage for each simulation based on the outputs from the finite element analysis. Two outputs were primarily used to support the classification of damage. The first was the distribution of maximum principal strains and erosion in the model, which reflect the predictions of cracking and spalling in simulation, respectively. The second was the residual axial force distribution in the strands of the girder following simulation of the impact. A script was written to parse the axial force in all strands in the girder and calculate three key indicators: 1) the largest percentage reduction in total prestress force in any cross section along the length of the girder (the transfer length at the ends of the girder excluded); 2) the number of individual strands exhibiting a loss of prestress greater than 25%; and, 3) the number of individual strands exhibiting a loss of prestress greater than 80%. The last indicator would capture both strands that were predicted to rupture as a result of the impact as well as strands that were fully exposed, resulting in a total or near total localized loss of prestress.

In an effort to classify the damage severity consistent with the conventional visual indicators described above, criteria for superficial damage was established as less than 5% loss of total prestress force and the absence of a clear indication of either shear cracking in the web of the girder or significant spalling from the plot of the maximum principal strain distributions across the surface of the impacted girder. Conversely, the criteria for severe damage was established as a total loss of prestress force exceeding 20%. All cases falling between these criteria were labeled as moderate damage. For illustration, Figure 5.5 presents maximum principal strain and erosion distributions across the front, bottom, and rear of the impacted girder for Scenario 1 impact at the midspan with the raised bed of the truck at an angle of 35° for three different initial velocities. Consistent with prior chapters, the colormap of the maximum principal strain is limited to 10% strain. In these distributions, dark blue highlights regions of predicted visible distress, such as cracking, and red indicates the location and extent of spalling identified by the finite element analysis by erosion of elements. Appendix C provides the maximum principal strain distributions for all 288 cases. The corresponding Table 5.1 summarizes the quantitative indicators calculated from the axial forces in the strands at the end of the simulation. The 15 mph case presented was selected because it is close to the threshold between superficial and moderate damage, but is classified as superficial due to the absence of definitive shear cracks along the front surface and spalling limited to a shallow depth. The indication of a longitudinal crack along the top of the web is expected under the action of the lateral load, but by itself is not considered a significant concern with respect to the strength or durability of the girder. The axial forces in the strands at the end of the simulation reflected essentially no loss of prestress following the impact, with only one strand exhibiting a loss of more than 25% of the original prestress force. As the velocity of the dump truck was increased from 15 to 35 mph, clear evidence of shear cracks developed in the maximum principal strain distribution and the predicted spalling increased to the extent that exposure of strands would be likely. The increased damage is also reflected in the quantitative indicators, which indicate 13 strands with at least 25% loss of prestress and a 7% loss of total prestress. Lastly, as the velocity of the dump truck was increased to 55 mph the loss of total prestress exceeded 20% with 22 of the strands experiencing a reduction in prestress force of at least 25%. As reflected in the distribution of maximum principal strain and erosion, the predicted damage to the girder is severe and expected to impact the structural capacity.

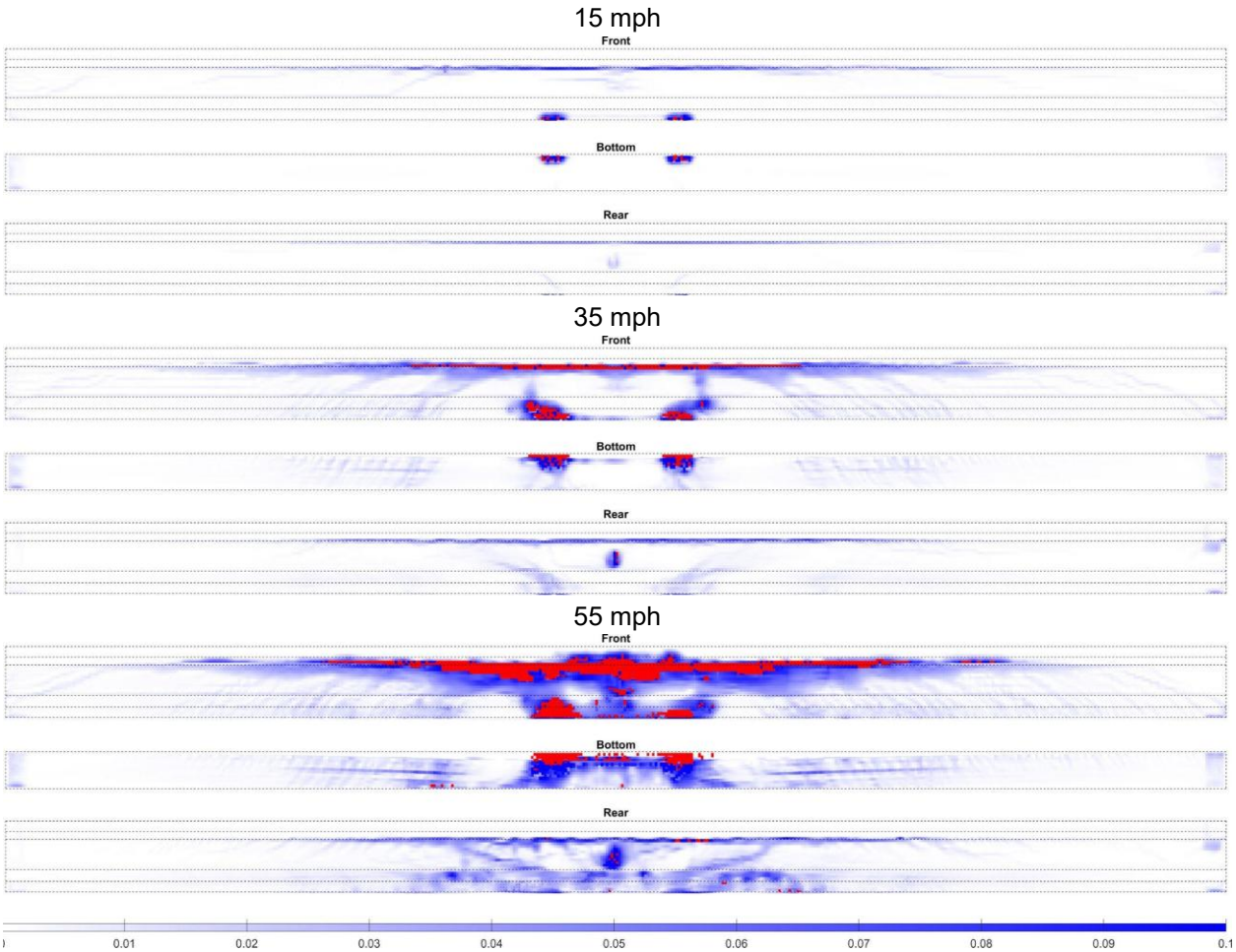

Figure 5.5. Representative maximum principal strain and erosion distributions for three simulations performed with a Scenario 1 impact at midspan with a bed angle of 35°

Table 5.1. Example of key damage indicators for three simulations performed with a Scenario 1 impact at the midspan with a bed angle of 35°

Initial velocity	Total prestress force loss %	Number of strands with 25% loss	Number of strands with 80% loss	Maximum Principal Strain	Damage Level
15 mph	0	1	0	0	Superficial
35 mph	7	13	0	2	Moderate
55 mph	22	22	0	2	Severe

The damage classification criteria was applied to all 288 simulations included in the parametric analysis conducted with the Bridge B model. Tables 5.2 through 5.5 provide the key indicators and assigned classification for each of the simulations. In these tables, the cells colored in green correspond to cases classified as superficial damage, those in yellow are classified as moderate damage, and those in red are classified as severe damage. There are four instances where the cells are empty and shaded grey. These four instances were identified as outliers due to unanticipated results. These four instances represent only 1% of the simulations, so their omission from the subsequent analysis is insignificant. The tables reveal underlying trends that suggest correlation between characteristics of the dump truck and the severity of

damage. As expected, increasing initial velocity of the dump truck correlates with increased severity of damage, especially for the scenarios involving collision of the back wall of the raised bed with the girder. Additionally, for these scenarios, lower angles of the raised bed correlate with increased damage severity. This is expected since increasing the angle of the raised bed increases the moment arm between the reaction force imparted on the truck and the center of gravity of the truck, thereby increasing the ease by which energy is released by raising the cab of the dump truck. Lastly, as expected, the severity of damage tends to decrease for the same velocity and angle of the raised bed as the vertical underclearance violation is reduced (i.e. from Scenario 1 down to Scenario 4). For the scenarios involving impact from the shield of the dump truck, only one of the cases was classified with severe damage.

Table 5.2. Classification of damage severity for Scenario 1 simulations

Impact at Midspan						
	15 mph	25 mph	35 mph	45 mph	55 mph	65 mph
35°	0%, 1, 0	1%, 8, 0	7%, 13, 0	23%, 22, 0	22%, 22, 0	34%, 22, 4
45°	0%, 0, 0	0%, 3, 0	4%, 16, 0	19%, 22, 0	26%, 22, 0	34%, 22, 2
55°	0%, 1, 0	0%, 1, 0	1%, 8, 0	9%, 16, 1	25%, 22, 0	34%, 22, 0
65°	0%, 0, 0	0%, 1, 0	0%, 3, 0	0%, 9, 0	1%, 11, 0	11%, 18, 2
Impact at Third Point						
	15 mph	25 mph	35 mph	45 mph	55 mph	65 mph
35°	0%, 1, 0	3%, 6, 0		24%, 22, 1	32%, 22, 1	36%, 23, 3
45°	0%, 1, 0	2%, 5, 0	8%, 20, 0	29%, 22, 3	38%, 22, 4	30%, 22, 4
55°	0%, 0, 0	0%, 1, 0	6%, 13, 0	17%, 22, 1	33%, 22, 2	29%, 22, 0
65°	0%, 0, 0	0%, 1, 0	1%, 7, 0	8%, 19, 0	11%, 21, 0	13%, 22, 1
Impact at Quarterpoint						
	15 mph	25 mph	35 mph	45 mph	55 mph	65 mph
35°	0%, 1, 0	4%, 7, 0	6%, 21, 0	15%, 9, 2	25%, 22, 1	27%, 22, 2
45°	0%, 1, 0	1%, 6, 0	11%, 22, 0	9%, 21, 0	16%, 22, 0	35%, 22, 8
55°	0%, 0, 0	0%, 3, 0	2%, 15, 2	11%, 22, 0	15%, 22, 1	28%, 22, 2
65°	0%, 0, 0	0%, 1, 0	1%, 6, 0	6%, 17, 0	8%, 21, 1	14%, 22, 0

Table 5.3. Classification of damage severity for Scenario 2 simulations

Impact at Midspan						
	15 mph	25 mph	35 mph	45 mph	55 mph	65 mph
35°	0%, 0, 0	1%, 7, 0	14%, 18, 0	45%, 22, 9	63%, 22, 3	43%, 22, 3
45°	0%, 0, 0	0%, 1, 0	2%, 12, 0	7%, 15, 2	26%, 22, 1	22%, 22, 2
55°	0%, 0, 0	0%, 1, 0	4%, 9, 0	12%, 15, 1	22%, 22, 3	33%, 22, 4
65°	0%, 0, 0			8%, 14, 0	12%, 15, 2	25%, 21, 2
Impact at Third Point						
	15 mph	25 mph	35 mph	45 mph	55 mph	65 mph
35°	0%, 0, 0	1%, 6, 0	13%, 19, 0	37%, 22, 8	60%, 22, 12	47%, 26, 9
45°	0%, 1, 0	0%, 1, 0	2%, 7, 0	10%, 21, 0	19%, 22, 2	22%, 22, 0
55°	0%, 0, 0	0%, 0, 0	13%, 20, 0	19%, 20, 2	24%, 22, 3	26%, 22, 0
65°	0%, 0, 0	0%, 1, 0	8%, 21, 0	5%, 16, 2	9%, 17, 4	12%, 19, 0
Impact at Quarterpoint						
	15 mph	25 mph	35 mph	45 mph	55 mph	65 mph
35°	0%, 2, 0	2%, 5, 0	6%, 12 , 0	31%, 22, 8	30%, 22, 12	29%, 22, 9
45°	0%, 0, 0	1%, 3, 0	3%, 7, 0	5%, 15, 0	11%, 22, 2	24%, 22, 0
55°	0%, 0, 0	0%, 1, 0	2%, 7, 0	3%, 12, 2	14%, 22, 3	11%, 22, 0
65°	0%, 2, 0	0%, 0, 0	0%, 6, 0	3%, 6, 2	13%, 11, 4	4%, 20, 0

Table 5.4. Classification of damage severity for Scenario 3 simulations

Impact at Midspan						
	15 mph	25 mph	35 mph	45 mph	55 mph	65 mph
35°	0%, 1, 0	0%, 0, 0	0%, 0, 0	9%, 16, 0	14%, 20, 1	29%, 22, 0
45°	0%, 0, 0	0%, 1, 0	0%, 0, 0	15%, 26, 0	11%, 20, 0	11%, 15, 0
55°	0%, 1, 0	0%, 1, 0	0%, 2, 0	12%, 18, 0	0%, 1, 0	1%, 0, 0
65°	0%, 0, 0		12%, 17, 1	19%, 17, 1	10%, 18, 2	5%, 10, 0
Impact at Third Point						
	15 mph	25 mph	35 mph	45 mph	55 mph	65 mph
35°	0%, 0, 0	0%, 0, 0	0%, 0, 0	5%, 13, 0	19%, 21, 2	18%, 19, 3
45°	0%, 0, 0	0%, 0, 0	0%, 0, 0	12%, 22, 0	4%, 20, 1	14%, 18, 2
55°	0%, 0, 0	0%, 1, 0	0%, 2, 0	4%, 15, 2	0%, 0, 0	5%, 13, 0
65°	0%, 0, 0	0%, 1, 0	2%, 13, 2	11%, 20, 1	5%, 17, 1	14%, 21, 0
Impact at Quarterpoint						
	15 mph	25 mph	35 mph	45 mph	55 mph	65 mph
35°	0%, 0, 0	0%, 0, 0	0%, 0, 0	0%, 1, 0	1%, 15, 0	5%, 12, 0
45°	0%, 0, 0	0%, 0, 0	0%, 0, 0	0%, 0, 0	1%, 14, 1	0%, 11, 0
55°	0%, 0, 0	0%, 0, 0	0%, 0, 0	0%, 0, 0	0%, 7, 1	4%, 13, 0
65°	0%, 0, 0	0%, 1, 0	0%, 0, 0	10%, 22, 2	6%, 17, 1	0%, 11, 1

Table 5.5. Classification of damage severity for Scenario 4 simulations

Impact at Midspan						
	15 mph	25 mph	35 mph	45 mph	55 mph	65 mph
35°	0%, 0, 0	1%, 0, 0	0%, 0, 0	0%, 0, 0	0%, 0, 0	14%, 19, 3
45°	0%, 0, 0	0%, 0, 0	0%, 0, 0	0%, 0, 0	4%, 3, 1	0%, 1, 0
55°	0%, 0, 0	0%, 0, 0	3%, 1, 1	0%, 0, 0	1%, 1, 0	0%, 0, 0
65°	0%, 1, 0	0%, 0, 0	4%, 5, 1	0%, 1, 0	0%, 0, 0	0%, 0, 0
Impact at Third Point						
	15 mph	25 mph	35 mph	45 mph	55 mph	65 mph
35°	0%, 0, 0	1%, 0, 0	0%, 0, 0	1%, 2, 0	14%, 22, 1	2%, 4, 1
45°	0%, 0, 0	0%, 0, 0	0%, 3, 0	2%, 2, 0	0%, 1, 0	0%, 0, 0
55°	0%, 0, 0	0%, 0, 0	0%, 0, 0	0%, 0, 0	0%, 0, 0	0%, 0, 0
65°	0%, 1, 0	0%, 0, 0	3%, 1, 1	0%, 0, 0	0%, 1, 0	0%, 0, 0
Impact at Quarterpoint						
	15 mph	25 mph	35 mph	45 mph	55 mph	65 mph
35°	1%, 0, 0	1%, 0, 0	0%, 0, 0	0%, 0, 0	0%, 1, 0	8%, 5, 2
45°	0%, 0, 0	0%, 0, 0	0%, 1, 0	0%, 1, 0	0%, 2, 0	0%, 1, 0
55°	0%, 0, 0	0%, 0, 0	0%, 0, 0	0%, 0, 0	0%, 0, 0	0%, 1, 0
65°	0%, 0, 0	0%, 0, 0	0%, 0, 0	0%, 0, 0	0%, 0, 0	0%, 0, 0

5.3 Development of Iso-Damage Curves for Overheight Vehicle Collisions

The literature review conducted for this study revealed no precedent for the development of a simplified prediction tool to forecast the expected severity of damage to prestressed concrete girder bridges from overheight vehicle impact. However, recent research related to the assessment of bridge columns subject to vehicular impact suggests that the peak force and impulse are sufficient explanatory factors to cluster classified damages for a given column design and vehicle type. To explore the possibility of extending this approach to overheight vehicle impacts to prestressed concrete girder bridges, the recorded force time histories for the contact between the dump truck and the girder were analyzed for the 288 simulations included in the parametric analysis of the Bridge B model. For each time history, the peak force was extracted from the time history and the total impulse was calculated by numerically integrating the area under the force time history response. The recorded contact force includes the individual Cartesian components, so both the total resultant force and the lateral component of force were investigated to identify the best discriminator. Ultimately, the peak lateral force and impulse were found to better distinguish the points with different damage classifications in the force-impulse space.

The nature of the impact and the force time histories were very different for collision simulations where the back wall first struck the girder compared to those where the shield impacted the girder (Figure 5.6). However, across Scenario 1 and Scenario 2 where the back wall struck the girder, the general shape and duration of the contact are similar. Likewise, similar time history characteristics were observed across Scenario 3 and Scenario 4 where the shield struck the girder. Since iso-damage curves are conventionally constructed for similar loadings, the data from the parametric analysis was separated into the 144 cases involving the collision of the back wall of the dump truck with the girder and the remaining 144 cases involving the collision of the shield with the girder.

The conventional function form of iso-damage curves originally introduced for blast-resistant design and subsequently extended to structural assessment of impact is:

$$(F - F_0)(I - I_0) = A\left(\frac{F_0 + I_0}{2}\right)^{\beta} \qquad \text{(Eq. 5.1)}$$

where F and I and the peak force and impulse respectively, F_0 is the peak force asymptote for the iso-damage curve, I_0 is the impulse asymptote, and A and β are scalar parameters that relate to the shape of the applied impact load (Ma et al. 2020). Wei et al. (2022) provides guidance on fitting parameters of iso-damage curves and simplifies the iso-damage function to:

$$(F - F_0)(I - I_0) = Z \qquad \text{(Eq. 5.2)}$$

where Z is a single shape parameter that controls the shape of the transition of the iso-damage curve between the peak force and impulse asymptotes. With the simplified form, the description of the iso-damage curve is reduced to three variables: F_0, I_0, and Z. Ultimately, to develop a generalized statistical model to predict iso-damage curves for generic bridges, a technique would need to be developed to predict the assignments for these three scalar values based on bridge characteristics. For this study, the variables were arrived at by optimizing the classification performance of the iso-damage curve while constraining each iso-damage curve to produce a conservative lower bound estimate wherein no cases associated with the damage level of the iso-damage curve would fall under the curve and therefore be mis-classified as less severe than predicted by the finite element analysis.

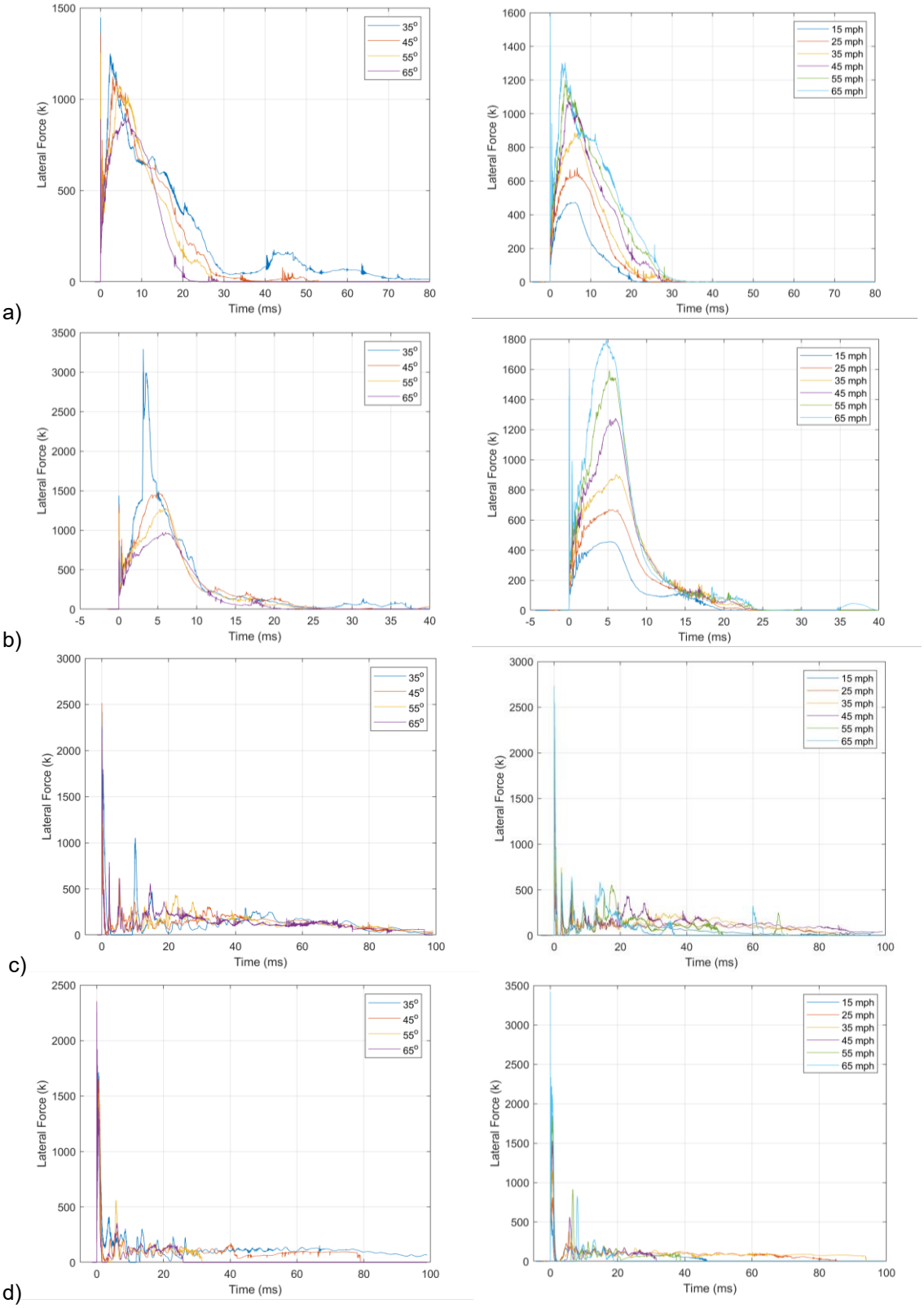

Figure 5.6. Representative impact force time histories for each of the four vehicular impact scenarios: a) Scenario 1; b) Scenario 2; c) Scenario 3; d) Scenario 4

Figure 5.7 presents the distribution of the individual simulation results for the back wall impact scenarios in the peak lateral force-impulse space as well as the iso-damage curves developed from these results. The distribution of individual simulation results indicates that the peak lateral force and impulse work well as explanatory variables to separate cases of superficial damage from moderate and severe damage. Likewise, the cases of moderate damage are generally well separated from the cases of severe damage. The developed iso-damage curves also serve well as boundaries between the damage classifications. Figure 5.8 presents the distribution of individual simulation results for the shield impact scenarios. In this figure, only a single developed iso-damage is shown because all but one of the cases exhibited damage that was classified as either superficial or moderate.

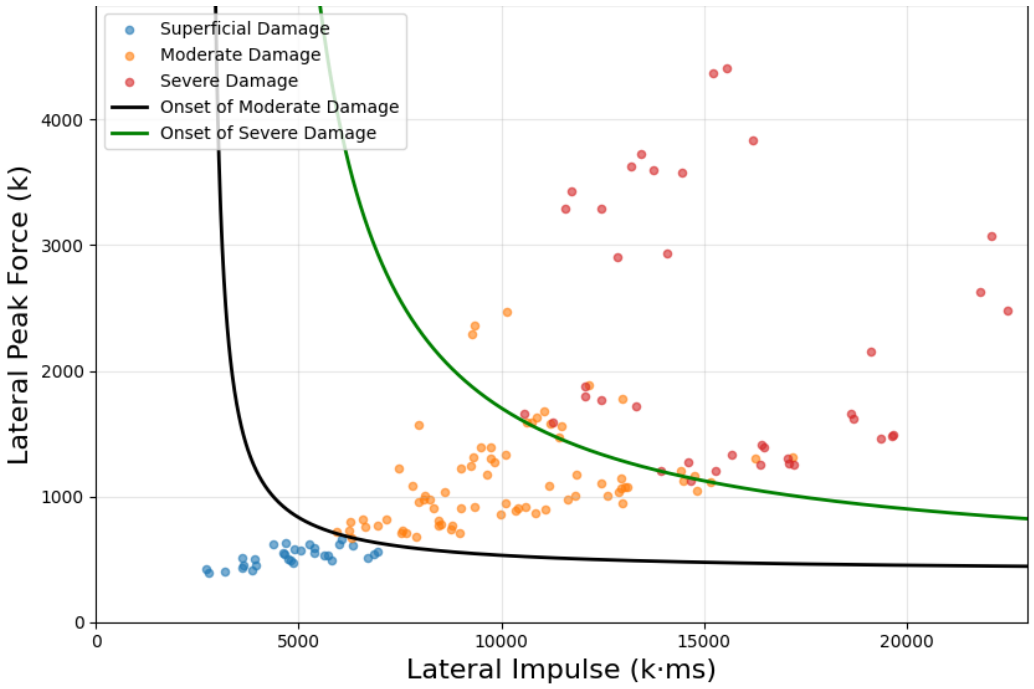

Figure 5.7. Distribution of simulation results for back wall impact scenarios in the peak lateral force-impulse space and developed iso-damage curves for Bridge B

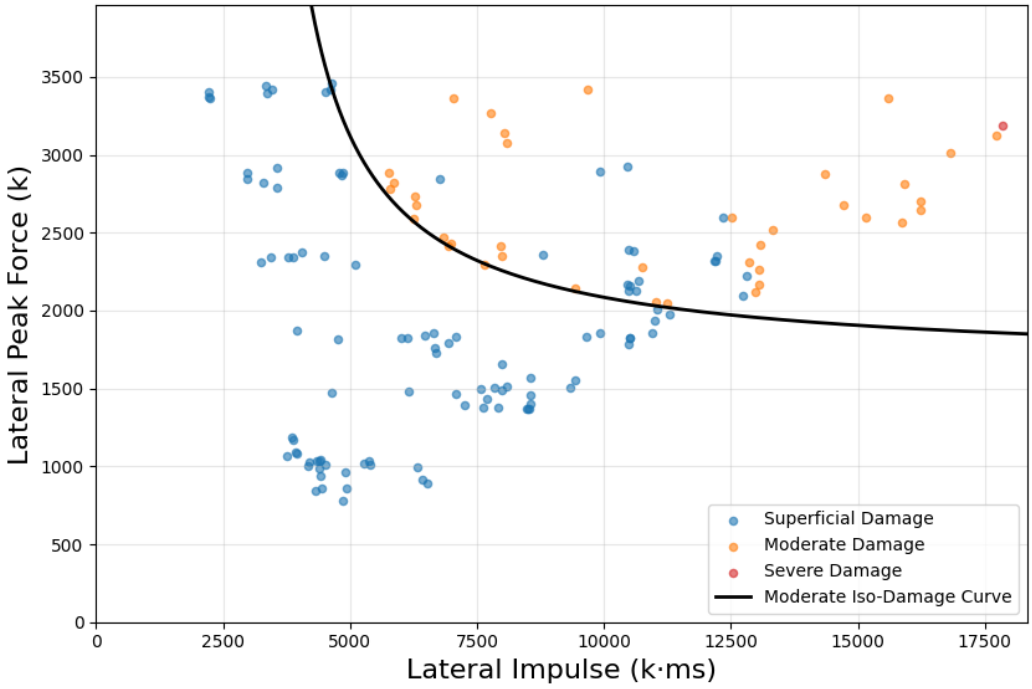

Figure 5.8. Distribution of simulation results for shield impact scenarios in the peak lateral force-impulse space and developed iso-damage curves for Bridge B

5.4 Prediction Models for Impact Force Characteristics of Dump Truck with Raised Bed

The iso-damage curves developed in the previous section form the basis of a simplified prediction model that could rapidly assess the likelihood and severity of damage to the girders for the modeled bridge. However, in order for the iso-damage curves to be applied to produce a rapid assessment of the likelihood of damage for a specific scenario without performing additional finite element analysis, a means of estimating the peak force and impulse for the incident is needed. To arrive at empirical prediction models for peak force and impulse associated with raised bed dump truck collisions, an effort was undertaken in the research project to gain an understanding of the key variables that influence the peak force and impulse associated with impact forces from dump trucks with raised beds and to develop a statistical model using nonlinear regression to predict these key quantities. For this effort, the same 288 cases performed for the parametric analysis of Bridge B described earlier in this chapter were performed for two additional bridge models. These models included the structure referred to as Bridge A in Chapter 4 and an additional bridge model that was constructed to add additional variation in girder type, skew angle, diaphragm type, and other structural features. The motivation behind including multiple bridge models in the study of the impact force characteristics was to provide insight into whether the impact force time history is significantly affected by bridge characteristics. By including all 288 cases per bridge model, the effects of vertical underclearance violation, velocity, angle of raised bed, and longitudinal location of impact could also be studied.

The additional bridge model included in this component of the study was a span consisting of five AASHTO Type III girders spaced at 9 ft 9 in supporting a 9-inch reinforced concrete deck with an out-to-out width of 45 ft 1 in and crowned with a slope of 0.025 ft/ft. The bridge has a skew angle of 30 degrees (60 degrees

from the bent angle). The modeled span has a length of 42 ft 9 in and is prestressed with 16 low relaxation Grade 270 strands of 0.5 in diameter. Intermediate diaphragms for this bridge were 8 in wide, reinforced concrete, and are oriented perpendicular to the webs of the girders. Due to the skew angle, this means that the intermediate diaphragm is located at the midspan of the first interior girder, but offset from the midspan of the exterior girder. Figure 5.9 depicts the cross section of the superstructure and provides a plan view of the span to indicate the location of the intermediate diaphragms. With the inclusion of this third bridge model, the study encompassed a set of structures with a range of span length, girder type, number of girders, skew angle, intermediate diaphragm type, and concrete compressive strength. Table 5.6 presents a summary of several of the dimensions and design details for the three bridges to document the ranges covered by the study.

For each of the three bridge models, overheight collisions of the dump truck with raised bed model described in Chapter 3 were performed for different vertical underclearance violations, initial truck velocities, angles of raised bed, and longitudinal location of impact. The four vertical underclearance violation scenarios presented previously in this chapter and shown in Figure 5.3 produced two different scenarios where the back wall of the raised bed first struck the girder (Scenarios 1 and 2) and two different scenarios where the shield of the dump truck first struck the girder (Scenarios 3 and 4). For each of these scenarios, collisions at the midspan, third point, and quarterpoint were simulated for initial velocities of 15, 25, 35, 45, 55, and 65 mph with raised bed angles of 35, 45, 55, and 65 degrees from the horizontal. Collectively, this resulted in 288 simulations per bridge, or a total of 864 finite element analyses. All simulations were performed for 100 ms, which was sufficient to capture the complete force time history for contact of the dump truck with the exterior girder.

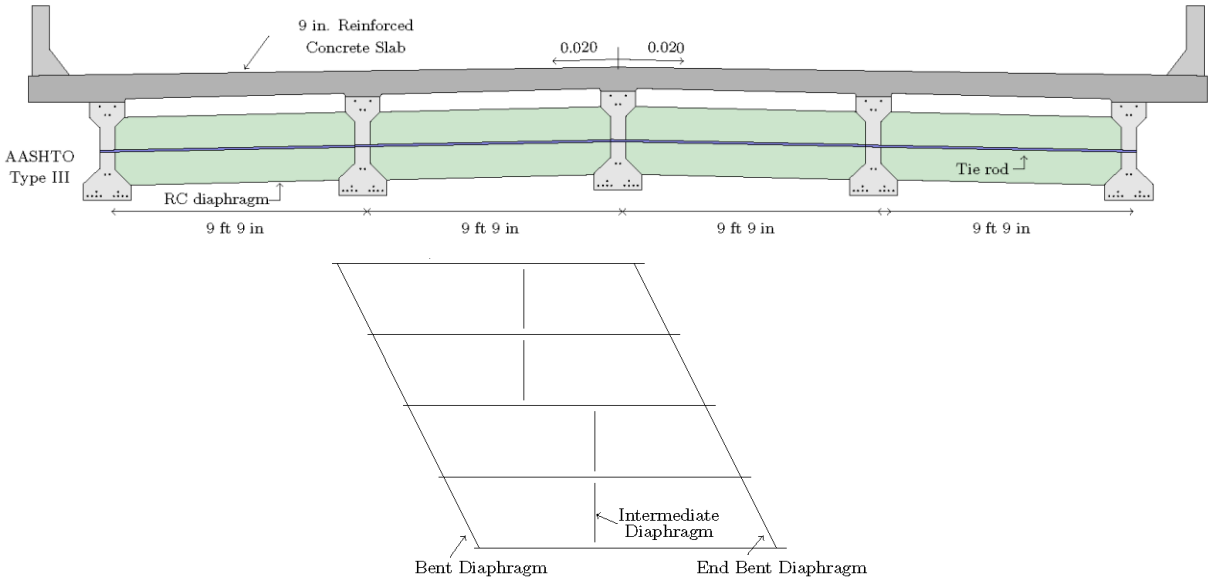

Figure 5.9. Dimensions and details for additional bridge span (Bridge C) included in investigation of impact force characteristics for collision of a dump truck with raised bed

Table 5.6. Summary of dimensions and design characteristics for bridge models included in investigation of impact force characteristics for dump truck collisions

	Bridge A	Bridge B	Bridge C
Span Length	98 ft 4 in	76 ft 5 in	42 ft 9 in
Girder Type	AASHTO Type IV	AASHTO Type IV	AASHTO Type III
Number of Strands Per Girder	28	26	22
Number of Girders	5	6	5
Intermediate Diaphragms	Steel Channel	Steel Channel	Reinforced Concrete
Skew	0^o	10^o	30^o
Concrete Compressive Strength	8000 psi	6000 psi	6000 psi

From the previous analysis of the contact force time histories for Bridge B, it has been demonstrated that the initial velocity of the dump truck and the angle of the raised bed both have a significant effect on the peak force and impulse. These effects were previously shown in Figure 5.6. In Figure 5.10, representative force time histories obtained for Bridge B at the three different longitudinal locations of impact are shown. For all scenarios, it can be seen that the longitudinal location of impact does not have a significant effect on the peak force or impulse. Likewise, since the intermediate diaphragm was located at the midspan, which was one of the longitudinal locations of impact simulated, the results further indicate that the presence of the intermediate diaphragm does not significantly affect the force time history characteristics. Figure 5.11 presents a representative comparison between force time histories obtained for each of the three bridge models for the same scenario, initial truck velocity, bed angle, and longitudinal location of impact. The results demonstrate that, despite the significant variation in span length, girder type, and other dimensions and structural details, the bridge characteristics do not appear to have a significant influence on the contact force time history. This is a particularly important finding, since it enables the development and use of a common prediction model for peak lateral impact force and impulse that could be universally applied for all prestressed concrete bridge girders. However, further analysis of larger girder sizes and different girder profiles, such as FIB and Modified Bulb Tee shapes, should be performed before extrapolating the results and conclusions from this study to other bridges. As can be seen by careful examination of Figure 5.11, the difference in the force time histories is most apparent for Bridge C, which was an AASHTO Type III girder while the other bridge models were based on AASHTO Type IV girders. The small difference doesn't warrant a different prediction model for the bridges, but does suggest the potential for more significant differences if the girder depth or profile is dissimilar from those used in this study.

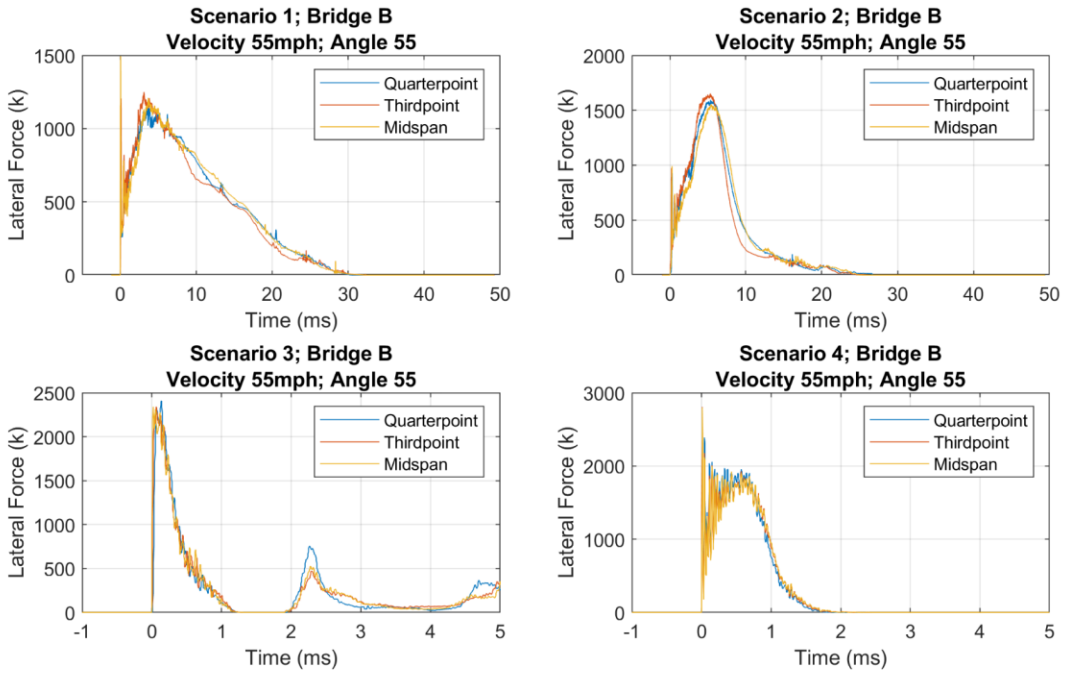

Figure 5.10. Influence of longitudinal location of collision on the contact force time history

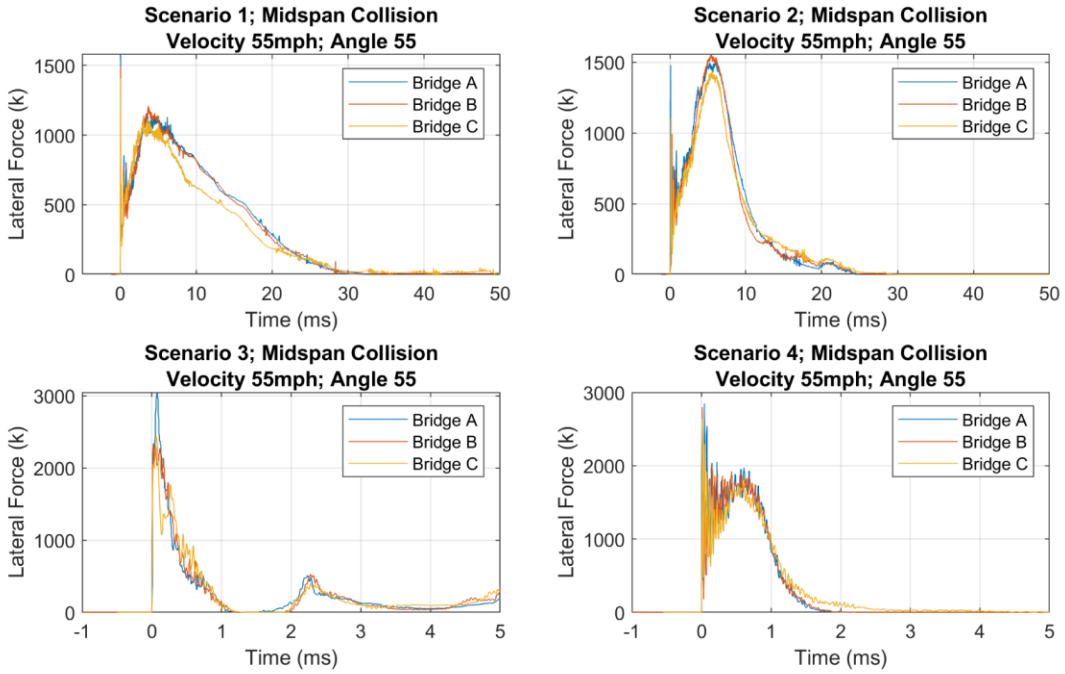

Figure 5.11. Influence of bridge characteristics on the contact force time history

The lateral force time histories for each of the 864 simulations were post-processed to extract the peak lateral force and calculate the impulse. Nonlinear statistical regression was then performed to arrive at prediction models for these quantities for each vertical underclearance violation scenario. When performing the nonlinear regression, eight different functional forms were considered for both the peak

lateral force and impulse models. These functional forms are shown in Figure 5.12. Since only the initial truck velocity, v, and angle of the raised bed, θ, were visually found to exhibit significant influence on the lateral force time histories, only these two variables were considered in the nonlinear regression models.

1. $$F = a\,v^{b}\,\theta^{c}$$
2. $$F = a\,v^{b}\left(1 + c\theta + d\theta^{2}\right)$$
3. $$F = a\left(1 + bv\right)\left(1 + c\theta\right)$$
4. $$F = a\left(1 + bv\right)\left(1 + c\theta + d\theta^{2}\right)$$
5. $$F = a\,v^{b}\left(1 + c\theta\right)$$
6. $$F = a\left(1 + bv + cv^{2}\right)\theta^{d}$$
7. $$F = a\left(1 + bv + cv^{2}\right)\left(1 + d\theta + e\theta^{2}\right)$$
8. $$F = a\,v^{b}\left(1 + c\theta^{2}\right)$$

Figure 5.12. Functional forms considered for development of statistical models to predict peak lateral impact force and impulse

The peak lateral force and impulse data from all of the 864 simulations were combined into a single database. Visual investigation of trends in the peak lateral force and impulse values revealed significant nonlinearity in the impulse with initial truck velocity for incidents involving collision of the shield of the dump truck with the girder (Scenarios 3 and 4). This nonlinearity can also be observed in Table 4.1. For initial velocities greater than approximately 35 mph to 55 mph (depending on the angle of the raised bed), the impulse unexpectedly decreased. Review of the simulation results revealed that at higher velocities the shield was exhibiting significant yielding or buckling causing a reduction in the contact time and, subsequently, the impulse. In order to avoid having the limit states of the shield (which vary by dump bed design) reflected implicitly in the peak lateral force and impulse models, any cases involving such behavior were first removed from the database. Nonlinear regression was then performed using each of the eight functional forms while dividing the filtered database into training and testing data sets. The performance of each model was assessed based on the statistical significance of the variables (p-values), the simplicity of the functional form, and the ability to capture trends across all scenarios based on the goodness of fit. Among the candidate functional forms, the first equation in Figure 5.12, a simple power-law formulation, was selected because it statistically predicted the training and test data as well as the more complex models. The resulting prediction models for each scenario are presented in Table 5.7. Figure 5.13 graphically presents each model and its fit to the full database of peak lateral force and impulse for each scenario. Most of the models achieved average training and test R^2 values greater than 0.90, indicating strong agreement between the predicted and actual values as well as indicating that the model does not overfit the data.

Table 5.7. Peak lateral force and impulse prediction models for dump truck with raised bed

	Peak Lateral Force (k)	Impulse (k·ms)
Scenario 1	$F = 1509.76\,v^{0.986}\,\theta^{-1.029}$	$I = 12128.332\,v^{0.839}\,\theta^{-0.796}$
Scenario 2	$F = 52713.676\,v^{1.051}\,\theta^{-1.926}$	$I = 9020.12\,v^{0.785}\,\theta^{-0.732}$
Scenario 3	$F = 160.206\,v^{0.762}\,\theta^{-0.052}$	$I = 312.049\,v^{0.846}\,\theta^{-0.132}$
Scenario 4	$F = 118.559\,v^{0.8}\,\theta^{0.032}$	$I = 3047.871\,v^{0.742}\,\theta^{-0.401}$

	Lateral Peak Force	Impulse
Scenario 1	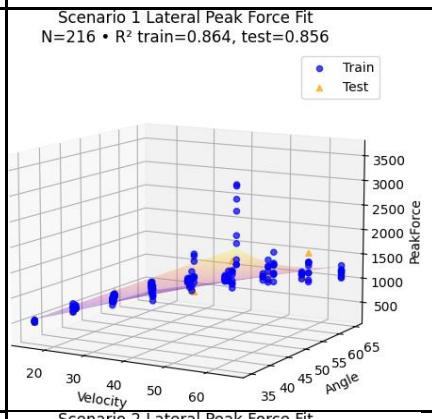	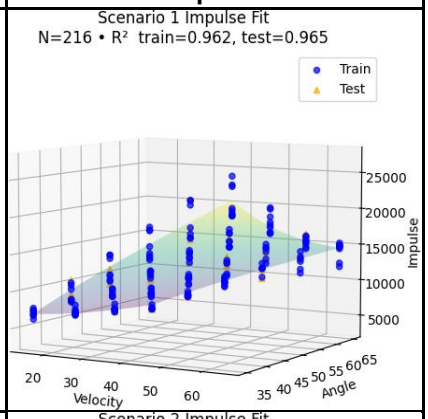
Scenario 2	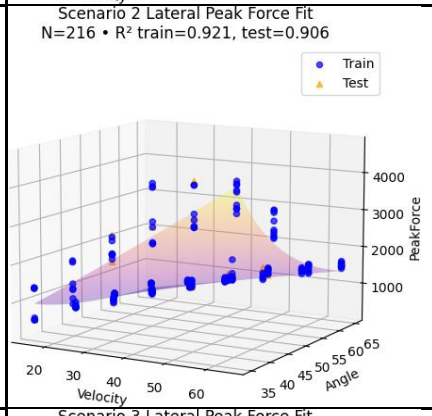	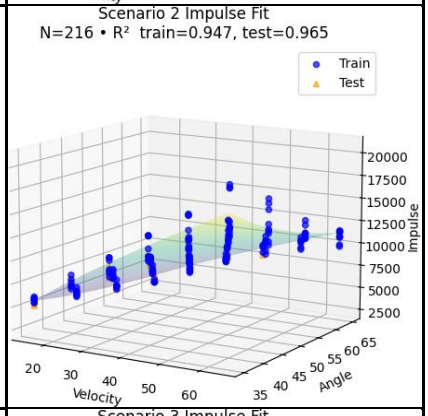
Scenario 3	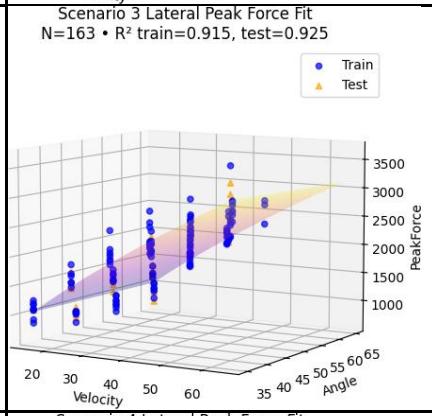	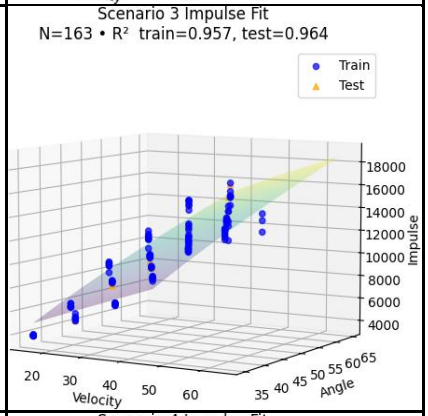
Scenario 4	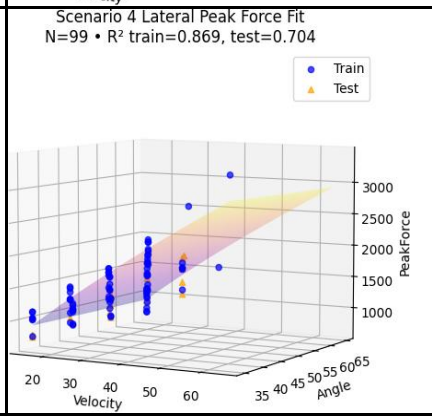	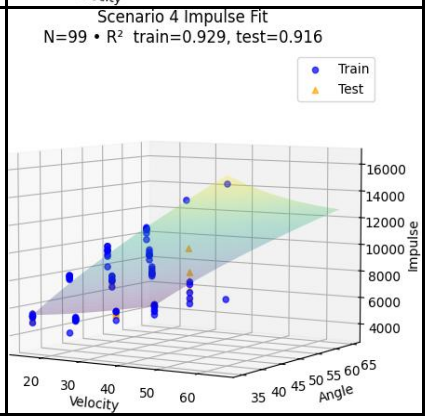

Figure 5.13. Comparison of developed prediction models against the full database of force characteristics developed through finite element analysis

5.5 Implementation of Simplified Prediction Models

The research effort resulted in the development of a framework for a simplified prediction model to assess damage to prestressed concrete girders from overheight vehicle impacts. This framework is based on iso-damage curves that delineate regions of the peak force-impulse space into superficial, moderate, and severe damage classifications. As detailed in section 5.3, these classifications are defined based on the expected need to either perform repairs to ensure long-term durability of the girders or structure repairs. Prediction models to estimate peak lateral force and impulse for collisions involving a dump truck with raised bed were also developed in section 5.4. In a practical implementation of the simplified assessment approach, a practitioner would need to estimate the initial truck velocity, angle of the raised bed, and approximate vertical underclearance violation (i.e. height of the raised bed relative to the bottom of the girder) and these estimates would be used to calculate the expected peak lateral force and impulse. These values correspond to a single point in the peak lateral force-impulse space, where the iso-damage curves for the structure reside (Figure 5.14). The predicted extent of damage corresponds to where the point falls relative to the iso-damage curves.

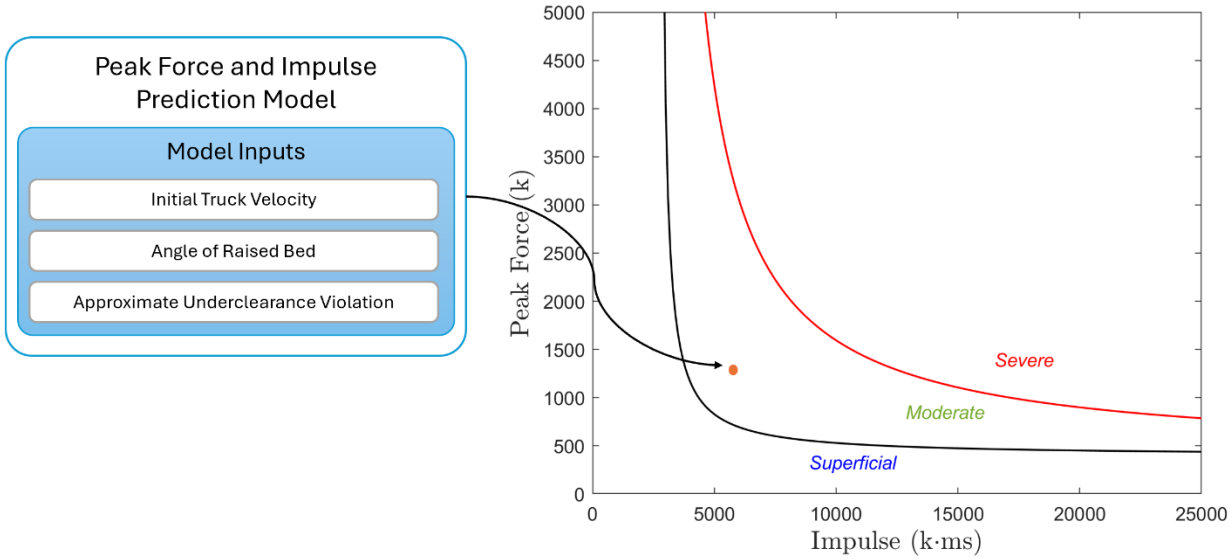

Figure. 5.14. Illustration of how peak lateral force and impulse prediction models are used alongside the iso-damage curves to forecast the likelihood and severity of damage

Since the method produces a graphical result, it is intuitive for a practitioner to assess the relative confidence of the prediction by how closely the point falls to an iso-damage curve, which is the boundary between two damage classifications. Additionally, if an input parameter is not known with high confidence, such as the angle of the raised bed, multiple points could be populated to fold the uncertainty into the damage assessment. Alternatively, the prediction models themselves can be mapped over the peak lateral force-impulse space alongside the iso-damage curves to provide direct insight into how the initial velocity and angle of the raised bed influence the damage estimate for each scenario. Figures 5.15 and 5.16 provide examples of such mapping for the Bridge B iso-damage curves. Since peak lateral force, impulse, and iso-damage curves are all relatively simple analytical functions, such figures are easily generated and could be rapidly produced within a spreadsheet.

While the research effort successfully developed this framework, the ability to generate iso-damage curves using a surrogate model that does not require parametric finite element analysis was not able to be produced within the period of performance of the project. Iso-damage curves are expected to be unique to individual structures, since they reflect the resistance of the structure to lateral impact, which should be a function of the girder type, span length, number and location of intermediate diaphragms, and other dimensions and design details. However, since the iso-damage curves are described by only three constants (F_0, I_0 and K), there is a probable path toward developing a statistical model to predict assignments for these variables based on key bridge characteristics. To do so, the parametric analysis detailed in sections 5.1 through 5.3 would need to be performed for a number of prestressed concrete girder bridges with a wide range of different bridge characteristics. The surrogate model could then be constructed by fitting the three constants in the iso-damage curves using the descriptors for the bridge characteristics.

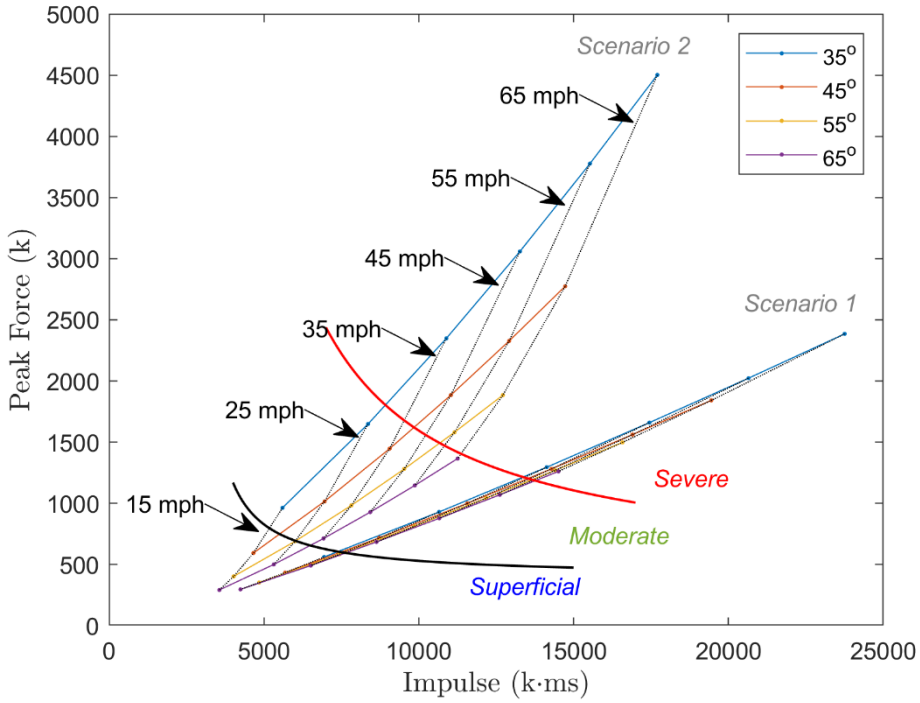

Figure 5.15. Overlay of peak lateral force and impulse prediction models with iso-damage curves for impact from rear wall of dump truck bed impact for Bridge B

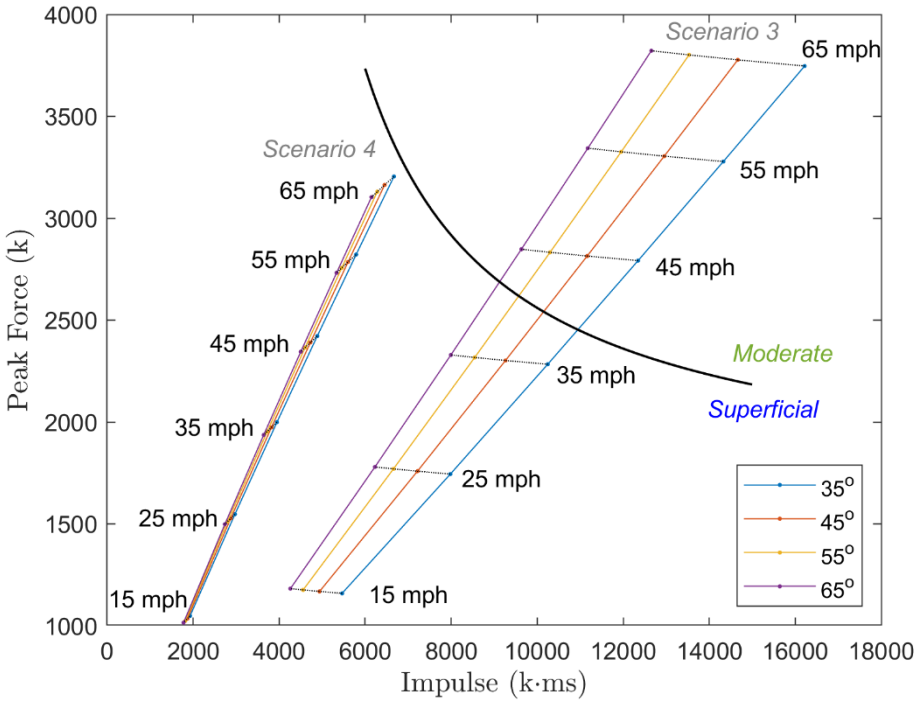

Figure 5.16. Overlay of peak lateral force and impulse prediction models with iso-damage curves for impact from shield of dump truck bed impact for Bridge B

6. CONCLUSIONS

This research project utilized high-fidelity finite element analysis to investigate factors affecting the severity and type of damage affecting in-service and partially constructed bridges with prestressed concrete girders when subject to lateral impact from a dump truck with raised bed. A library of software routines was developed to automate the generation of bridge models from parameters read from as-built bridge plans, constitutive models used in the collision simulations were validated against published experimental test data for beam specimens, and contact modeling of the collision forces from overheight impactors was verified through comparison with published results. A high-fidelity model of a dump truck with raised bed was developed by modifying an existing validated model of an F-800 truck and the plausibility of this model for simulating overheight vehicle impacts to bridges was supported by comparing simulation results to damages observed following an actual accidental overheight collision of a raised bed dump truck with a bridge under construction. Parametric analysis was performed using variants of a bridge model to investigate differences in failure mechanisms and vulnerability to collapse in prestressed concrete girders at different stages of construction completion. The effect of the presence and type of intermediate diaphragm on the performance of prestressed concrete bridge girders subject to overheight impact prior to placement of the deck was also studied. Lastly, a framework for developing simplified models to predict the severity of damage from dump truck collisions based on estimates of truck velocity, angle of raised bed, and approximate vertical underclearance violation was developed. The framework utilizes iso-damage curves to classify the likelihood of damage based on the peak lateral impact force and impulse. A model of a bridge span created using as-built plans of an existing bridge demonstrated the application and suitability of the framework. Furthermore, prediction models were developed using nonlinear regression to provide a means for estimating the peak lateral force and impulse for collisions involving dump trucks with raised beds. Collectively, the iso-damage curves and prediction models for the impact force characteristics enable rapid forecasting of whether superficial, moderate, or severe damage is anticipated for a particular impact scenario without performing additional finite element analysis.

6.1 Key Findings and Products of the Research

- The research effort resulted in the development of an extensive library of scripts capable of automating the generation of detailed finite element models of bridges with prestressed concrete girders, as well as a high-fidelity model of a dump truck with a raised bed. Forensic analysis of future incidents involving the collision of raised beds of dump trucks with prestressed concrete girder bridges could be easily and rapidly simulated with the software infrastructure developed through this project. Such analysis would be able to provide information to NCDOT about the likelihood and severity of prestress losses and damage to concrete within impacted girders to help inform repair and replacement decisions. The research team is eager and willing to assist NCDOT with any such assessments using this developed computational capability. The developed CAE library was written to develop finite element models for the LS-DYNA finite element analysis software. This software was selected based on the prevalence of use within recent literature that informed the research tasks, as well as existing computational support available to the research team through the High Performance Computing resources at the University of North Carolina at Charlotte. The research team can make the CAE library available directly to NCDOT, but NCDOT would need to maintain a license for LS-DYNA to run simulations independently from the research

team. In addition, the time required for such simulations may exceed several days without the benefit of High Performance Computing resources to enable parallel processing of the models.

It is the understanding of the research team that NCDOT uses and maintains software licenses for the LUSAS finite element analysis software. It may be possible to port the CAE library to the LUSAS environment, as LUSAS does offer the capability to perform nonlinear explicit analysis, staged construction through restart analysis, plasticity models with hardening laws. NCDOT may need to purchase the LUSAS Dynamic and LUSAS Nonlinear options to enable such capabilities, if these options are not included in the existing license agreement. Revising the CAE scripts to build the geometries of bridge models and configure analyses would likely be a very minor effort. However, a more extensive verification effort would be required due to the need to implement a different concrete constitutive model and different contact algorithms in LUSAS. The Continuous Surface Cap Model (CSCM) that was selected for this research based on extensive validation is not available in the LUSAS software, although an alternative advanced nonlinear concrete model is available. It is unclear whether this concrete constitutive model accounts for strain rate effects, which is important for impact analysis, or if any effort has previously been made to validate the LUSAS concrete model for simulating the response of reinforced or prestressed concrete to impact loads. Furthermore, the simulation of impact and modeling of the raised bed dump truck in LS-DYNA relied on several contact algorithms and advanced constraints. Based on review of materials available on the LUSAS website, it is unclear whether equivalent contacts and constraints are available within LUSAS. Technology transfer of the CAE ported over to the LUSAS environment would require verification and validation of the concrete constitutive model, contact algorithms, and constraints, which would likely require a six-month effort. The success of such an effort would also be dependent upon the current capabilities of the LUSAS software.

- The research successfully formulated a framework for developing a simplified tool to assess the likelihood and severity of damage to prestressed concrete girders subjected to overheight vehicle impacts. The framework is based on iso-damage curves and was demonstrated using a model of a representative bridge created from as-built plans. Iso-damage curves were developed for two levels of intervention: moderate damage, which was defined as the threshold at which repairs are expected to be required to ensure long-term durability, and severe damage, which was defined as the threshold at which structural repairs would be required. The simplified tool requires only the estimation of the dump truck initial velocity, angle of raised bed, and approximate vertical underclearance violation. The iso-damage curves can be presented graphically with an overlay of vehicle characteristics to produce an easily interpreted, risk-based framework for assessing the likelihood and severity of damage. This feature is described and shown graphically in section 5.5 of this report.

The formulation of the iso-damage framework for damage assessment of prestressed concrete girder bridges subjected to overheight vehicle impact is a significant contribution to the state-of-practice, as no existing literature on this topic has proposed a generalizable technique that could lead to simplified tools suitable for routine implementation by practitioners. The need to formulate this framework left the research team with insufficient time to build a general statistical model to generate iso-damage curves for any prestressed concrete girder bridge based on a set of descriptive inputs. Naturally, iso-damage curves for each bridge will be different, as they reflect the resistance

of the girder to lateral impact, which will be a function of girder type, span length, number and design of intermediate diaphragms, and other design parameters. In order to construct a generalized model such that the iso-damage framework could be implemented by NCDOT without requiring case-specific finite element analysis, additional research would need to be performed to arrive at the statistical model(s) needed to produce the three constants that define each iso-damage curve from a set of significant bridge characteristics. This research effort would involve modeling several tens of prestressed concrete girder bridge superstructures using bridge plans provided by NCDOT, performing parametric analysis on each bridge model to arrive at iso-damage curves following the damage classification and segregation techniques described in sections 5.2 and 5.3 of this report. This parametric analysis would also need to consider oblique vehicular impacts in cases of bridges with skew. Statistical models could then be established using the database of iso-damage constants and associated design characteristics of the bridge models. This effort would be significantly expedited by the developed CAE library. Given the computational time required to initialize, run, and post-process the simulation results, it is anticipated that a 24 month second phase effort would be required to arrive at a complete set of simplified models suitable for application to AASHTO girders, Florida I-beams, and Modified Bulb Tees. The research effort could be contracted on a shorter timeline by focusing the work on development of models for only one girder type per phase, which also would derisk the additional investment in research funding.

- A large parametric analysis performed with the developed dump truck model revealed that the impact force characteristics required for efficient use of iso-damage curves are influenced most significantly by the initial truck velocity, angle of raised bed, and vertical underclearance violation. Bridge characteristics, such as span length, longitudinal location of impact, number of girders, and girder type, did not have a significant effect on the peak lateral impact force or impulse. This is an important finding because it suggests that a common set of simple nonlinear formulae can be used to estimate the peak lateral impact force and impulse for any bridge, rather than requiring a structure-specific analysis or model.
- Finite element analysis of a case study bridge under construction that was impacted by a dump truck with raised bed prior to the placement of the deck and subsequent parametric analysis of another bridge model during several stages of construction highlighted differences in failure mechanisms and vulnerability to collapse of girders as the bridge is constructed. Prior to the placement of the deck, damage to the girder adjacent to sole plate connections is a particular concern for girders that have been welded to the sole plate. Finite element simulations for a range of initial truck velocities suggest that this failure mechanism is the first to occur during lateral impact to the girder at this stage of construction. After the deck has been placed, the additional mass and stiffness contributions provided by the deck suppress the likelihood of this type of failure occurring prior to significant damage at the location of impact. In general, before the deck is placed, the bridge girders exhibit significant minor and major axis flexure under lateral impact. Once the deck has been placed, the behavior of the girder under impact becomes more dominated by torsional response leading to D-shaped regions of shear-torsion cracking and shear push-out failure. The differences in behavior and failure mechanisms of the girder at the different stages of construction lead to significant differences in vulnerability of the girders to severe damage and collapse.
- For bridges under construction, the presence of intermediate diaphragms is beneficial for reducing flexural cracking by promoting load sharing among the girders. Furthermore, the results from this research suggest that reinforced concrete intermediate diaphragms offer improved lateral impact

resistance compared with steel channel intermediate diaphragms. However, neither the presence of the intermediate diaphragm nor the type was found to eliminate or reduce the severity of damage adjacent to the sole plate connection. For even low initial truck velocities, the finite element analyses revealed susceptibility of the girders to damage at this location in all cases. When prestressed concrete girders are subjected to accidental overheight vehicle impacts during construction prior to the placement of the deck, NCDOT should carefully inspect the girders of the impacted bridge in the region of the supports to identify any evidence of this type of damage. The simulations performed in this study suggest that girders will be damaged at this location, even at low-speed impacts, and likely require replacement if impacted prior to the placement of the deck.

6.2 Recommendations for Future Research

The following recommendations are offered for future research:

- The research effort successfully developed and demonstrated a simplified approach for assessing the likelihood and severity of damage to prestressed concrete bridge girders subjected to accidental overheight collision from a dump truck with raised bed. The simplified approach is based on iso-damage curves, which were shown to separate cases of superficial, moderate, and severe damage using peak lateral force and impulse. Furthermore, statistical models were developed to predict the peak lateral force and impulse with a high degree of accuracy for different raised bed dump truck collision scenarios. These statistical models enable the iso-damage curves to be used to provide an assessment of damage for hypothetical incidents using only an estimate of the vehicle speed, angle of raised bed, and approximate vertical underclearance violation. However, at the conclusion of this effort, iso-damage curves were only developed for a single structure. The iso-damage curves are expected to be unique to individual structures, since they reflect the resistance of the structure to lateral impact, which should be a function of the girder type, span length, number and location of intermediate diaphragms, and other dimensions and design details. Since the iso-damage curves are described by only three variables (F_0, I_0 and K), there is a probable path toward developing a statistical model to predict assignments for these variables based on key bridge characteristics. It is recommended that future research be conducted to apply the CAE finite element model technique and iso-damage framework developed in this research report to a large number of bridges encompassing a wide range of bridge characteristics and then develop a surrogate model to predict the iso-damage variable assignments directly from the bridge characteristics.
- Parametric analysis of overheight vehicle impacts to partially constructed bridges suggest that the damage observed adjacent to the sole plate connections in one case study incident featured in this report is a particularly critical failure mechanism to inspect for when bridges under construction are subjected to accidental lateral impact. Finite element analyses performed on models representative of assemblies of bridge girders and intermediate diaphragms prior to the placement of the concrete deck suggest that damage adjacent to the sole plate connection may be the first damage mechanism initiated and that damage may be present adjacent to the sole plate connection even if the lateral impact does not result in spalling or cracking at the location of the impact. Future research should be directed toward additional numerical modeling and, if possible, experimentation to better understand the risk of damage to sole plate connections from accidental lateral impacts, particularly at magnitudes that result in only superficial damage to the directly impacted region of the girder. If future research confirms the susceptibility of prestressed concrete girders to this damage mechanism prior to the construction of the deck, then research on techniques to mitigate

this risk, as well as to nondestructively inspect for the presence of damage near the connection, should be considered.

- The review of news articles involving incidents of overheight collision of vehicles revealed that the overwhelming majority of incidents involve either a dump truck with a raised bed or an excavator carried on a trailer. This research effort produced a high-fidelity model for a dump truck with raised bed that was demonstrated to produce plausible predictions of damage for the case study structure involving collision to a partially constructed bridge. Future research should address cases involving impact from the boom of an excavator. The damage resulting from such a vehicle is expected to be very different, since the boom of an excavator is narrower than the bed of a dump truck. Furthermore, some of the energy during the collision of a dump truck with a bridge will be directed toward raising the cab of the truck, while less energy is expected to be directed toward such a mechanism during collision from an excavator since the front of the trailer is connected to the truck.
- With the exception of simulation of the case study involving collision of a raised bed dump truck with a partially constructed bridge, all of the simulations performed assumed that the direction of travel of the dump truck was perpendicular to the impacted girder. Future research should investigate how the angle of incidence of the dump truck collision affects the resulting damage to the girder as well as the peak lateral force and impulse.
- Simulations involving collision of the shield of the dump truck with the girder exhibited yielding and buckling of the shield at higher initial truck velocities. Dump truck shields vary in design, with some shields being significantly longer or constructed of thinner steel than assumed for the representative dump truck. A sensitivity analysis could be conducted for several different shield designs to provide a better understanding of the significance of the shield strength and stiffness on the expected damage to the structure.

6.3 Implementation and Technology Transfer

There are two main products that were developed based on this research: (1) the Collision Analysis Engine and (2) the Isodamage Framework. The team is eager to engage with the NCDOT and provide guidance on the implementation of these products.

- UNC Charlotte developed the capability to rapidly construct simulations to reconstruct overheight vehicle collisions to prestressed concrete girder bridges. We are eager to support NCDOT with simulations following any future incidents. This software infrastructure enables rapid analysis of potential collisions between dump trucks and bridges, offering vital insights to NCDOT on prestress losses and damage assessments for maintenance. The scripts are compatible with LS-DYNA, utilizing high-performance computing at the University of North Carolina at Charlotte. While NCDOT uses LUSAS for finite element analysis, there may be potential to adapt the library to this platform, though additional software licenses might be needed for specific capabilities. Revising the scripts for LUSAS will require extensive verification due to differences in concrete models and algorithms, as well as the validation of the LUSAS concrete model for impact analysis. This transition is estimated to take about six months.
- The research resulted in a framework for a simplified prediction model to assess damage to prestressed concrete girders from overheight vehicle impacts. This framework uses iso-damage curves to categorize damage into superficial, moderate, and severe classifications, and informs the

decisions for repairs to maintain girder strength and durability. The framework was demonstrated with a representative bridge model. The formulation of the iso-damage framework represents a significant advancement, as there is no existing generalizable technique for practitioners. Each bridge will have different iso-damage curves reflecting the girder's resistance to impact, influenced by factors such as girder type, span length, and diaphragm design.

To implement this framework without case-specific finite element analysis, further research is needed to develop statistical models that define iso-damage curves based on key bridge characteristics. This research would involve modeling several prestressed concrete girder bridges using NCDOT plans and conducting parametric analysis, including oblique impacts for skewed bridges. A comprehensive database of iso-damage constants would facilitate model development and could be expedited by a CAE library. A complete set of simplified models for various girder types is projected to take 24 months, though the timeline could be shortened by focusing on one girder type per phase to mitigate funding risks.

In a practical implementation of the simplified assessment approach, practitioners need to estimate the initial truck velocity, angle of the raised bed, and vertical underclearance violation. These estimates are used to calculate the expected peak lateral force and impulse, which indicate a point in the peak lateral force-impulse space. The predicted extent of damage is determined by the point's position relative to the iso-damage curves for the structure. The method offers a visual assessment of prediction confidence based on the proximity of the point to the iso-damage curves and allows for the incorporation of uncertainties. Although the research successfully established the framework, creating iso-damage curves using a surrogate model without parametric finite element analysis wasn't achieved within the project timeframe. These curves are unique to each structure, reflecting various design characteristics. Future work may involve statistical modeling to predict iso-damage curve constants based on specific bridge features through extensive parametric analysis.

APPENDIX A. FIELD OBSERVATIONS OF DAMAGE TO PRESTRESSED CONCRETE GIRDERS

Damages resulting from actual incidents of overheight vehicular collisions with bridge girders in North Carolina are documented to provide readers with a perspective on typical damage mechanisms and extent, as well as the wide variability of damage severity.

A.1 Incident Reports Provided by NCDOT

At the beginning of the research project, the Steering and Implementation Committee provided the research team with three supplemental element inspection reports from recent damage inspections conducted on bridges with prestressed concrete girders subjected to accidental overheight collisions. A summary of the incidents and observed damage is provided here to assist in justifying decisions made in the execution of the research plan and contribute to the limited number of case studies documented in the literature for damage caused by overheight collision to prestressed concrete bridge girders.

A.1.1 Girders of Partially Constructed Bridge Displaced by Impact

In 2021, prestressed concrete modified bulb-tee girders of a bridge under construction in Wade, NC were impacted by an overheight construction vehicle. At the time of the incident, all four girders in the span had been placed and intermediate diaphragms located at the midspan of the 63 ft 7 in span were installed. However, the deck, end bent, and thru bent diaphragms were not yet constructed. Furthermore, field welding of the embedded plates at the bearing surfaces of the girders to the sole plate over the elastomeric bearings at the thru bent had not yet been performed and the end bent was an integral abutment design so the girders were simply resting on elastomeric bearings on that end of the span. Consequently, the lateral impact to the partially constructed bridge caused the impacted girder to be lifted from the bearings and displaced by 34 inches on the thru bent side and 15 inches on the end bent side. On the thru bent side, the girder was lifted over an anchor bolt and ultimately came to rest on top of the bolt. Spalling of the girder flange indicated that the girder struck the bolt before being lifted over it. Photographs obtained from the damage inspection report of visible damage are provided in Figure A.1. Spalling at the location of the impact was limited to a ¼ inch deep region approximately 10 inches in length. The intermediate diaphragm, a k-brace constructed with bolted angles, was visibly deformed following the incident. The girders adjacent to the impacted girder also exhibited translational motion at both ends, but of significantly lower magnitude.

Figure A.1. Damage observed in modified bulb-tee girder of a partially constructed bridge in Wade following overheight impact [Courtesy of North Carolina Department of Transportation]

A.1.2 Moderately Damaged Modified Bulb-Tee Girder in Greensboro

An overheight impact occurred at approximately the third point of the span of a newly constructed bridge in Greensboro in 2021. The 92.5 ft span consisted of five 63-inch modified bulb tee girders spaced at 11 ft. The impact was reported to have occurred at the underside of the exterior girder. Photographs obtained from the damage inspection report of visible damage are provided in Figure A.2. The impact was significant enough to cause delamination of a 10.5 ft section of the bottom flange of the girder extending approximately 8 inches wide. The delamination propagated outward along the vertical surface of the bottom flange on each side at a shallow angle, resulting in a total length of delamination that was approximately three times the length of the delamination at the bottom surface of the flange. A continuous ⅛ inch wide crack was visible along the top surface of the bottom flange, extending to the web. No damage to the deck, diaphragms, or any other girders was reported in the inspection report. The extent of the damage was determined to be repairable and the priority level assigned to the repair was 2 (priority maintenance).

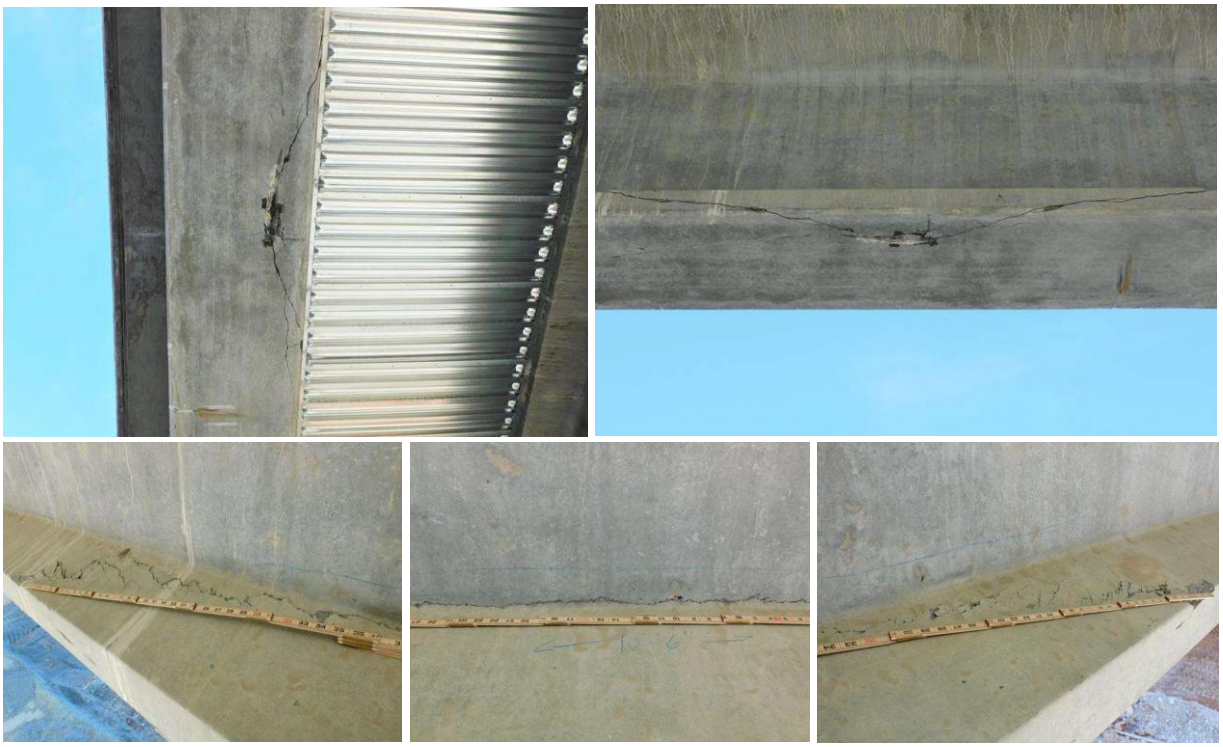

Figure A.2. Damage observed in modified bulb-tee girder of a Greensboro bridge following overheight impact [Courtesy of North Carolina Department of Transportation]

A.1.3 Severely Damaged Girders from Collision by Excavator Boom in Greenville

The boom of an excavator being pulled on an 18 wheeler flatbed lowboy trailer struck a prestressed concrete girder bridge outside of Greenville, NC in 2020. The affected span of the bridge was 85 ft in length, comprised six girders, and was 22 years old at the time of the incident. The impact occurred just to one side of a reinforced concrete intermediate diaphragm positioned at the midspan. Photographs obtained from the damage inspection report of visible damage are provided in Figure A.3. Damage to the exterior girder was severe, with a total of 17 severed strands and an additional two strands that were partially ruptured. Spalling of the bottom flange around the location of the impact was extensive, occurring over 19 ft of the girder length and exposing multiple layers of strands. As has been typically reported in the literature, the delamination propagated outward along the bottom surface of the girder, resulting in a longer region of spalling on the rear side of the impacted girder relative to the impacted side. Spalling on the rear surface of the bottom flange extended the full thickness of the flange (Figure A.3b). Although a D-shaped shear push-out failure of the girder did not occur, horizontal cracking was observed at the web-to-top flange transition on both sides of the girder. On the rear side of the girder, this horizontal cracking extended a total length of 9 ft and was present on both sides of the intermediate diaphragm (Figure A.3c). On the impacted side of the girder, the horizontal cracking was twice as long, extending for a total of 18 ft. In addition to the damage to the exterior girder, four of the remaining five girders were noted to have some level of damage due to secondary impacts from the excavator boom. Damage to these girders included delamination, spalling, exposure of strands, rupture of strands, and horizontal cracking at the interface of the web to the top flange. The damage inspection report did not note nor provide any photographic evidence of any damage to the intermediate diaphragms or the deck. The exterior girder was replaced, while the remaining girders with reported damage were repaired.

Figure A.3. Damage observed in a Greenville bridge following impact from the boom of an excavator: a) exposed and severed strands and spalling around location of impact; b) spalling across the rear side of the bottom flange; c) horizontal cracking at the web-to-top flange transition present on both sides of the intermediate diaphragm; d) horizontal cracking at the web-to-top flange transition on the impacted side of the girder [Courtesy of North Carolina Department of Transportation]

A.2 Incidents with Site Visits Conducted by the Research Team

Over the course of the research effort, the Steering and Implementation Committee regularly notified the research team of overheight vehicle collisions that occurred within a few hours drive from the University

of North Carolina at Charlotte campus. These incidents were not limited to bridges with prestressed concrete girders.

A.2.1 Impact Damage to Partially Constructed Prestressed Concrete Girder Bridge in Raleigh

On March 15, 2024 a dump truck with a raised bed impacted a bridge under construction in Wake County, NC. The bridge was designed as a two-span prestressed concrete girder bridge with reinforced concrete deck. However, at the time of the incident, only the girders had been placed, along with the mid-span steel MC intermediate diaphragms (Figure A.4). The bridge spans a total of 174.875 ft (Span A is 88.708 ft and Span B is 86.167 ft) and is comprised of five 45-inch FIB prestressed concrete girders with typical girder spacing of 8 ft 8 in. Significant damage occurred at the baseplates at the end bent and interior bent as shown in Figure A.5. The elevation of the exterior girder (girder 1) was slightly higher than that of the other girders, allowing the truck bed to clear the initial girder without making contact. However, subsequent impacts occurred to girders 2, 3, and 4. Spalling occurred near the impact location on the vertical face of the bottom flange as well as the underside of girders 2, 3, and 4 as shown in Figures A.6 and A.7.

Figure A.4. Partially constructed bridge

Figure A.5. Typical damage at base plate at bents [Courtesy of North Carolina Department of Transportation]

Figure A.6. Spalling at impact location [Courtesy of North Carolina Department of Transportation]

Figure A.7. Spalling and scraping at impact locations of girders 2, 3, and 4

A.2.2 Impact Damage to Prestressed Concrete Girder Bridge in Cary

On August 1, 2023, a dump truck traveling at highway speed with its bed raised initially struck an overhead sign structure and subsequently impacted the girders of a bridge positioned ahead; the impact force caused the bed to separate from the truck. Both the sign structure and the detached bed are shown in Figure A.8. The two-span bridge was comprised of nine AASHTO type IV prestressed concrete girders, spaced at 8 ft 9 in, and a reinforced concrete deck. The bridge had a minimum vertical underclearance of 17.5 ft. Figure A.9 shows the location of the impact to the exterior girder, and Figure A.10 shows the damage concentrated on the exterior girder.

Figure A.8. Sign structure impacted and detached dump truck bed [Courtesy of North Carolina Department of Transportation]

Figure A.9. Location of bridge and impact location [Courtesy of North Carolina Department of Transportation]

Figure A.10. Exterior girder damage [Courtesy of North Carolina Department of Transportation]

A.2.3 Impact Damage to Steel Stringer Bridge in Hillsborough

On May 31, 2023, the boom of an excavator being carried on a trailer collided with a 4-span, steel stringer bridge in Orange Country, NC. All girders were 12 in wide and 36.375 in deep. Figure A.11 shows the location of the impact and damage to the bridge. Figure A.12 shows the overall extent of the damage. Note

the impact occurred in an area with existing soot and fire damage from a previous truck impact and fire during September 2022. The steel beam has both local and global deformations. Figure A.13 shows the excavator after the impact incident. Figure A.14 shows the detail of the damage at the initial impact site, including bottom flange rotation and cracking in the bottom cover plate. Figure A.15 shows damage at the diaphragm, including member rotation and broken weld, and a longitudinal view of the damaged girder. There is significant deformation and cracking in the impacted girder, but limited damage in the adjacent beams. Ultimately, the decision was made to repair the beams.

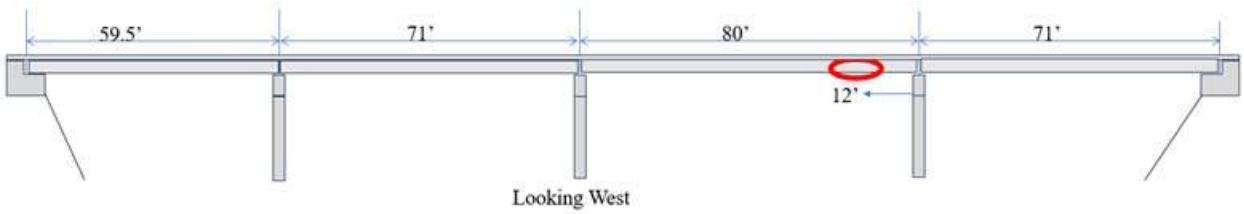

Figure A.11. Location of impact.

Figure A.12. Overall damage to exterior girder [right photo Courtesy of North Carolina Department of Transportation]

Figure A.13. Photo of excavator after incident [Courtesy of North Carolina Department of Transportation]

Figure A.14. Rotation and fracture at impact site. [Courtesy of North Carolina Department of Transportation]

Figure A.15. Broken weld and member rotation at diaphragm [Courtesy of North Carolina Department of Transportation] and deformation in beam 4 looking south

A.2.4 Impact Damage to Steel Stringer Bridge in Charlotte

On April 11, 2024, a truck with a raised boom impacted the bottom flange of an exterior steel stringer in an overpass in Mecklenburg County, NC. The research team visited the site to document the damage to the structure using photography and LiDAR scanning. Figure A.16 provides the measured out-of-plane deformation of the stringer obtained from processing the point cloud obtained from the LiDAR scans along with photographs of the damaged girder and intermediate diaphragms. The bridge is composed of several steel girders. There was visible local deformation at the location of impact as well as out-of-plane deformation along the impacted girder (Figure A.17). The diaphragm closest to the point of impact appeared to buckle (Figure A.18).

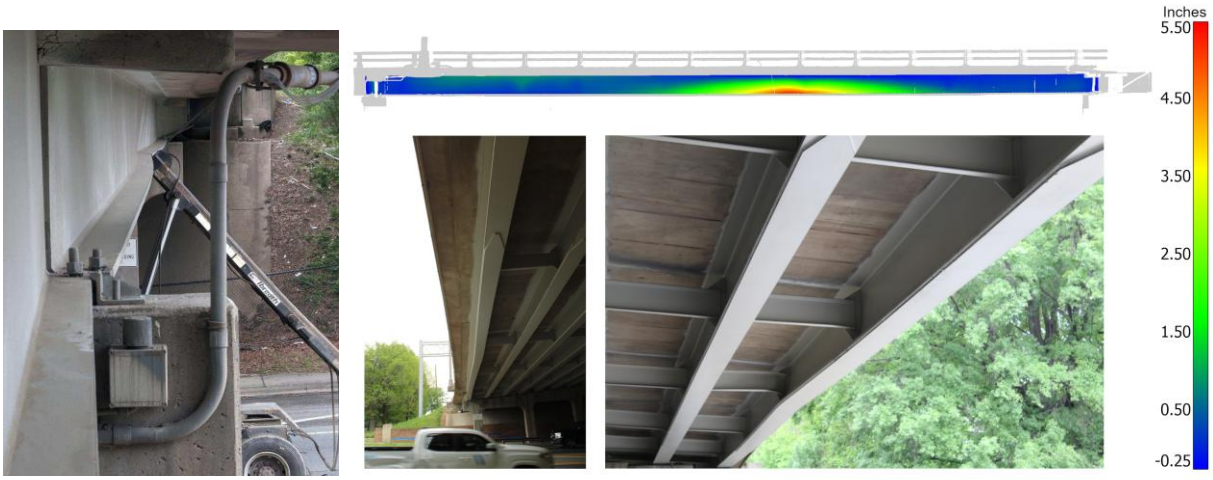

Figure A.16. Damage observed in a steel stringer bridge following overheight impact [Image of Offending Vehicle Courtesy of North Carolina Department of Transportation]

Figure A.17. View of steel girders in bridge and lateral deformation of impacted girder

Figure A.18. Buckling intermediate diaphragm closest to impact site

A.2.5 Impact Damage to Plate Girder Bridge in Lexington

On October 4, 2023, a plate girder bridge in Lexington was struck by the raised bed of a dump truck. News reports indicated that the bed detached from the truck after impact, and video revealed what appeared to be a backwall impact from the truck bed. Figure A.19 shows the bridge and plate girders. The bottom angle member of the intermediate diaphragm closest to the impact location was bent upward nearly 4 in (Figure A.20a) and at least one flange to a connecting bracket partially ruptured, which propagated from the bottom face (Figure A.20b). The cross bracing was shown to exhibit buckling behavior as well (Figure A.20c). Local deformation appeared on the exterior girder face where the cross bracing was bolted nearest to the impact location (Figure A.20d).

Figure A.19. Bridge view and girder detail

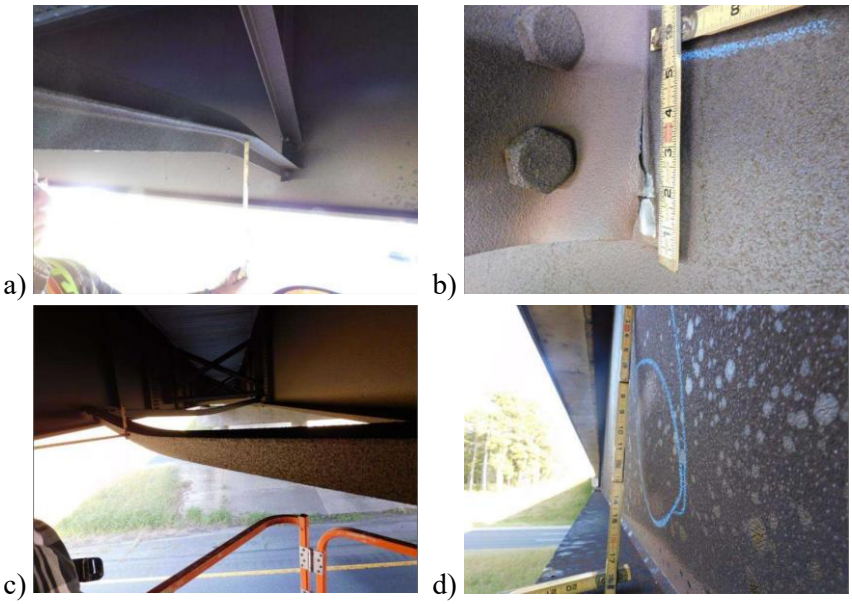

Figure A.20. Damage to impacted girder: a) intermediate diaphragm; b) connection rupture; c) buckled cross bracing; and d) deformation on exterior girder face [Courtesy of North Carolina Department of Transportation]

APPENDIX B. OVERHEIGHT VEHICLE INCIDENTS REPORTED IN NEWS ARTICLES

Month	Year	Location	Vehicle Type
January	2020	Madison County, Florida	Excavator
September	2020	Greenville , North Carolina	Excavator
May	2021	Layton, Utah	Excavator
June	2021	Madisonville, Kentucky	Excavator
July	2021	Harwich, Massachusetts	Excavator
July	2021	Cornwall, Connecticut	Excavator
July	2021	Soperton, Georgia	Dump truck
August	2021	Savannah, Georgia	Dump truck
August	2021	Lafayette, Indiana	Dump truck
August	2021	Willison, Vermont	Dump truck
August	2021	Huntsville, Alabama	Dump truck
September	2021	Muskoka (Canada)	Excavator
September	2021	Elmira, New York	Dump truck
September	2021	Stafford, Virginia	Dump truck
October	2021	Albany, New York	Excavator
October	2021	Belchertown, Massachusetts	Excavator
October	2021	Falmouth, Maine	Excavator
October	2021	Tulsa, Oklahoma	Dump truck
November	2021	Ottawa (Canada)	Dump truck
December	2021	Brunswick, Maine	Excavator
February	2022	Stafford, Virginia	Excavator
February	2022	Ann Arbor, Michigan	Excavator
March	2022	York, Pennsylvania	Excavator
March	2022	Abilene, Texas	Excavator
April	2022	Fargo , North Dakota	Excavator
April	2022	Levittown, Pennsylvania	Dump truck
May	2022	Calgary, Canada	Garbage truck
May	2022	Winona County, Minnesota	Excavator
May	2022	Pittsfield, Massachusetts	Dump truck
May	2022	Lawrence, Kansas	Garbage truck
May	2022	Martin County, Florida	Dump truck
June	2022	Renton, Washington	Excavator
June	2022	Brighton, New York	Dump truck
June	2022	West Bridgewater, Massachusetts	Dump truck
July	2022	Westfield, Indiana	Dump truck
July	2022	Providence, Rhode Island	Excavator
July	2022	Raleigh, North Carolina	Dump truck
August	2022	Outagamie County, Wisconsin	Dump truck
August	2022	Pinehurst, North Carolina	Excavator
August	2022	Mead, Colorado	Excavator
August	2022	Middlesex, Ontario	Dump truck
August	2022	Cameron, Missouri	Dump truck
August	2022	Taylorsville, Indiana	Excavator
August	2022	York, Pennsylvania	Dump truck
August	2022	Nashville, Tennessee	Dump truck
September	2022	Lexington County, South Carolina	Dump truck
September	2022	Tolland, Connecticut	Dump truck

September	2022	Hollywood , Florida	Dump truck
October	2022	Lawrence, Kansas	Dump truck
October	2022	Buffalo, New York	Garbage truck carrying natural gas tanks
October	2022	Toronto (Canada)	Dump truck
November	2022	Allen County, Indiana	Excavator
November	2022	Lexington, Massachusetts	Dump truck
November	2022	Indianapolis, Indiana	Garbage truck
December	2022	St Johns County, Florida	Dump truck
December	2022	Springfield, Ohio	Dump truck
December	2022	Houston, Texas	Semi-trailer
December	2022	Cornwall, Connecticut	Excavator
December	2022	Newton, Massachusetts	Dumpster truck without dumpster but with raised lift
January	2023	Amarillo , Texas	Garbage truck carrying dumpster
January	2023	Lafayette, Louisiana	Excavator
February	2023	Greensboro, North Carolina	Excavator
February	2023	New Bedford, Massachusetts	Excavator
January	2023	Montgomery, Alabama	Boom truck
February	2023	Richmond, Vancouver	Dump truck
February	2023	Toledo, Ohio	Tractor trailer
February	2023	San Antonio, Texas	Dump truck
February	2023	Ocala, Florida	Tractor trailer
March	2023	Mechanicville, New York	Excavator
March	2023	Ann Arbor, Michigan	Tractor trailer with no box, but raised lift
March	2023	Miami, Florida	Tractor trailer hauling construction material
March	2023	Liverpool, New York	Tractor trailer
March	2023	Calgary	Excavator
April	2023	Levittown, Pennsylvania	Dump truck
April	2023	Clarksburg, West Virginia	Excavator
April	2023	Jacksonville, Illinois	Excavator
April	2023	Atlanta, Georgia	Dump truck
May	2023	Abbottsford, Canada	Excavator
May	2023	Dartmouth, Nova Scotia	Dump truck
May	2023	Clemmonsville, North Carolina	Raised hydraulic lift of truck
May	2023	Downer, Minnesota	Excavator
June	2023	Dorchester, Massachusetts	Tractor trailer carrying glass panels
June	2023	Canton, Mississippi	Dump truck
June	2023	Ocala, Florida	Dump truck
June	2023	Syracuse, New York	Tractor trailer
June	2023	Edmonton (Canada)	Excavator
June	2023	Austin, Texas	Semi-truck
July	2023	Newberry, South Carolina	Excavator
July	2023	Hanson, Kentucky	Excavator
July	2023	Pennsylvania	Coca-Cola truck
July	2023	Pleasantville, New York	Tractor-trailer
July	2023	Hays, Kansas	Truck carrying oversized load (tank)
August	2023	Cary, North Carolina	Dump truck/container truck

APPENDIX C. MAXIMUM PRINCIPAL STRAIN DISTRIBUTIONS FOR IMPACT SCENARIOS

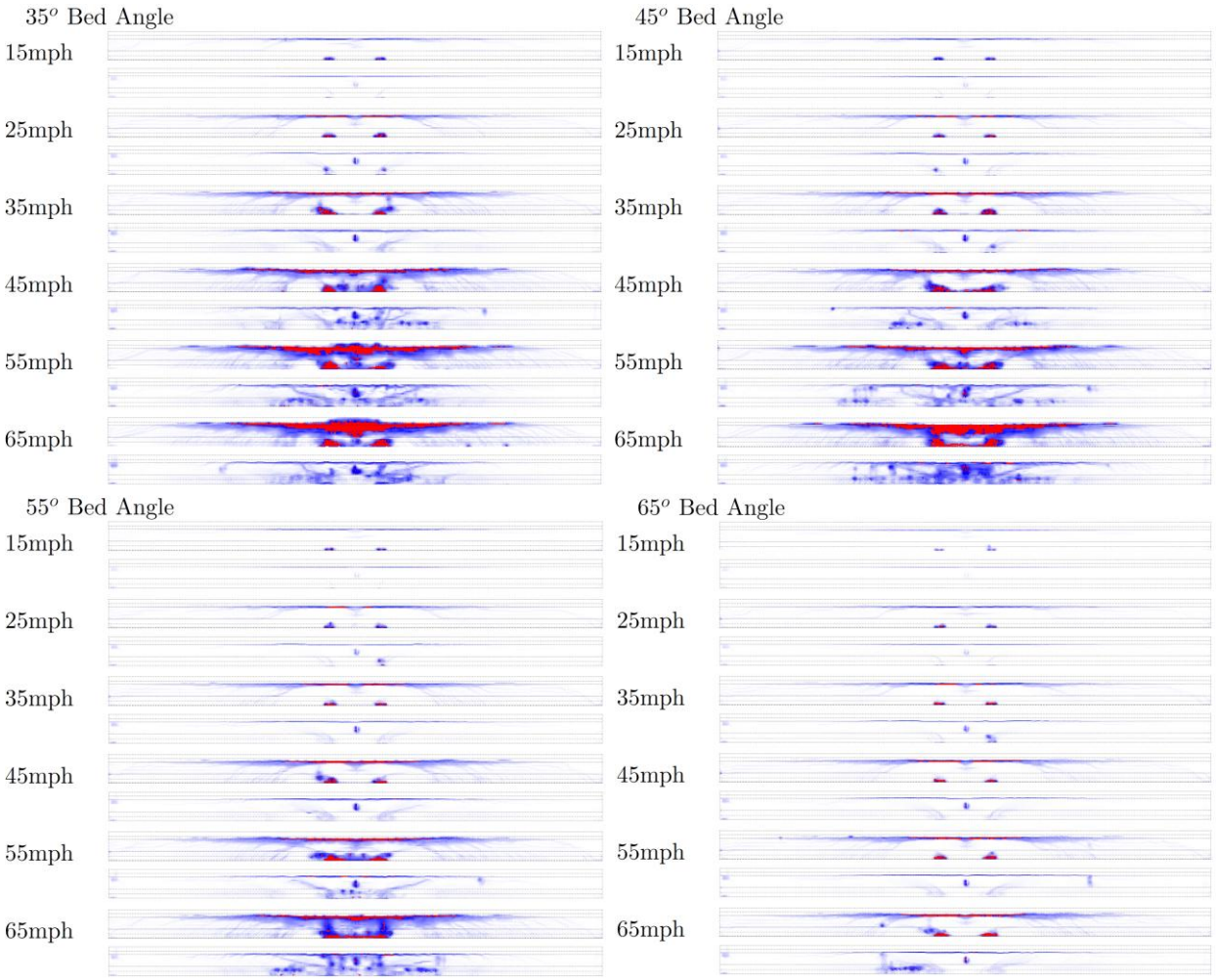

Figure C.1. Maximum principal strain distributions for Scenario 1 impact at midspan (front of exterior girder and rear of exterior girder shown)

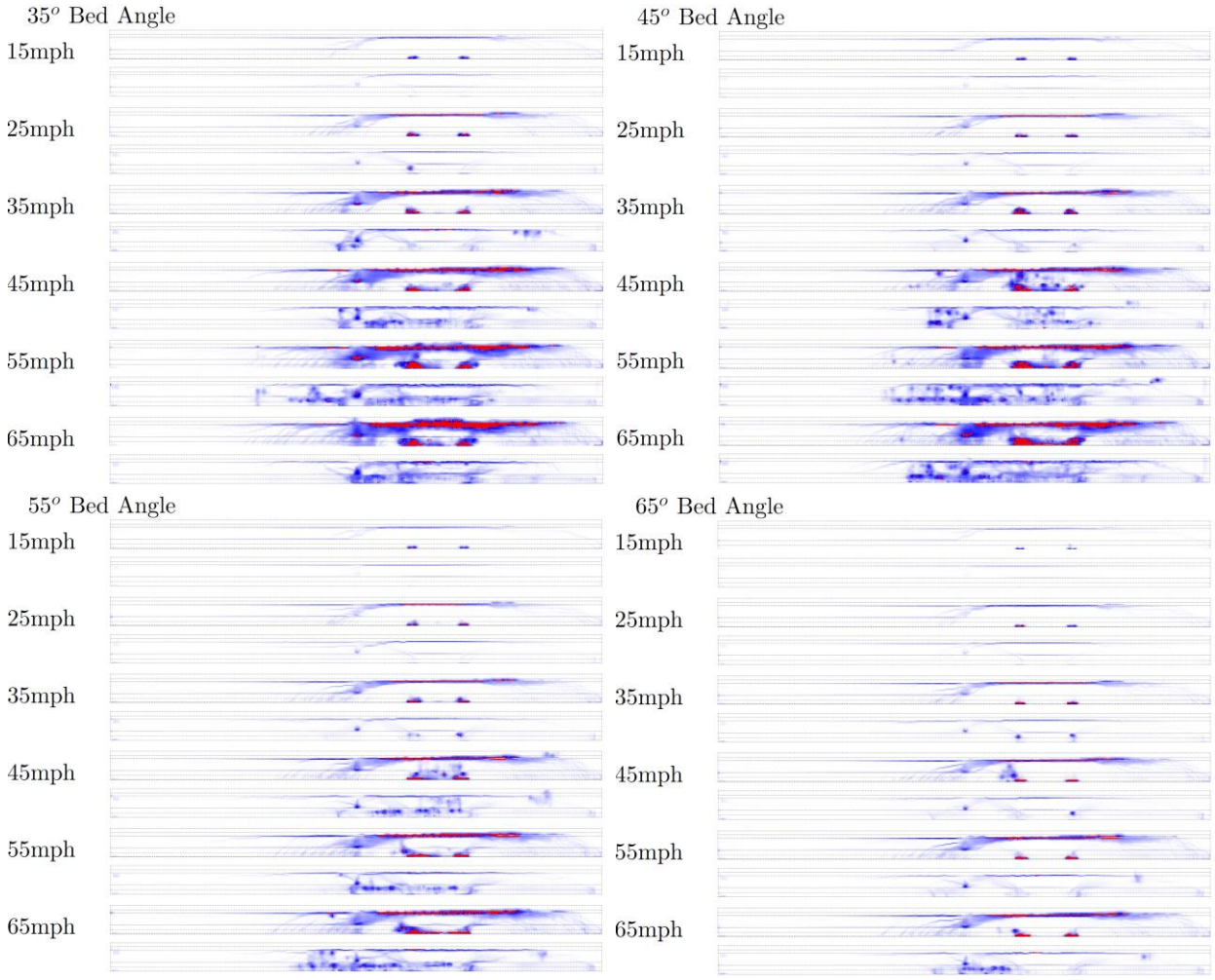

Figure C.2. Maximum principal strain distributions for Scenario 1 impact at third point (front of exterior girder and rear of exterior girder shown)

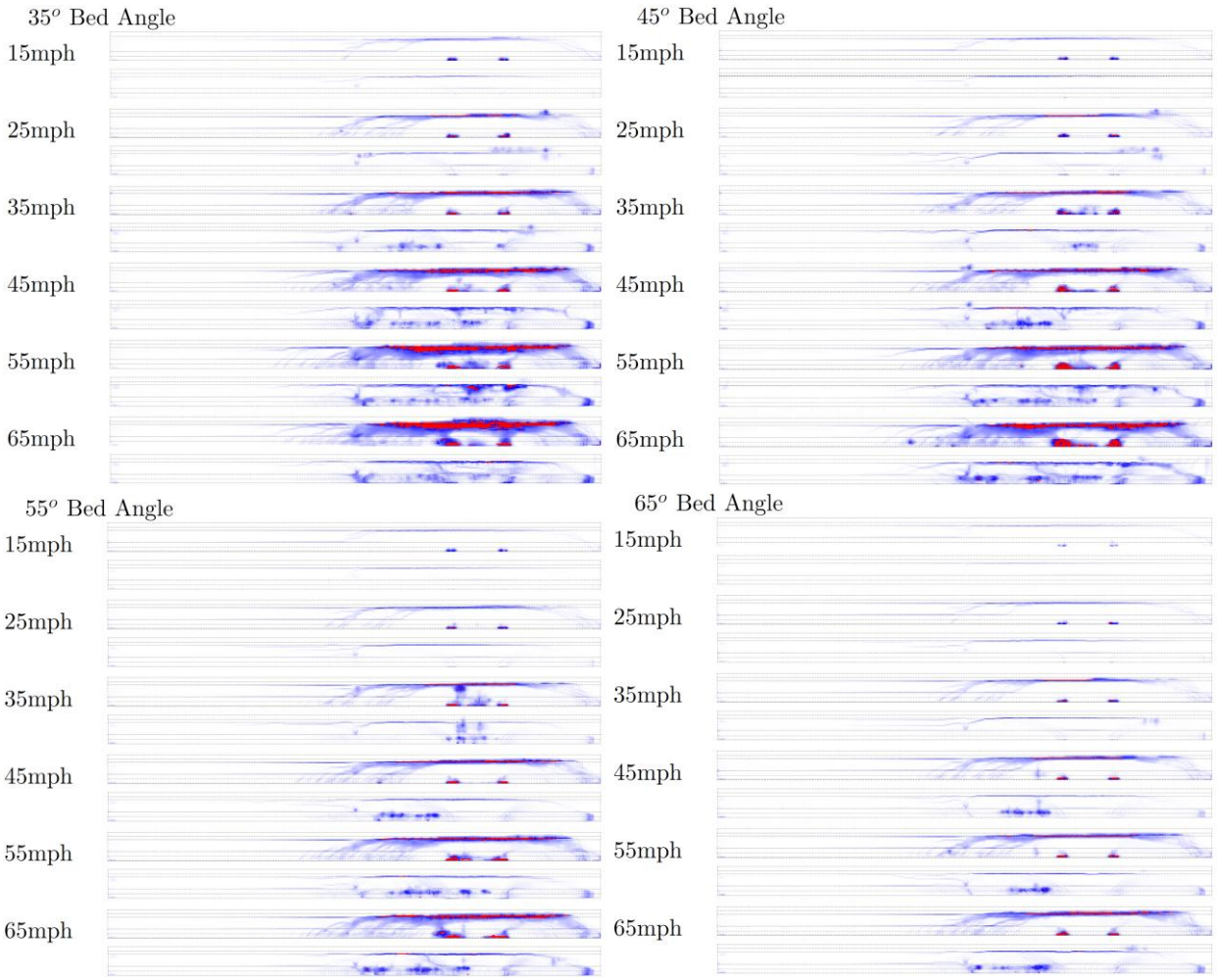

Figure C.3. Maximum principal strain distributions for Scenario 1 impact at quarterpoint (front of exterior girder and rear of exterior girder shown)

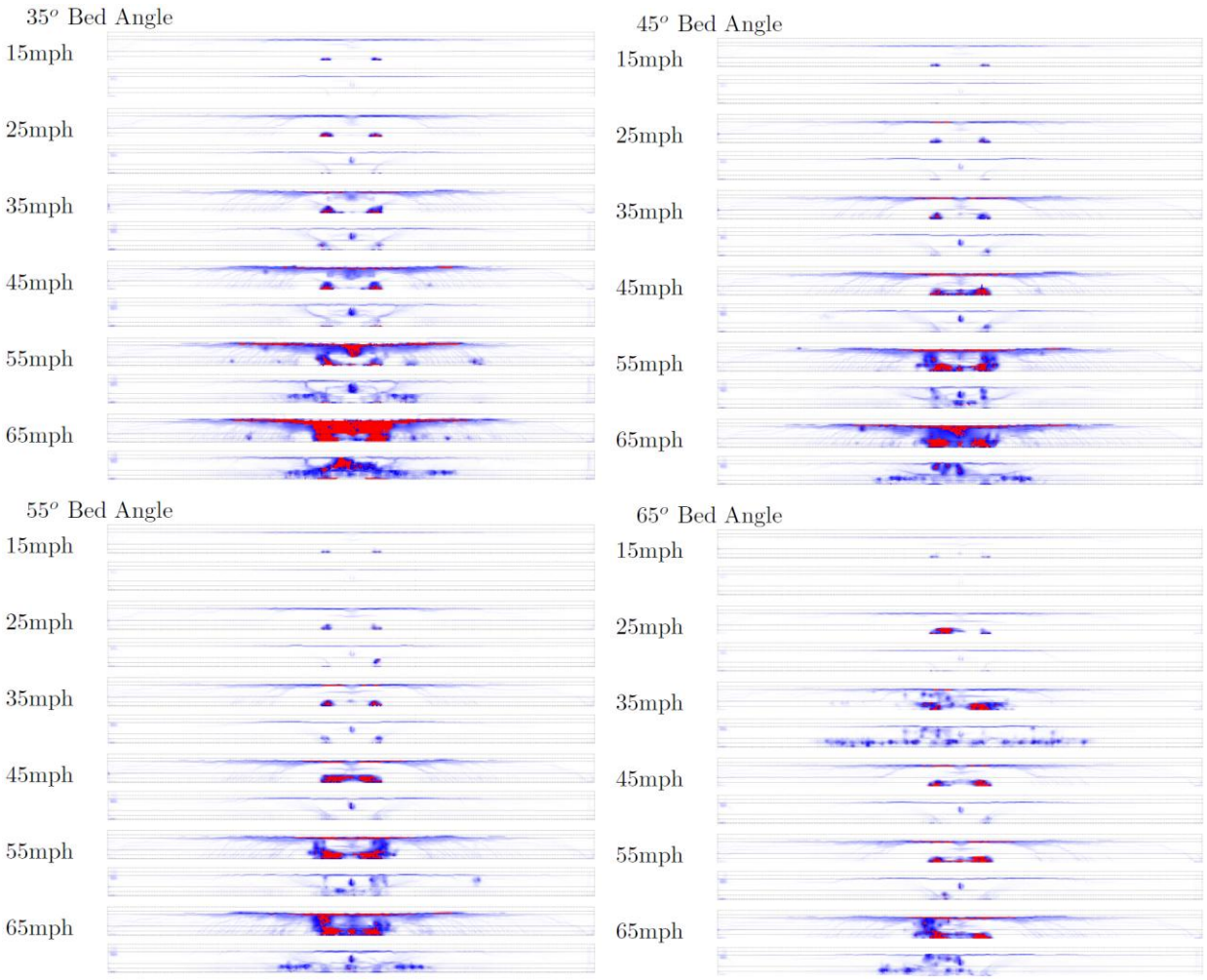

Figure C.4. Maximum principal strain distributions for Scenario 2 impact at midspan (front of exterior girder and rear of exterior girder shown)

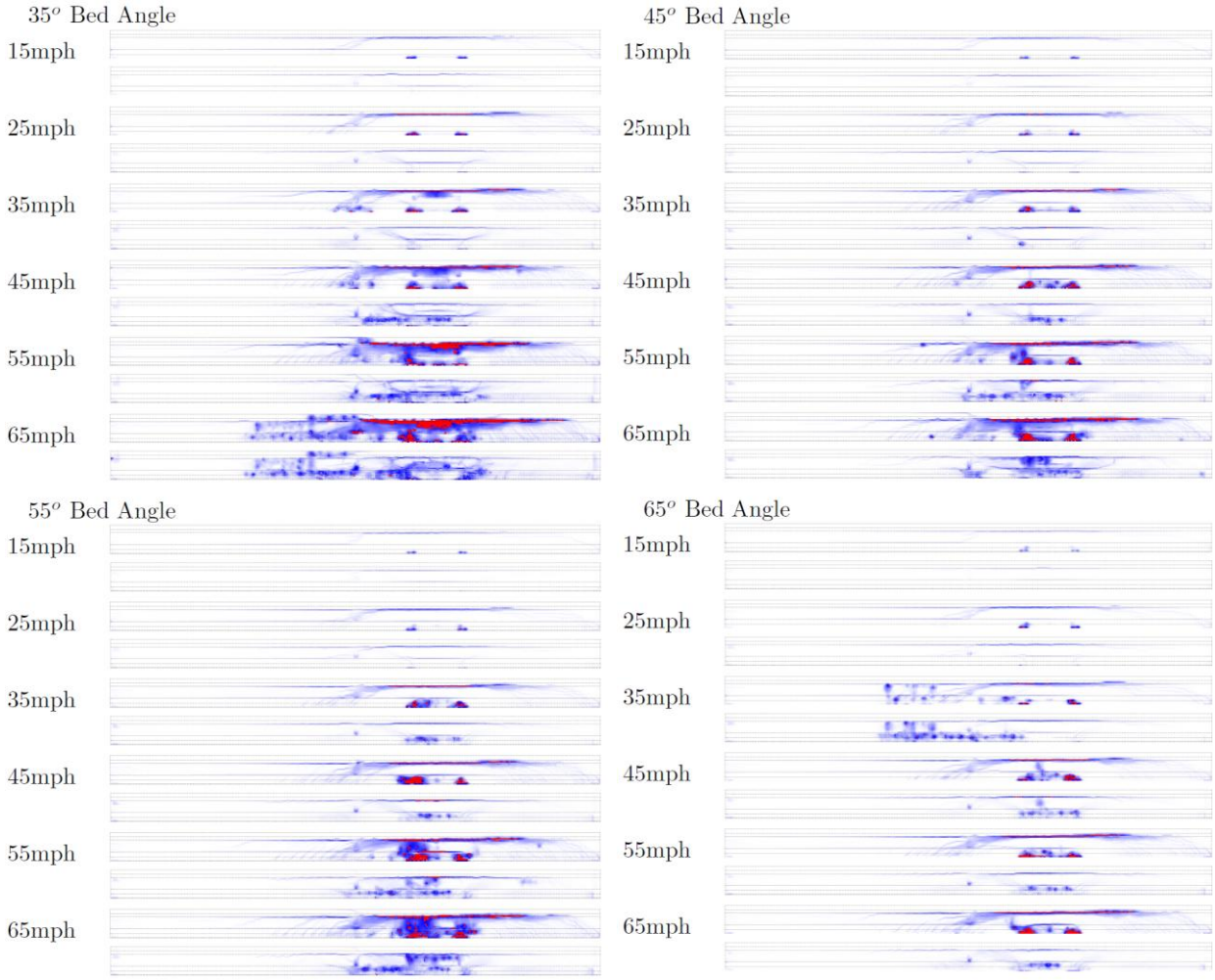

Figure C.5. Maximum principal strain distributions for Scenario 2 impact at third point (front of exterior girder and rear of exterior girder shown)

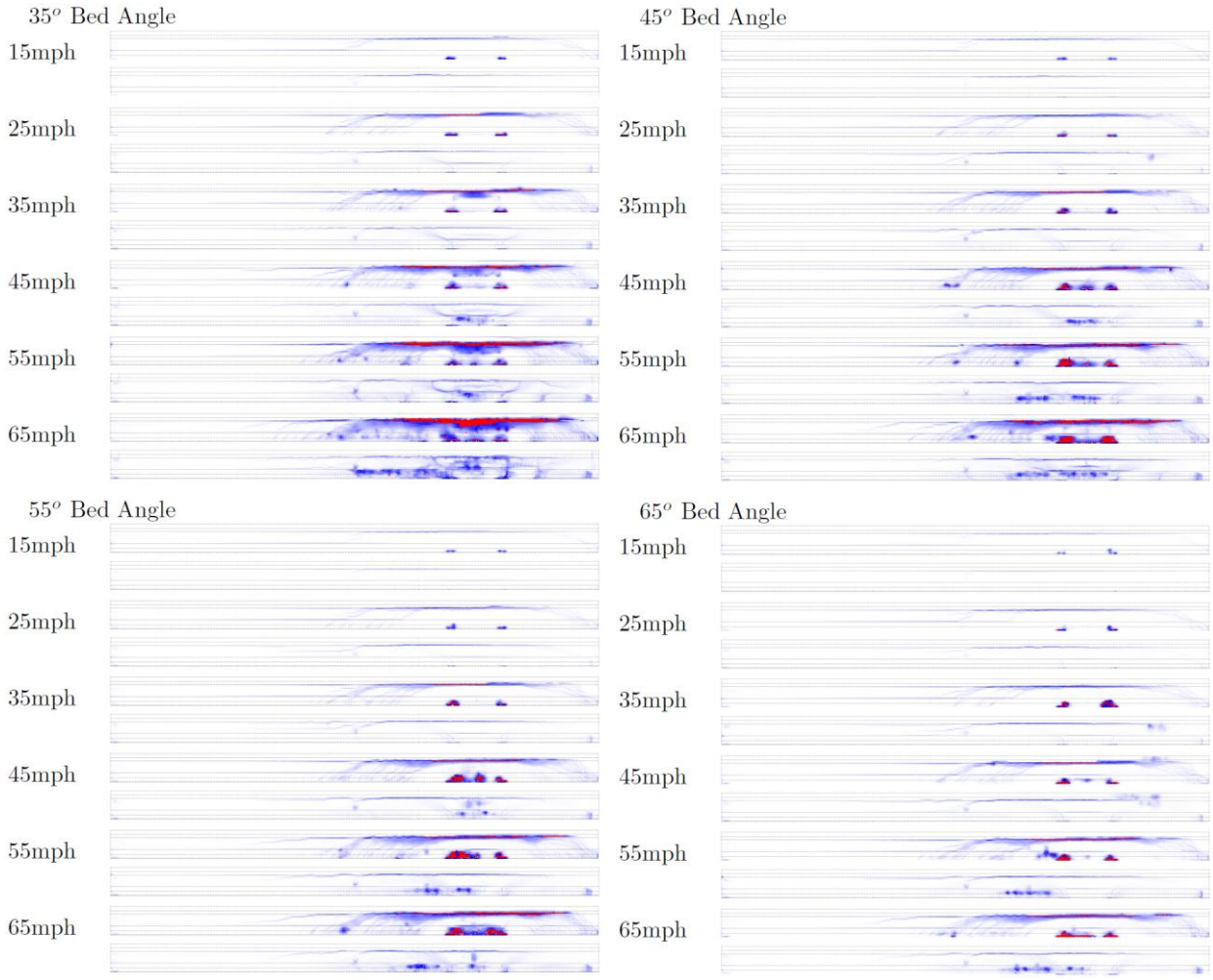

Figure C.6. Maximum principal strain distributions for Scenario 2 impact at quarterpoint (front of exterior girder and rear of exterior girder shown)

Figure C.7. Maximum principal strain distributions for Scenario 3 impact at midspan (front of exterior girder and rear of exterior girder shown)

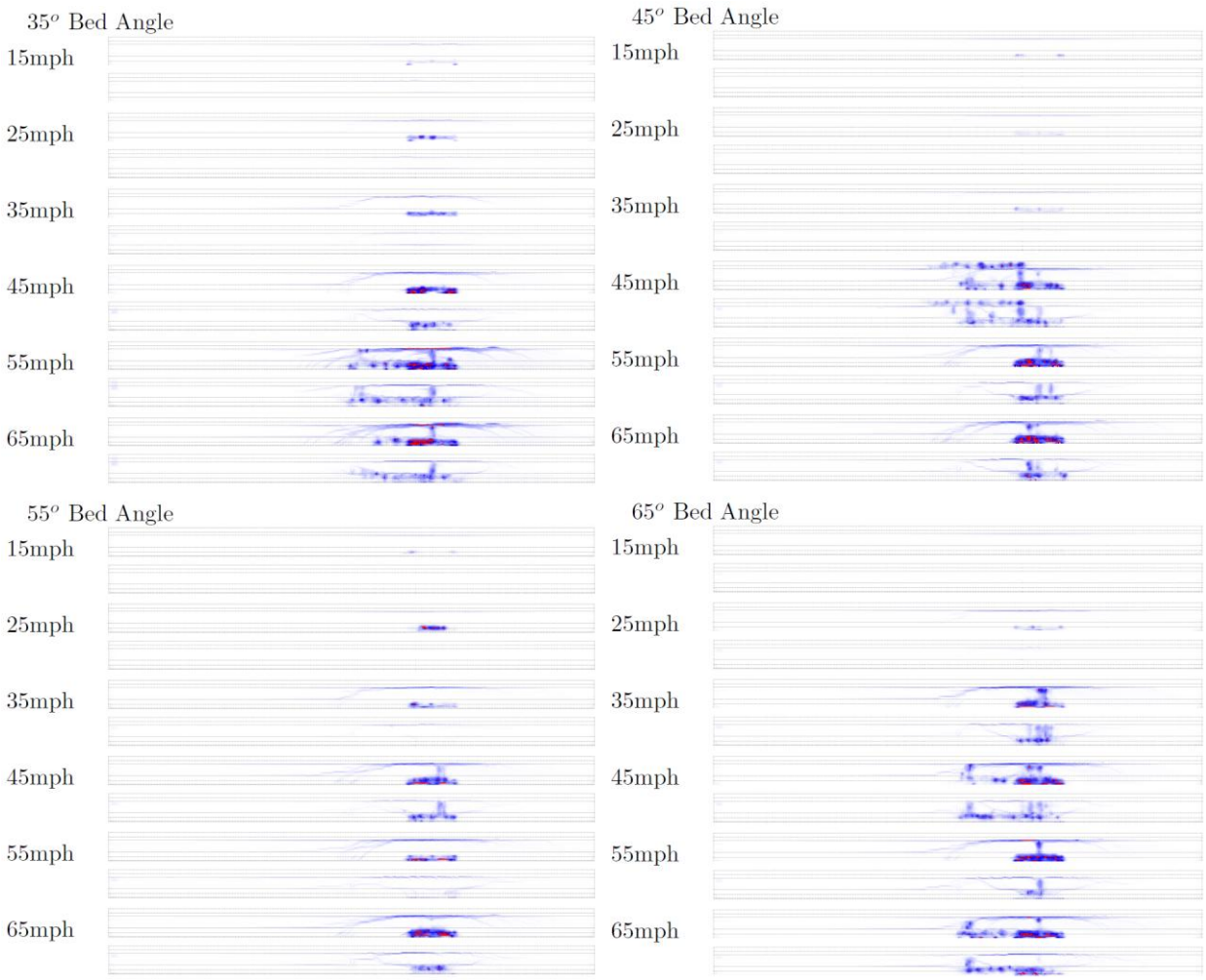

Figure C.8. Maximum principal strain distributions for Scenario 3 impact at third point (front of exterior girder and rear of exterior girder shown)

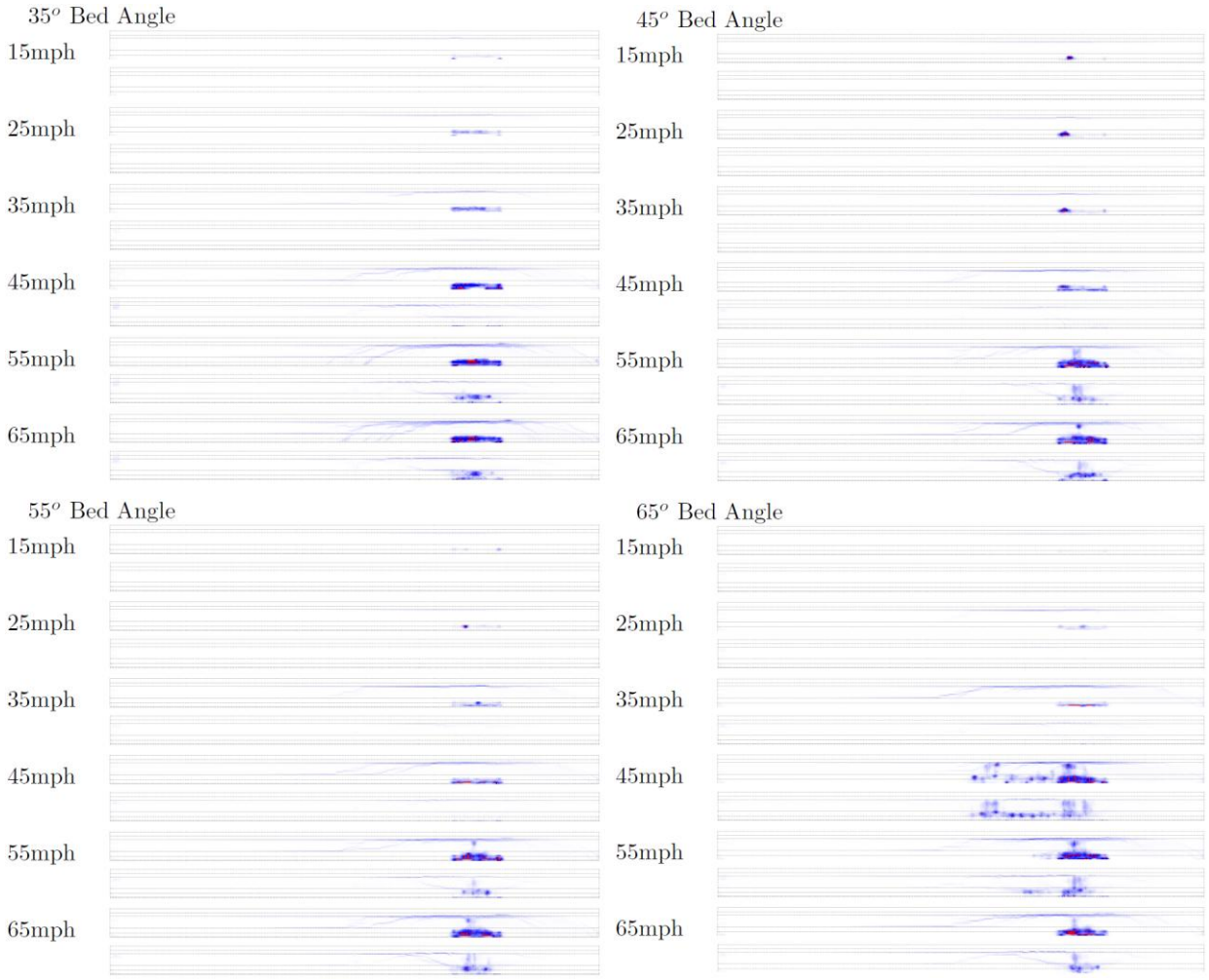

Figure C.9. Maximum principal strain distributions for Scenario 3 impact at quarterpoint (front of exterior girder and rear of exterior girder shown)

Figure C.10. Maximum principal strain distributions for Scenario 4 impact at midspan (front of exterior girder and rear of exterior girder shown)

Figure C.11. Maximum principal strain distributions for Scenario 4 impact at third point (front of exterior girder and rear of exterior girder shown)

Figure C.12. Maximum principal strain distributions for Scenario 4 impact at quarterpoint (front of exterior girder and rear of exterior girder shown)

REFERENCES

AASHTO. (2012). LRFD Bridge Design Specifications, 6th Edition, Washington, DC.

ABC-UTC (2020), “Guide for Repair of Reinforced and Prestressed Concrete Bridge Girders,” Accelerated Bridge Construction University Transportation Center (ABC-UTC), Reno, NV.

Abendroth, R., Klaiber, F., and Shafer, M. (1995) “Diaphragm effectiveness in prestressed concrete girder bridges,” Journal of Structural Engineering, 121(9), 1259-1379.

Abendroth, R., Fanous, F., and Andrawes, B. (2004) “Steel diaphragms in prestressed concrete girder bridges,” Center for Transportation Research and Education, Iowa State University, Report # TR-424, 151p.

Adhikary, S.D. (2014) Dynamic Behavior of reinforced concrete beams under varying rates of concentrated and impact loadings, Ph.D. Thesis, Nanyang Technological University, Singapore.

Agrawal, A., Xu, X., and Chen, Z. (2011) Bridge-vehicle impact assessment. University Transportation Research Center, New York State Department of Transportation (UTRC/NYSDOT), Final report number C-07-10, 157p.

Aimi H. and Sennah K. (2013). "Parametric effects on evaluation of an impact-damaged prestressed concrete bridge girder repaired by externally bonded carbon-fiber-reinforced polymer sheets," Journal of Performance of Constructed Facilities, vol. 29, p. 04014147.

Andrawes, B. (2001) Lateral impact response for prestressed concrete girder bridges with intermediate diaphragms,” Master of Science Thesis, Iowa State University, Department of Civil, Construction, and Environmental Engineering, 195p.

Andrawes B., Shaw I., and Zhao H. (2018). "Repair & Strengthening of Distressed/Damaged Ends of Prestressed Beams with FRP Composites," Illinois Center for Transportation/Illinois Department of Transportation.

Brice, R. (2013) “Precast-Prestressed Concrete Bridge Girders Damaged by Over-Height Load Impacts,” 2013 PCI Convention and National Bridge Conference, Grapevine, Texas, September 21-24.

Buth, C., Williams, W., Brackin, M., Lord, D., Geedipally, S., and Abu-Odeh, A. (2010) “Analysis of large truck collisions with bridge piers: Phase 1: Report of guidelines for designing bridge piers and abutments for vehicle collisions,” Texas Department of Transportation, Report # FHWA/TX-10/9-4973-1, 186p.

.

Cai, C., Araujo, M., Chandolu, A., Avent, R., and Alaywan, W. (2007) “Diaphragm effects of prestressed concrete girder bridges: review and discussion,” Practice Periodical on Structural Design and Construction, 12(3), 161-167.

Cai, C. and Xia, M. (2015). "Repairing/strengthening of bridges with post-tensioned FRP materials and performance evaluation," Louisiana Transportation Research Center (LA): Baton Rouge.

Cerullo, D., Sennah, K., Azimi, H., Lam, C., Fam, A., and Tharmabala, B. (2013). "Experimental study on full-scale pretensioned bridge girder damaged by vehicle impact and repaired with fiber-reinforced polymer technology," Journal of Composites for Construction, vol. 17, pp. 662-672.

Chan, A. (1986) Impact behaviour of model prestressed concrete beams, Ph.D. Thesis, University of Sheffield, 236 p.

Comite Euro-International du Beton (CEB). (2013) CEB-FIP model code for concrete structures 2010. Lausanne, Switzerland: International Federation for Structural Concrete.

Cowper, G. and Symonds, P. (1957) "Strain-hardening and strain-rate effects in the impact loading of cantilever beams," Office of Naval Research, Technical Report 28.

Das, S., Brenkus, N.R. and Tatar, J. (2022) „Strategies for Prevention, Protection, and Repair of Bridge Girders Vulnerable to Over-height Vehicle Impacts: A State-of-the-Art Review," Structures, 44, 514-533.

Dunne, R., Thorkildsen, E. (2020) "Case Study: Response to Bridge Impacts – An Overview of State Practices," FHWA_HIF-20-087, FHWA, Springfield, VA.

ElGawady, M. and Abdulazeez, M. (2024) "Over-height vehicle impact with bridge girders having different boundary conditions," Mid-American Transportation Center, Report # MATC-MS&T: 133-5, 25p.

ElGawady, M., Malek, H., and Abdulazeez, M. (2024) "Performance of Prestressed Bridge Girders Subjected to Vehicle Impact," Mid-American Transportation Center, Report # MATC-MS&T: 133-4, 34p.

ElSafty, A. and Graef, M. (2012) "The Repair of Damaged Bridge Girders with CFRP Laminates," Final Report No. BDK82 977-03, Florida DOT, Tallahassee, FL.

Elshazli, M., ElGawady, M., Xing, T., and Ibrahim, A. (2025) "Failure analysis of prestressed concrete girder bridges under over-height truck impacts," Transportation Research Record, doi: 10.1177/03611981251339178

Feldman, L., Jirsa, J., Fowler, D., and Carrasquillo, R. (1996) "Current practice in the repair of prestressed bridge girders," Center for Transportation Research, The University of Texas at Austin, Report # FHWA/TX-96/1370-1, 86p.

Feldman, L. R., Jirsa, J. O., and Kowal, E. S. (1998). "Repair of bridge impact damage." Concr. Int., 20(2), 61–66.

Fujikake, K., Li, B., and Soeun, S. (2009) "Impact response of reinforced concrete beam and its analytical evaluation." Journal of Structural Engineering, 135(8), 938-950.

Gangi, M., Jones, M., Liesen, J., Zhou, J., Pino, V., Cousins, T., Roberts-Wollmann, C.L., Koutromanos, I., Nanni, A., (2017) “Evaluation of Repair Techniques for Impact-Damaged Prestressed Beams,” Virginia Transportation Research Council, Charlottesville, VA.

Gangi, M., Jones, M., Liesen, J., Zhou, J., Pino, V., Cousins, T.E., Roberts-Wollmann, C.L., Koutromanos, I. and Nanni, A. (2018) “Evaluation of Repair Techniques for Impact-Damaged Prestressed Beams,” Final Report VTRC 18-R8, Virginia Transportation Research Council (VA): Charlottesville.

Ghaffary, A. and Moustafa, M.A., (2020) “Synthesis of Available Methods for Repair of Reinforced Concrete and Prestressed Concrete Bridge Girders,” Final Report, Accelerated Bridge Construction University Transportation Center, Reno, NV.

Harries, K., Kasan, J., Miller, R., and Brinkman, R. (2012) “Updated research for collision damage and repair of prestressed concrete beams,” NCHRP Project 20-07, Task 307 Final Report, 228p.

Harries K. A., Kasan J., and Brinkman R. (2012b). "Guide to Recommended Practice for The Repair of Impact-Damaged Prestressed Concrete Bridge Girders." NCHRP20-07(307) Appendix, TRR, Washington, DC.

Hasenkamp C. J., Badie S. S., Hanna K. E., and Tadros M. K. (2012). "Proposed evaluation and repair procedures for precast, prestressed concrete girders with end-zone cracking," PCI journal, vol. 57.

Hughes, B. and Mahmood, A. (1984) “Impact behavior of prestressed concrete beams in flexure” Magazine of Concrete Research, 36(128), 157-164.

Jiang, H. and Chorzepa (2015) “An effective numerical simulation methodology to predict the impact response of pre-stressed concrete members,” Engineering Failure Analysis, 55, 63-78.

Jing, Y., Ma, Z., and Clarke, D. (2016) “Full-scale lateral impact testing of prestressed concrete girder,” Structural Concrete, 17(6), 947-958.

Jing, Y. (2017) Experimental and analytical study of dynamic behavior of bridge superstructures subjected to overheight vehicle collisions. Ph.D. Dissertation, University of Tennessee, Knoxville, Department of Civil and Environmental Engineering, 116p.

Jones M. (2015). "Repair of Impact Damaged Prestressed Bridge Girders with Strand Splices and Fabric Reinforced Cementitious Matrix Systems," Master’s Thesis, Virginia Tech, (VA): Blacksburg.

Kasan J. L. (2012). "On the repair of impact damaged prestressed concrete bridge girders," University of Pittsburgh.

Kasan J. L., Harries K. A., Miller R., and Brinkman R. J. (2012). "Limits of application of externally bonded CFRP repairs for impact-damaged prestressed concrete girders," Journal of Composites for Construction, vol. 18, p. A4013013.

Kim Y. J., Green M. F., and Fallis G. J. (2008). "Repair of bridge girder damaged by impact loads with prestressed CFRP sheets," Journal of Bridge Engineering, vol. 13, pp. 15-23.

Ma, H., Cao, Z., Shi, X., Hu, K., and Zhou, J. (2020) “Performance assessment of reinforced concrete columns under vehicle impact load using P-I diagram,” Structural Concrete, vol. 21, 1625-1643.

Miele, C., Plaxico, C., Stephens, D., and Simunovic, S. (2010) “U26: Enhanced Finite Element Analysis Crash Model of Tractor-Trailers (Phase C)” National Transportation Research Center, Inc.

Miller A. D. (2006). "Repair Of Impact-Damaged Prestressed Concrete Bridge Girders Using Carbon Fiber Reinforced Polymer (CFRP) Materials” Thesis, North Carolina State University, Raleigh, NC.

Mohan, P., Marzougui, D., and Kan, C-D. (2007) “Validation of a Single Unit Truck Model for Roadside Hardware Impacts,” International Journal of Vehicle Systems Modelling and Testing,” 2(1), 1-15.

Nanni A., Huang P., and Tumialan J. (2001). "Strengthening of impact-damaged bridge girder using FRP Laminates," in Ninth International Conference on Structural Faults and Repair, pp. 4-6.

Nanni A. (2004). "Strengthening of an Impact-Damaged PC Girder." Concrete Repair Bulletin, May/June 2004, 16-17.

National Center for Statistics and Analysis (2025) “Traffic safety facts 2022: A compilation of motor vehicle traffic crash data,” National Highway Traffic Safety Administration, Report # DOT HS 813 656. 210p.

Nguyen, B. and Brilakis, I. (2016) “Understanding the Problem of Bridge and Tunnel Strikes Caused by Over-height Vehicles,” Transportation Research Procedia, 14, 3915-3924.

Oak Ridge National Laboratories (2025) “FEM Models for Semitrailer Trucks,” thyme.ornl.gov/FHWA/TractorTrailer/download Accessed September 12, 2025.

Oppong, K., Saini, D., and Shafei, B. (2021) “Characterization of impact-induced forces and damage to bridge superstructures due to over-height collision. Engineering Structures, 236: 112014.

Pantelides C. P., Reaveley L. D., and Burningham C. A. (2010). "Repair of prestressed concrete girder ends and girder collision repair." Report UT-10.04, UDOT, Salt Lake City, Utah.

Pino V. and Nanni A. (2015a). "FRCM and FRP composites for the repair of damaged PC girders," Research on Concrete Applications for Sustainable Transportation.

Pino, V. and Nanni, A. (2015b) “Repair of Damaged PC Girder with FRCM and FRP Composites,” Final Report, RE-CAST University Transportation Center, Rolla, MO.

Pino V., Nanni A., Arboleda D., Roberts-Wollmann C., and Cousins T. (2017). "Repair of damaged prestressed concrete girders with FRP and FRCM composites," Journal of Composites for Construction, vol. 21, p. 04016111.

Qiao, P., Yang, M., and McLean, D. (2008) “Effect of intermediate diaphragms to prestressed concrete bridge girders in over-height truck impacts,” Washington State Transportation Center (TRAC), Report # WA-RD 696.1, 141p.

Rabbat, B. and Russell, H. (1985) “Friction coefficient of steel on concrete or grout,” Journal of Structural Engineering, 111(3), 505-515.

Rizkalla, S., Zia, P. and Storm, T. (2011) “Predicting Camber, Deflection, and Prestress Losses in Prestressed Concrete Members,” Final Report #2010-05, North Carolina DOT, Raleigh, NC.

Saati, S. and Vecchio, F.J. (2009) “Effects of shear mechanisms on impact behavior of reinforced concrete beams”. ACI Structural Journal, 106(1), 78-86.

Saini, D. and Shafei, B. (2019) “Concrete constitutive models for low velocity impact simulations,” International Journal of Impact Engineering, 132, 103329.

Samadzad, A. and Whelan, M. (2024) “Effect of Hourglass Control on LS-DYNA Concrete Constitutive Models in Low Velocity Impact Simulations,” 17th International LS-DYNA Conference, Metro Detroit, Michigan.

Samadzad, A., S. Cathey, M. Whelan, N. Braxtan, and S. Chen. (2024) "Finite element analysis of over-height vehicle collisions on prestressed girder bridges." Bridge Maintenance, Safety, Management, Digitalization and Sustainability: Proceedings of the 12th International Conference on Bridge Maintenance, Safety and Management, Copenhagen, Denmark.

Samadzad, A., Whelan, M., Cathay, S., Braxtan, N., and Chen. S. (2025) “Investigation of concrete constitutive models for predicting the response, damage, and residual capacity of reinforced concrete beams subject to low velocity impact,” International Journal of Impact Engineering, 202, 105310.

Scheer, J. (2010) Failed Bridges - Case Studies, Causes and Consequences, Ernst and Sohn, Hannover, Germany.

Schiebel S., Parretti R., and Nanni A. (2001). "Repair and strengthening of impacted PC girders on Bridge A4845, Jackson County, Missouri." Report RDT01-017, MoDOT.

Shanafelt, G. and Horn, W. (1980) “Damage Evaluation and Repair Methods for Prestressed Concrete Bridge Members,” National Cooperative Highway Research Program, Report 226, 66p.

Shanafelt, G.O. and Horn, W.B. (1985) “Guidelines for Evaluation and Repair of Prestressed Concrete Bridge Members,” NCHRP 280, Transportation Research Board, Washington, D.C.

Simunovic, S. and Zisi, N. (2005) “F800 Single Unit Truck Model for Crash Simulations with LS-DYNA,” thyme.ornl.gov/FHWA/F800WebPage/description/

Tabatabai, H. and Nabizadeh, A. (2019) “Strength and Serviceability of Damage Prestressed Girders,” Final Report 0092-17-02, Wisconsin DOT, Madison, WI.

Xu, L., Lu, X., Guan, H., and Zhang, Y. (2013) “Finite-element and simplified models for collision simulation between overheight trucks and bridge superstructures,” Journal of Bridge Engineering, 17(1): 151-160.

Weathersby, J.H. (2003) “Investigation of bond slip between concrete and steel reinforcement under dynamic loading conditions,” Louisiana State University and Agricultural and Mechanical College, Ph.D. Dissertation, Department of Civil and Environmental Engineering, 263 p.

Wei, W., Su, J., and Huang, F. (2022) “Development of pressure-impulse diagram to predict the damage of simply supported RC beams under close-in explosion,” Process Safety and Environmental Protection, vol. 167, 126-145.

Whelan, M. and Janoyan, K. (2012) “Assessment of simplified linear dynamic analysis of a multispan skew bridge on steel-reinforced elastomeric bearings,” Journal of Bridge Engineering, 17(1), 151-160.

Zobel, R., Jirsa, O., Fowler, D., and Carrasquillo, R. (1997) “Evaluation and repair of impact-damaged prestressed concrete bridge girders,” Center for Transportation Research, The University of Texas at Austin, Report # FHWA/TX-97/1370-3F, 209p.